CRYSTAL PLASTICITY BASED ANALYSIS OF CRACK PROPAGATION AT MICROSCALE BY EXTENDED FINITE ELEMENT METHOD

A THESIS SUBMITTED TO
THE GRADUATE SCHOOL OF NATURAL AND APPLIED SCIENCES
OF
MIDDLE EAST TECHNICAL UNIVERSITY

BY

UMUT YILMAZ

IN PARTIAL FULFILLMENT OF THE REQUIREMENTS
FOR
THE DEGREE OF MASTER OF SCIENCE
IN
MECHANICAL ENGINEERING

JANUARY 2023

Approval of the thesis:

CRYSTAL PLASTICITY BASED ANALYSIS OF CRACK PROPAGATION AT MICROSCALE BY EXTENDED FINITE ELEMENT METHOD

submitted by **UMUT YILMAZ** in partial fulfillment of the requirements for the degree of **Master of Science** i**n Mechanical Engineering, Middle East Technical University** by,

Prof. Dr. Halil Kalıpçılar
Dean, Graduate School of **Natural and Applied Sciences** _____

Prof. Dr. M. A. Sahir Arıkan
Head of the Department, **Mechanical Engineering** _____

Prof. Dr. Haluk Darendeliler
Supervisor, **Mechanical Engineering, METU** _____

Examining Committee Members:

Prof. Dr. Fevzi Suat Kadıoğlu
Mechanical Engineering, METU _____

Prof. Dr. Haluk Darendeliler
Mechanical Engineering, METU _____

Assoc. Prof. Dr. Hüsnü Dal
Mechanical Engineering, METU _____

Asst. Prof. Dr. Orkun Özşahin
Mechanical Engineering, METU _____

Prof. Dr. Can Çoğun
Mechatronics Engineering, Çankaya University _____

Date: 27.01.2023

I hereby declare that all information in this document has been obtained and presented in accordance with academic rules and ethical conduct. I also declare that, as required by these rules and conduct, I have fully cited and referenced all material and results that are not original to this work.

Name Last name : Umut Yılmaz

Signature :

ABSTRACT

CRYSTAL PLASTICITY BASED ANALYSIS OF CRACK PROPAGATION AT MICROSCALE BY EXTENDED FINITE ELEMENT METHOD

Yılmaz, Umut
Master of Science, Mechanical Engineering
Supervisor: Prof. Dr. Haluk Darendeliler

January 2023, 99 pages

Crack propagation is conventionally treated by employing analytical methods at macroscale. Investigation of the relations between the crack propagation, dislocation movement and the crystalline grain properties in the material microscale provides better understanding of the crack propagation mechanism. In this work, the crystal plasticity constitutive model is incorporated to a commercial finite element software as an user-defined subroutine to simulate crack propagation in the material microscale. The effects of grain properties and material selection on the crack growth behavior are examined by considering different damage criteria. The extended finite element method (XFEM) is employed to analyze the crack propagation in single crystal and polycrystal structures by constructing multiple models, including pre-cracks. In these analyses, plates made of 316L stainless steel, AA2024 aluminum alloy and nickel-based supper alloy (MD2) materials with face-centered cubic crystal structures are subjected to quasi-static loading. The results of the analyses show that crack propagation behavior is dependent to the grain orientation, grain size and intrinsic material parameters such as hardening property and anisotropic stiffness.

Keywords: Crystal Plasticity, Crack Propagation, Microstructure, Extended Finite Element Method

ÖZ

ÇATLAK İLERLEMESİNİN GENİŞLETİLMİŞ SONLU ELEMANLAR METODU İLE MİKRO ÖLÇEKTE KRİSTAL PLASTİSİTE TEMELLİ ANALİZİ

Yılmaz, Umut
Yüksek Lisans, Makina Mühendisliği
Tez Yöneticisi: Prof. Dr. Haluk Darendeliler

Ocak 2023, 99 sayfa

Çatlak ilerlemesi geleneksel olarak makro ölçekteki analitik metotların kullanımı ile ele alınmaktadır. Çatlak ilerlemesi, dislokasyon hareketi ve kristal tanecik özellikleri arasındaki ilişkilerin malzeme mikro ölçeğinde incelenmesi çatlak ilerleme mekanizmasının daha iyi anlaşılmasını sağlar. Bu çalışmada, çatlak ilerlemesinin malzeme mikro ölçeğinde benzetimi amacıyla kristal plastisite bünye modeli ticari bir sonlu elemanlar yazılımına kullanıcı tanımlı bir alt program ile dahil edilmiştir. Tanecik özellikleri ve malzeme seçiminin çatlak büyüme davranışına etkileri farklı hasar kriterleri göz önünde bulundurularak incelenmiştir. Genişletilmiş sonlu elemanlar metodu (XFEM) başlangıç çatlağı da içeren modeller oluşturularak tek kristalli ve çok kristalli yapılarda çatlak ilerlemesinin analizi için kullanılmıştır. Bu analizlerde, yüzey merkezli kübik kristal yapılara sahip 316L paslanmaz çelik, AA2024 alüminyum alaşımı ve nikel bazlı süperalaşım (MD2) malzemelerinden yapılmış levhalar yarı statik yüklemeye tabi tutulmuştur. Analiz sonuçları çatlak ilerlemesi davranışının tane yönüne, tane boyutuna ve pekleşme ve anizotropik katılık gibi içsel malzeme özelliklerine bağlı olduğunu göstermiştir.

Anahtar Kelimeler: Kristal Plastisite, Çatlak İlerlemesi, Mikro Yapı, Çoklu Kristal, Genişletilmiş Sonlu Elemanlar Metodu

To my family who always supported me

ACKNOWLEDGMENTS

I would like to express my sincere gratitude and respects to my supervisor Prof. Dr. Haluk Darendeliler for his guidance, advice, criticism, encouragements and insight throughout the research.

I would also like to thank my beloved Huri Asena for his support, encouragement and help. I could not be able to cope this work in the absence of her.

I would like to express my happiness, chance, and confidence as I have such a family to inspire and motivate me in every stressful moments.

TABLE OF CONTENTS

LIST OF TABLES

TABLES

LIST OF FIGURES

FIGURES

LIST OF ABBREVIATIONS

ABBREVIATIONS

BCC	Body Centered Cubic
CPFEM	Crystal Plasticity Finite Element Model
FCC	Face Centered Cubic
HCP	Hexagonal-Closed Packed
MAXPS	Maximum Principal Stress
MAXPE	Maximum Principal Strain
MAXACSS	Maximum Accumulated Shear Strain
MAXRSS	Maximum Resolved Shear Stress
UDMGINI	User-defined Damage Initiation Criterion

LIST OF SYMBOLS

SYMBOLS

τ_{cr}	Critical Resolved Shear Stress
ϕ	Angle between the normal of the slip plane and stress direction
λ	Angle between the slip and stress direction
γ	Taylor Shear Strain
$\tau^{(\alpha)}$	Resolved Shear Stress of αth Slip System
f	Fracture Criterion
$\sigma_1, \sigma_2, \sigma_3$	Principal Stresses
$\varepsilon_1, \varepsilon_2, \varepsilon_3$	Principal Strains
$F_\alpha(x)$	Enrichment Function
$H(x)$	Heaviside Function
u	Finite Element Displacement Vector
$\bar{\varepsilon}_f^{pl}$	Equivalent Failure Plastic Strain
σ_{Y0}	Damage Onset Stress
$\bar{\varepsilon}_0^{pl}$	Damage Onset Equivalent Plastic Strain
G_f	Fracture Energy
L	Characteristic Length

CHAPTER 1

INTRODUCTION

1.1 Background and Motivation

Material failures are the major engineering design problems which may cause harmful effects to both economic and human life. As an striking example for the economical effect of the material failures, material failure related cost was estimated as 119 billion dollars per year [1]. Also, another work stated that 1885 aircraft accidents associated with metallic failure were recorded between 1927 and 1984 [2]. Thus, cracks which could have catastrophic results should be considered during the design phases of the structures as the one of the major design concerns.

Commonly used conventional analytical approaches for design of the structural components can be employed against the crack growth only if the presence of well-established stress and strain fields at the crack tip are formulated. Throughout researches arising the question of how to examine the crack problem, there are plenty of analytical methods are derived such as Airy stress functions, Griffith's energy release rate method [3], Westergaard's stress field solutions [4] and introduction of stress intensity factor by Irwin [5]. However, conventional analytical methods mainly work with the stress values calculated at the crack tip which theoretically approach to the infinity by making assumption of elastic material behavior, namely elasticity theory is taken into account at crack surrounding. While these robust analytical methods are making possible to get practical solutions in engineering, physical reality underlying the crack growth behavior is ignored.

Crystal plasticity finite element model (CPFEM) has been becoming a powerful finite element tool which is able to provide physics-based modelling of the crystalline structures over times. Further, physical parameters based on observations made during experiments can be conveyed to computer aided simulations. Modeling of the fracture problem in crystalline scale can be performed to investigate effects of the intrinsic material properties on the crack growth behavior of crystalline metals by adopting damage criteria based on crystalline parameters.

Crystal plasticity finite element method is able to model crystalline texture by considering anisotropic nature of the metals in the crystalline scale. The reason of the anisotropy of a crystalline material is coming from the differences of the grain orientation, size, shape and elastic resistance which is the function of the direction in the frame of crystalline. Therefore, crystalline anisotropy should be taken into account to obtain more realistic and physics-based simulations.

Microscale crack growth behavior can not be imagined without the crystalline anisotropy. In the presence of the crack located within crystalline, crack growth is a result of the irreversible crack tip dislocation events [6]. Dislocation motion takes place due to shear stress on grain slip planes exceeding critical stress value and varies among grains. Shear stress on slip planes alters depending on grain orientations, hence activated slip systems at the crack tip differ due to the different grain orientation.

As crack advances into the crystalline depth, it induces different type and number of slip systems at the crack tip. As a consequence of the crack growth into the crystalline depth, new crack tip encounters difficulty to propagate through crystalline due to the surrounding grain which is boundary condition for the newly introduced crack tip.

Grains located at the vicinity of the crack tip provide mechanical restraint to the crack to propagate, how degree of material resists to crack propagation depends on the material properties. As soon as dislocation activities occurring in the crack tip

achieves to the critical level, crack penetrates into the grains by overcoming mechanical constraints, i.e. surrounding grain resistance.

Damage criterion established by considering crystalline scale parameters provides more precise and accurate result than macro-scale assessment of the crack propagation problem.

1.2 Objective of the Thesis

The main objective of this thesis is to investigate the crack propagation at crystalline scale and the relationships between crack propagation of crystalline metal and its intrinsic material properties. Four different damage criteria have been introduced to examine crack propagation behavior of the single crystal and polycrystal materials by implementing them to crystal plasticity formulation and using the extended finite element method. First damage criterion is maximum resolved shear stress criterion. Maximum principal stress criterion has been utilized as an allegory of the resolved shear stress to compare results as second damage criterion. Maximum accumulated shear strain criterion has been introduced as an third damage criterion. Further, maximum principal strain criterion has been implemented into crack propagation model.

1.3 Scope of the Thesis

This thesis first covers the analysis results of V-notch introduced plates made of MD2 material and in plane stress condition to understand the effect of grain orientation on the crack propagation under four different criteria; maximum principal stress, maximum principal strain, maximum resolved shear stress and maximum accumulated shear strain. Then, the polycrystal plates which are in plane stress condition, are made of MD2, AA2024 aluminum alloy and 316L stainless steel and includes pre-crack are studied by the finite element method of to find impact of grain orientation and material selection on the crack growth behavior

under aforementioned four criteria. Finally, the finite element analyses of AA2025 aluminum alloy polycrystalline plates with pre-crack which are in plane stress condition are performed to evaluate the effect of grain size to the crack propagation behavior.

1.4 Outline of the Thesis

This thesis includes eight chapters devoted different topics and references as following:

- Chapter 1 presents the motivation lying on carrying out examination, brief background mainly devoted to physical mechanism behind the crack propagation and the scope of the thesis.
- Chapter 2 is separated only for literature survey regarding the researches dealing with crack growth investigation in crystalline scale.
- Chapter 3 gives overview of the theoretical explanation of the crystalline mechanics.
- Chapter 4 introduces constitutive relations to be used in numerical models.
- Chapter 5 offers the brief theory of the finite element and extended finite element method which has been employed to take care of discontinuity within material.
- Chapter 6 focuses on the damage criteria to be implemented into models and finite element models description.
- Chapter 7 is devoted to finite element models, their results and discussion.
- Chapter 8 gives the conclusion of this thesis and recommendations for the future works.

CHAPTER 2

LITERATURE REVIEW

Numerical modeling of the crack propagation in the frame of crystalline scale is an on-going research topic to obtain more in-depth knowledge regarding the microscale crack propagation behavior. The material model reflecting mechanical behavior of the crystalline materials is thrivingly studied throughout the years, and the crystal plasticity became a robust material model capturing mechanical behavior in the scale of crystalline as an accumulation of the results of these studies. Another challenge is to model material discontinuity, i.e. crack, in the crystalline scale by ceasing classical crack finite element modelling approach which causes burden of remeshing. The introduction of the extended finite element method (XFEM) overcomes the difficulty of the classical approach.

There are plenty of work combining both realistic material behavior and extended finite element method which provides crack propagation modeling without necessity of remeshing.

Irreversible deformation of a material was discovered as the slip motion of the dislocations throughout slip planes by Taylor [7] in 1934. Then, the crystal plasticity finite element method was very firstly utilized by subjecting tensile loading to the single crystal specimen by Peirce, Asaro and Needleman [8] in 1982. Hill [9] proposed constitutive relations for crystalline metals by establishing relation between slip and hardening and correlation between the stress rate and strain rate in 1965. Rice [10] extended the crystal plasticity constitutive relations by introducing new thermodynamical internal variable to obtain work conjugate of stress and strain to slip by maintaining normality principle of the small deformation in 1971. Rice and Hill [11] developed new constitutive relations to introduce lattice rotation due to elastic deformation and rotation caused by slip motion to the model

in 1972. Peirce et al. [12] investigated the rate dependency of the deformation behavior of the single crystal and concluded that deformation of crystals can be considered in the frame of viscoplasticity. Asaro [13] and Wu, Bassani and Laird [14] investigated the hardening behavior of the single crystals and proposed new definitions for hardening withing the frame of rate-dependent crystal plasticity constitutive model by representing three hardening stages of the single crystal.

Following part is solely devoted for research confined with research regarding crack propagation in crystalline scale combined with extended finite element.

Farukh et al. [15] mapped the experimental polycrystalline texture of the nickel-based superalloy material whose crystalline type is face centered cubic to the finite element medium as a representative volume element by means of image processing code. The accumulated plastic strain computing in according to crystal plasticity finite element model was introduced as a crack initiation criterion. As a result, the dependency of the crack growth rate to the grain orientation was quantified as a material intrinsic property. In the extended finite element method, the crack propagation direction was defined by considering principal strain direction. The shape of the crack path was obtained as a straight line.

Wilson and Dunne [16] investigated microscale crack growth behavior for face centered cubic nickel superalloy, body centered cubic ferritic steel and hexagonal-closed packed titanium and zircalloy examples to establish the relationship between the experimental results and numerical model by combining both crystal plasticity and extended finite element. The observed phenomena in the experiments for each crystalline structure have been quantified and tried to interpret by means of constructed numerical model. Wilson and Dunne concluded that the accumulated stored energy and slip activity at the crack tip are leading mechanical feature of the microstructural cracks depending on the crack length. Experimental results were correlated with crystal plasticity finite element models such as crack length and crack growth rate at the grain boundaries.

Zhao et al. [17] focused on Ni-based superalloy, MD2, single crystal material to study differentiation of the active slip system under different operational temperature conditions, 24°C and 625°C. Zig-zag type of crack propagation attribute monitored in the experiments has been acknowledged through finite element model by defining crack initiation and propagation criterion as the maximum accumulated shear strain of each individual slip system. In this work, crack path was manually altered for the sake of numerical convergence, since extended finite element model is not able to change crack direction in wide angle.

Abdolvand [18] compared the crystal plasticity finite element models constructed for notched hexagonal-close packed zirconium polycrystal specimen with the experimental data by assessing crack propagation with respect to several damage criteria: maximum principal stress, maximum principal strain, maximum slip and maximum energy stored among the slip systems. Author interpreted the appropriateness of the employed criteria conditions by comparing accuracy of the crack behavior modeled in finite element model and detected in zirconium polycrystal experiments.

Zhang and Dunne [19] focused on two nickel grains including grain boundary to study crack propagation behavior for variety of twist and tilt configurations of the grains. Crack propagation parameters used in paper for the crack propagation have been specified as the maximum shear strain and elastic stored energy density by using the combination of crystal plasticity finite element and XFEM tools. The criterion of elastic stored energy has been found more sensitive to both tilt and twist angles and their mixture configurations than the maximum shear strain criteria. As a result, strong dependency on grain twist angle rather than grain tilt angle was found on the crack propagation direction and rate by evaluating results of finite element models constructed for different tilt and twist angles.

Hu and Liu et al. [20] offered a model to investigate crack propagation behavior considering accumulated shear strain criterion for nickel-based supper alloy FGH96. Researchers investigated the performance of the accumulated shear strain

criterion utilized for different grain properties, e.g. grain size grain orientation and grain impediment and compared the accumulated shear strain criterion with other conventional criteria.

Wilson and Dunne [21] proposed a new criterion based on plastic strain energy stored at the crack tip for the small size crack propagation modeling of hexagonal-closed packed zirconium material for the first time. Physical motivation of the new criterion lies behind that incipient crack surfaces form due to the plastic strain energy causing dislocation in which occur at the crack tip. Constructed finite element model leading to crack according to newly proposed plastic strain energy criterion was compared with the principal stress criterion in terms of crack propagation direction and rate by varying grain orientation. Plastic strain energy criterion was found comprehensive criterion which able to simulate crack retardation and deflection observed in experiments.

Karamitros et al. [22] performed an investigation for the crack propagation direction and rate for nickel-based superalloy single crystal. The crack propagation behavior of the nickel-based superalloy single crystal was examined by introducing stored energy density criterion forming by stored plastic strain energy, statistically stored and geometrically necessary dislocation. Finite element results obtained by implementing stored energy density criterion was compared with experimental results. Finite element models varying with grain orientation showed the coherent results in terms of zig-zag type of crack propagation and alternating growth rates observed in experiments.

Zhang and Johnston et al. [23] examined crack propagation of AA2024 aluminum alloy in microscale by implementing plastic strain energy to the finite element model to justify fatigue life and crack propagation direction. In their experiments, crack initiation was observed at the intermetallic regions in which iron-rich particles were piled up in an abundant way. Authors presented the new model introduced to the finite element model which is statistical volume element approach

for AA2024 aluminum test specimen instead of representative volume element, which provide more cost-efficient analyses.

Efthymiadis et al. [24] conducted fatigue test for the AA2024 aluminum with the hole located at the middle of the specimen to acquire stress and strain fields at the stress singularity region. Efthymiadis offered new damage initiation criterion by combining maximum accumulated slip and dissipated energy for AA2024 aluminum polycrystalline, which provide reliable results according to experiments.

CHAPTER 3

PHYSICS OF CRYSTALLINE STRUCTURE

In macroscale, metals are modeled as if continuum medium in which solid occupies the space in a continuous way without considering its physical nature, i.e. atomic structure. Unlike macroscale modeling, in physical reality, the repetitive arrangement of the metal atoms forms crystalline nature of the metals which is not in the case of continuum approach. Further, whilst physical properties of the metals are considered to have isotropic attribute in the macroscopic scale; mechanical behaviors of the metals in crystalline scale abundantly rely on crystalline direction as opposed to macroscopic scale assumption. In this section, basics of the physical behavior of the crystalline are discussed.

3.1 Crystalline Structures

Crystalline materials are formed by settling material atoms in regular order which induces periodic pattern in the space during solidification. The smallest group of the periodic arrangement of atoms is called as the unit cell, and unit cells are categorized according the way of aggregation of atoms, such as face centered cubic (FCC), body centered cubic (BCC), and hexagonal-closed packed (HCP). The representation of the unit cells commonly encountered in metals is given in Figure 3.1.1. As a result of identical unit cell cluster, the lattice term is used to define aggregated unit cells as illustrated in Figure 3.1.2.

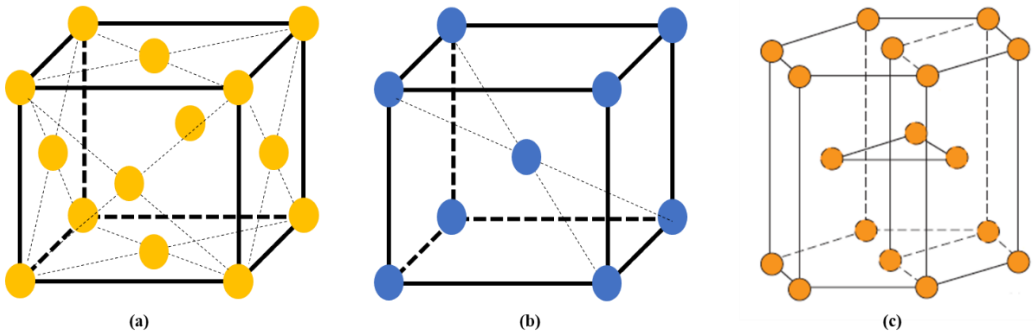

Figure 3.1.1 Unit cell types (a) face centered cubic (FCC), (b) body centered cubic (BCC), (c) hexagonal-closed packed (HCP) (Figure (c) [27])

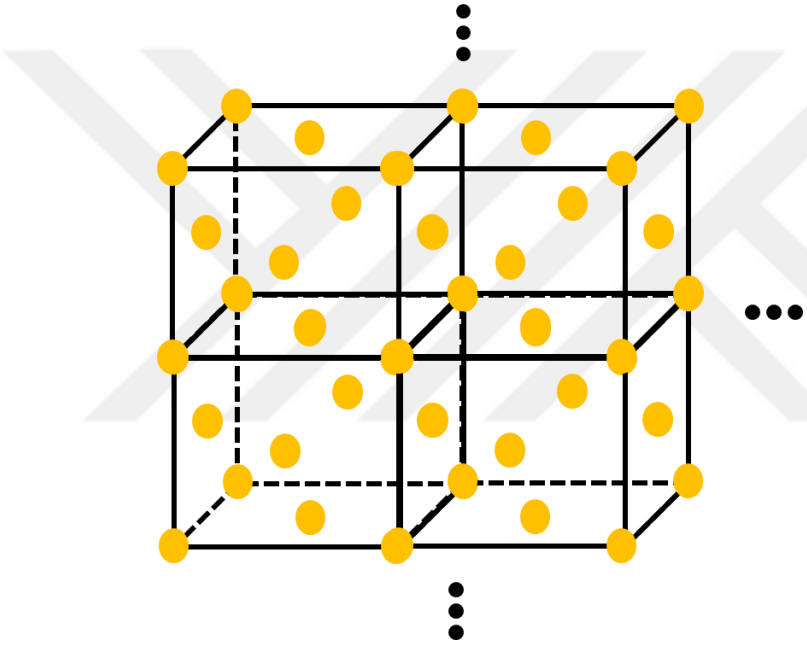

Figure 3.1.2 Representation of the lattice as an aggregation of the unit cells

If the unit cells whose orientations are identical with other unit cells come together, single crystal structure is formed. Therefore, single crystal solid has only one orientiation with no grain boundaries. On the other hand, the most commonly crystalline structure in reality is the polycrystalline structures. During solidification or crystallization of solid, crystal nuclei start to grow in different directions; and grains which have different orientations intersect each other by creating grain boundary. Representative schematic of the solidification process of a polycrystalline can be seen in Figure 3.1.3.

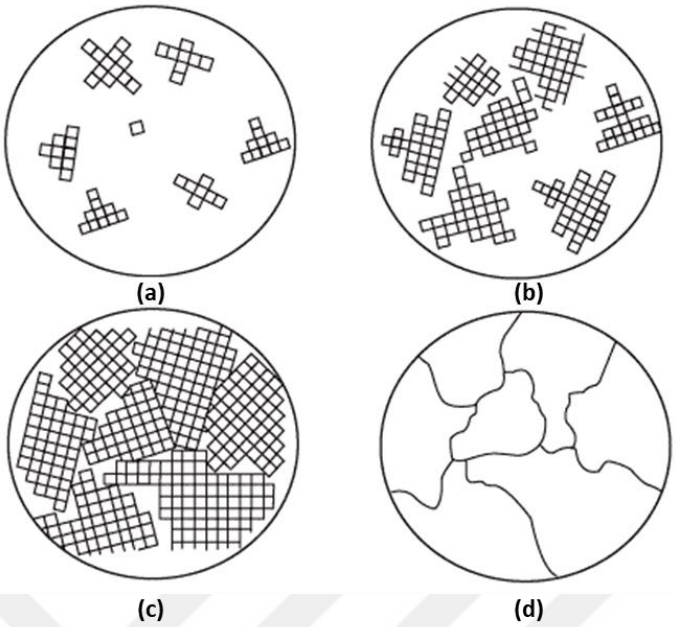

Figure 3.1.3 Solidification of a polycrystalline solid (a) crystal nuclei, (b) grain growth (c) intersect of crystals with mismatch (d) microscopic view of grain boundaries [28]

In crystalline scale, definition of the crystallographic direction and plane of atoms is required, therefore a labeling convention is used by enclosing three numbers with square brackets, e.g. [xyz], for crystallographic direction and with parantheses, e.g (hkl), for crystallographic plane. Especially, usage of labeling convention is needed to specify slip phenomena in crystalline in terms of direction and plane.

It is difficult to establish ideal crystalline structure, the fact that crystalline structures consists of edge and screw dislocations or both. Edge and screw dislocations are the member of line defects which occur due to the sudden change in the repetitive atomic pattern; edge dislocation occurs in the case of extra half atomic plane or absence of the half atomic plane within the lattice and dislocation movement is parallel to the loading direction, whereas screw dislocation takes place under shear loading and dislocation motion is perpendicular to the loading direction. In reality, combined dislocations which are the combination of edge and screw dislocations are observed in the crystalline solids. The schematic of the edge and screw dislocations is depicted in Figure 3.1.4.

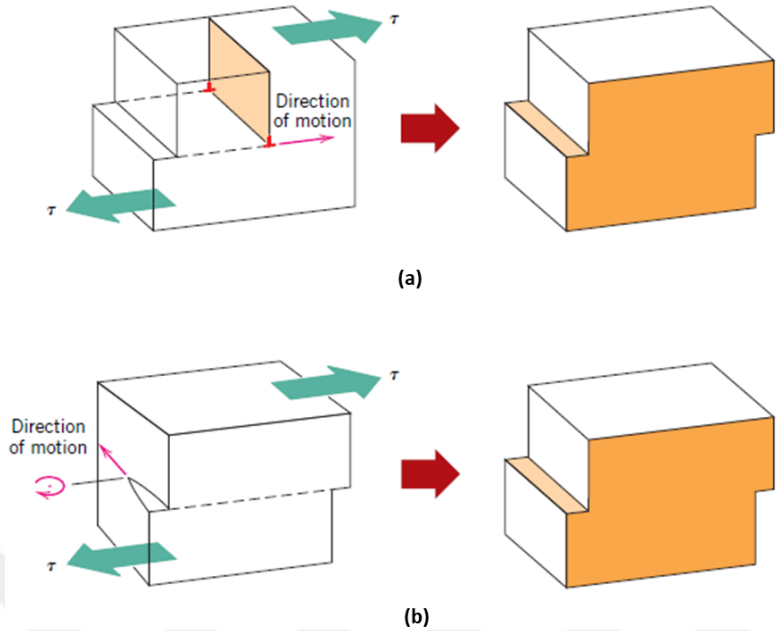

Figure 3.1.4 Edge and screw dislocation representation (a) edge dislocation (b) screw dislocation [29]

These defects have a share in the irreversible deformation of the crystalline solid, since, for example, extra atom plane breaks atomic bound which is in the steady state condition and moves into the parallel direction of the shear load and re-establish new atomic bounds with atoms located at the neighbour atoms in edge dislocation. Irreversible deformation observed in macroscale stems form dislocation of the atoms which is called as slip. Representative dislocation motion of the atomic array can be seen in Figure 3.1.5.

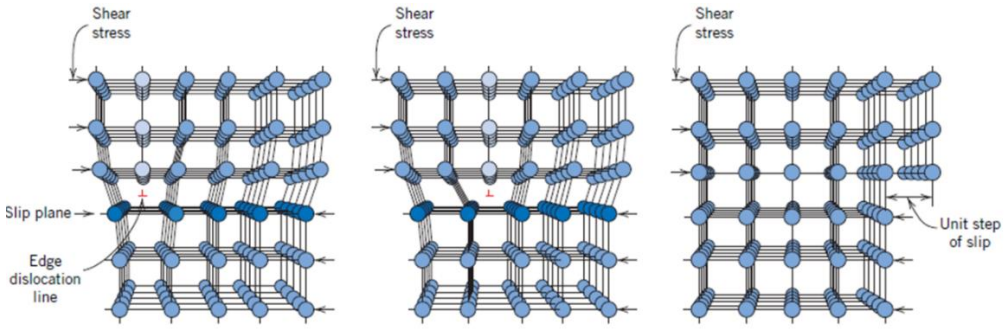

Figure 3.1.5 Dislocation motion in the lattice [30]

Dislocation occurs in the specific direction and plane which correspond to the densest atomic packing and cause minimum energy to slip depending on the metal crystalline type. This direction and plane are named as slip direction and plane, respectively. Also, the term of slip system is used to define combination of the slip direction and plane. Number of slip systems in which slip motion is able to occur for metal crystalline is 12 in {111} plane set for FCC; 12 in {110} plane set, 12 in {211} plane set and 24 {321} plane set for BCC; 3 in {0001} plane set, 3 in $\{10\bar{1}0\}$ plane set and 6 in $\{10\bar{1}1\}$ plane set for HCP crystallines. As an example, illustration for the slip systems of FCC crystalline is provided in Figure 3.1.6.

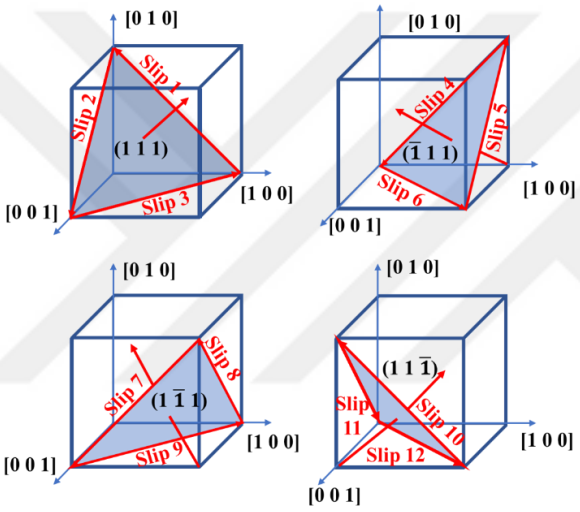

Slip System	Slip Plane Normal	Slip Direction
1	(1 1 1)	[1 1̄ 0]
2	(1 1 1)	[0 1 1̄]
3	(1 1 1)	[1 0 1̄]
4	(1̄ 1 1)	[1 1 0]
5	(1̄ 1 1)	[0 1 1̄]
6	(1̄ 1 1)	[1 0 1]
7	(1 1̄ 1)	[1 1 0]
8	(1 1̄ 1)	[0 1 1]
9	(1 1̄ 1)	[1 0 1̄]
10	(1 1 1̄)	[1 1̄ 0]
11	(1 1 1̄)	[0 1 1]
12	(1 1 1̄)	[1 0 1]

Figure 3.1.6 Slip systems of face centered cubic crystalline [31]

As described in preceding paragraphs, dislocation due to the defects within the lattice is activated by the presence of shear stress along with dislocation line, even a tensile macroscopic load is applied in macroscopic scale, a stress component arises in the direction lying on slip system which might be perpendicular to the applied load direction depending on grain orientation. This stress component is called resolved shear stress and depends on both applied load and angles between slip plane-load application direction and slip direction-load application direction. The resolved shear stress, τ_r, is formulated as

$$\tau_r = \sigma \cos\phi \cos\lambda \tag{1}$$

where σ is the stress due to applied load in macroscopic scale, ϕ and λ are the angle between the normal of the slip plane and the axial normal stress direction, and the angle between the slip and axial normal stress direction, respectively. Also, $cos\,\phi\,cos\,\lambda$ is called as Schmid's factor. The geometric definition of the resolved shear stress can be seen in Figure 3.1.7.

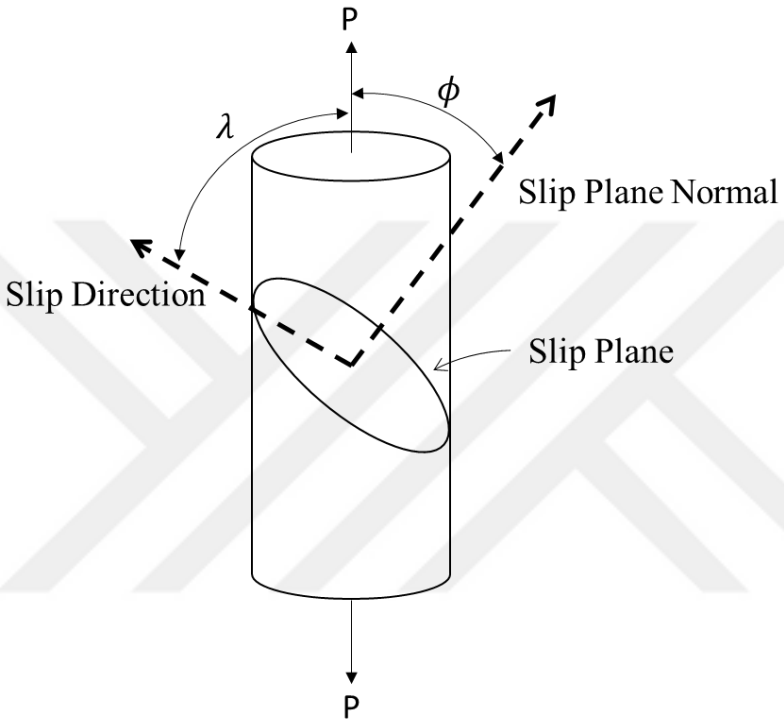

Figure 3.1.7 Geometrical representation of the resolved shear stress [43]

Further, there is a threshold stress value to evoke dislocation to move, it is called as critical resolved shear stress. When the resolved shear stress reaches to the critical resolved shear stress value, dislocation motion takes place in specified direction over the specified plane depending on crystal structure and orientation. The critical resolved shear stress is a intirinsic material property.

CHAPTER 4

CONSTITUTIVE RELATIONS

4.1 Crystal Plasticity Constitutive Relations

Crystal plasticity is a material model that is employed to simulate mechanical behavior of a crystal in the microscale medium. Crystal plasticity material model can be reviewed in three subgroups; kinematics, constitutive laws and kinetics. In this work, Huang [25] crystal plasticity finite element ABAQUS UMAT subroutine is employed.

4.1.1 Kinematics

Kinematic formulations of the crystal plasticity are dependent on experimental observation which indicates that any irreversible deformation takes place solely by dislocation movements occuring within grain. Thus, deformation of a material arises from elastic deformation, rotation and plastic deformation due to crystalline slip. Hence, deformation gradient can be defined in terms of its plastic and elastic parts by multiplicative decomposition as in below

$$\boldsymbol{F} = \boldsymbol{F}^{e} \cdot \boldsymbol{F}^{p} \tag{2}$$

where $\boldsymbol{F}^{e}$ is the elastic deformation gradient including elastic stretching and rotation and $\boldsymbol{F}^{p}$ is the plastic deformation gradient which represents plastic flow. In this sense, deformation of a crystalline takes place due to undergoing plastic deformation by translating crystalline structure from the reference configuration to the intermediate configuration leading by $\boldsymbol{F}^{p}$ and then elastic deformation governing by $\boldsymbol{F}^{e}$, which is illustrated in Figure 4.1.1. Slip direction of the α^{th} slip system, $\boldsymbol{s}_0^{(\alpha)}$, and unit normal to the slip plane of the α^{th} slip system, $\boldsymbol{m}_0^{(\alpha)}$, are

shown for both reference and intermediate configurations as can be seen in Figure 4.1.1; as slip direction and unit normal to the slip plane of the α^{th} slip system of the current configuration have been represented as $\boldsymbol{s}^{(\alpha)}$ and $\boldsymbol{m}^{(\alpha)}$.

Slip direction of the α^{th} slip system, $\boldsymbol{s}_0^{(\alpha)}$, and unit normal to the slip plane of the α^{th} slip system, $\boldsymbol{m}_0^{(\alpha)}$, are conserving their orientation during lattice plastic deformation and are transfered to intermediate configuration from reference configuration by plastic deformation gradient $\boldsymbol{F}^p$; whereas, stretching and rotation of the lattice ending up transformation of intermediate configuration to current configuration are led by elastic deformation gradient, $\boldsymbol{F}^e$ with slip direction $\boldsymbol{s}^{(\alpha)}$ and surface normal $\boldsymbol{m}^{(\alpha)}$.

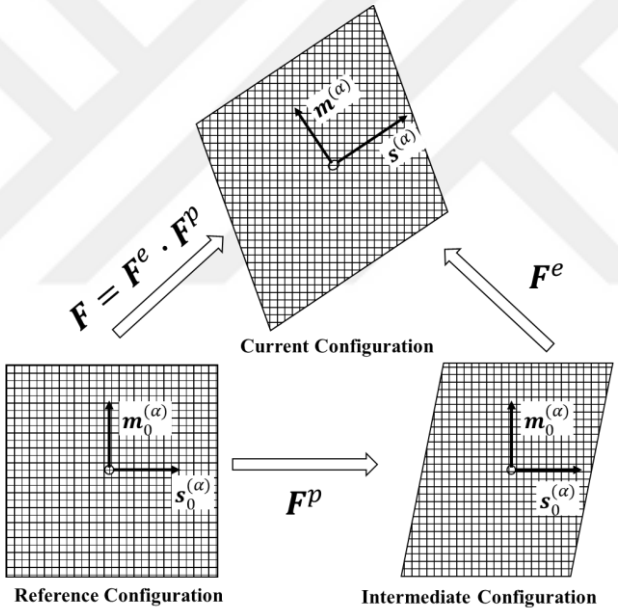

Figure 4.1.1 Kinematic decomposition of the deformation gradient

Velocity gradient can be defined as

$$\boldsymbol{L} = \dot{\boldsymbol{F}} \cdot \boldsymbol{F}^{-1} \tag{3}$$

Taking time derivative of the deformation gradient following equation can be written

$$\dot{\boldsymbol{F}} = \dot{\boldsymbol{F}}^e \cdot \boldsymbol{F}^p + \boldsymbol{F}^e \cdot \dot{\boldsymbol{F}}^p \tag{4}$$

By substituting Equations (2) and (4) into Equation (3), velocity gradient can be rewritten

$$\boldsymbol{L} = \left(\dot{\boldsymbol{F}}^{e} \cdot \boldsymbol{F}^{p} + \boldsymbol{F}^{e} \cdot \dot{\boldsymbol{F}}^{p}\right) \cdot \boldsymbol{F}^{p-1} \cdot \boldsymbol{F}^{e-1} = \dot{\boldsymbol{F}}^{e} \cdot \boldsymbol{F}^{e-1} + \boldsymbol{F}^{e} \cdot \dot{\boldsymbol{F}}^{p} \cdot \boldsymbol{F}^{p-1} \cdot \boldsymbol{F}^{e-1} \quad (5)$$

Equation (5) can be defined as follow

$$\boldsymbol{L} = \boldsymbol{L}^{e} + \boldsymbol{F}^{e} \cdot \boldsymbol{L}^{p} \cdot \boldsymbol{F}^{e-1} \quad (6)$$

where $\boldsymbol{L}^{e} = \dot{\boldsymbol{F}}^{e}.\boldsymbol{F}^{e-1}$ is the definition of the elastic velocity gradient, and $\boldsymbol{L}^{p} = \dot{\boldsymbol{F}}^{p} \cdot \boldsymbol{F}^{p-1}$ is the plastic velocity gradient. $\boldsymbol{L}^{p}$ can be defined overall of the slip rate on the each individual slip system as

$$\boldsymbol{L}^{p} = \sum_{\alpha=1}^{n} \dot{\gamma}^{(\alpha)} \boldsymbol{s}^{(\alpha)} \otimes \boldsymbol{m}^{(\alpha)} \quad (7)$$

where $\dot{\gamma}^{(\alpha)}$ is slipping rate of the α^{th} slip system, $\boldsymbol{s}^{(\alpha)}$ and $\boldsymbol{m}^{(\alpha)}$ are slip direction and unit normal to slip plane vectors in the current configuration, respectively.

Slip direction and unit normal to slip plane vectors for α^{th} slip system in the current configuration given in Equation (7) can be determined as follows

$$\boldsymbol{s}_{0}^{(\alpha)} = \boldsymbol{F}^{e} \cdot \boldsymbol{s}^{(\alpha)} \quad (8)$$

$$\boldsymbol{m}_{0}^{(\alpha)} = \boldsymbol{m}^{(\alpha)} \cdot \boldsymbol{F}^{e-1} \quad (9)$$

Also, the velocity gradient can be written in terms of its symmetric stretching rate and asymmetric spin tensor as

$$\boldsymbol{L} = \boldsymbol{D} + \boldsymbol{W} \quad (10)$$

Further, stretching rate and spin tensors can be decomposed into its elastic and plastic parts

$$\boldsymbol{D} = \boldsymbol{D}^{e} \cdot \boldsymbol{D}^{p} \quad (11)$$

$$\boldsymbol{W} = \boldsymbol{W}^{e} \cdot \boldsymbol{W}^{p} \quad (12)$$

which satisfies

$$\boldsymbol{D}^{e} + \boldsymbol{W}^{e} = \dot{\boldsymbol{F}}^{e} \cdot \boldsymbol{F}^{e-1} \quad (13)$$

$$\boldsymbol{D}^p + \boldsymbol{W}^p = \sum_{\alpha=1}^{n} \dot{\gamma}^{(\alpha)} \boldsymbol{s}^{(\alpha)} \otimes \boldsymbol{m}^{(\alpha)} \tag{14}$$

4.1.2 Constitutive Law

In preceding section, the equation for the motion of a crystal structure is provided without relating deformations and stresses. In this section, constitutive laws that provide the equation sets which relate the deformations and stresses are presented.

The elastic law of crystals under large deformation proposed by Hill and Rice [11] can be written by using an objective stress rate and elastic rate of deformation as

$$\boldsymbol{\sigma}^{\Delta e} + \boldsymbol{\sigma}(\boldsymbol{I} : \boldsymbol{D}^e) = \mathbb{C} : \boldsymbol{D}^e \tag{15}$$

where $\boldsymbol{I}$ is the second order identity tensor, $\mathbb{C}$ is the fourth order elastic tensor moduli in which property of tensor symmetry is valid $\mathbb{C}_{ijkl} = \mathbb{C}_{jikl} = \mathbb{C}_{ijlk} = \mathbb{C}_{klij}$. In the above equation $\boldsymbol{\sigma}^{\Delta e}$ is the Jaumann rate of Cauchy stress $\boldsymbol{\sigma}$, defined as

$$\boldsymbol{\sigma}^{\Delta e} = \dot{\boldsymbol{\sigma}} - \boldsymbol{W}^e \cdot \boldsymbol{\sigma} - \boldsymbol{\sigma} \cdot \boldsymbol{W}^e \tag{16}$$

The Jaumann stress rate, $\boldsymbol{\sigma}^{\Delta e}$, that is the corotational stress rate on the axes following rotation of the crystal lattice can be linked with the corotational stress rate on the axes following rotation of the material, $\boldsymbol{\sigma}^{\Delta}$ as follows

$$\boldsymbol{\sigma}^{\Delta e} = \boldsymbol{\sigma}^{\Delta} + (\boldsymbol{W} - \boldsymbol{W}^e) \cdot \boldsymbol{\sigma} - \boldsymbol{\sigma} \cdot (\boldsymbol{W} - \boldsymbol{W}^e) \tag{17}$$

where the corotational stress rate on the axes following rotation of the material can be defined as follows

$$\boldsymbol{\sigma}^{\Delta} = \dot{\boldsymbol{\sigma}} - \boldsymbol{W} \cdot \boldsymbol{\sigma} + \boldsymbol{\sigma} \cdot \boldsymbol{W} \tag{18}$$

The slipping rate occuring in th α^{th} slip system, $\dot{\gamma}^{(\alpha)}$, is stemmed from Schmid stress, $\tau^{(\alpha)}$, which is the resolved stress of the stress state throughout slip direction. Rice [26] proposed a resolved shear stress definition including elastic deformation

by considering work conjugate stress and strain measures in the finite deformation case by

$$\tau^{(\alpha)} = \boldsymbol{m}_0^{(\alpha)} \cdot \frac{\rho_0}{\rho}\, \boldsymbol{\sigma} \cdot \boldsymbol{s}_0^{(\alpha)} \tag{19}$$

where ρ_0 and ρ are the mass densities in the reference and current states. The Schmid stress rate is given by

$$\dot{\tau}^{(\alpha)} = \boldsymbol{m}_0^{(\alpha)} \cdot [\boldsymbol{\sigma}^{\Delta e} + \boldsymbol{\sigma}(\boldsymbol{I} : \boldsymbol{D}^e) - \boldsymbol{D}^e \cdot \boldsymbol{\sigma} + \boldsymbol{\sigma} \cdot \boldsymbol{D}^e] \cdot \boldsymbol{s}_0^{(\alpha)} \tag{20}$$

4.1.3 Hardening Law

Hardening laws are given in the framework of viscoplasticity. The slipping rate, $\dot{\gamma}^{(\alpha)}$, corresponding to the α^{th} slip system is computed by considering resolved shear stress, $\tau^{(\alpha)}$, occuring in the α^{th} slip system in the rate-dependent crystalline framework as

$$\dot{\gamma}^{(\alpha)} = \dot{a}^{(\alpha)} f^{(\alpha)} \frac{\tau^{(\alpha)}}{g^{(\alpha)}} \tag{21}$$

where $\dot{a}^{(\alpha)}$ is the reference strain rate on the α^{th} slip system, $g^{(\alpha)}$ is the current strength of the α^{th} slip system, and $f^{(\alpha)}$ is the function which is nondimensional for defining the dependency of the strain rate to the stress state. Power law for polycrystalline creep proposed by Hutchinson [44] is given as

$$f^{(\alpha)}(x) = x|x|^{n-1} \tag{22}$$

where n is the rate sensitivity exponent.

The evolution of the strength, $g^{(\alpha)}$, comes from the strain hardening as given in below

$$\dot{g}^{(\alpha)} = \sum_{(\beta)} h_{(\alpha\beta)} \dot{\gamma}^{(\beta)} \tag{23}$$

where $h_{(\alpha\beta)}$ is the slip hardening tensor. Whilst subscripts equal to each other $(\alpha=\beta)$ is called as self hardening modulus, otherwise it is called as latent hardening modulus. Self hardening modulus can be written as

$$h_{\alpha\alpha} = h(\gamma) = h_0 sech^2 \left| \frac{h_0 \gamma}{\tau_s - \tau_0} \right| \tag{24}$$

where h_0 is the initial hardening modulus, τ_0 is the critical resolved shear stress, τ_s is the saturated resolved shear stress corresponding to stage I stress, and γ is the Taylor cumulative shear strain which is given in below

$$\gamma = \sum_{\alpha} \int_0^t \left| \dot{\gamma}^{(\alpha)} \right| dt \tag{25}$$

The latent hardening modulus is given by

$$h_{(\alpha\beta)} = q h(\gamma) \tag{26}$$

where q is a constant. Note that, definitions of the hardening moduli do not consider Bauschinger effect on the crystalline solids.

CHAPTER 5

EXTENDED FINITE ELEMENT METHOD

5.1 Finite Element Method

In sophisticated engineering applications, there is a difficulty to predict behavior of the structure in an exactly way. Hence, discretization of the whole into the subdomains, i.e. finite elements, provides ability to examine the behavior of the whole structure by analyzing the subdomains whose behavior can be easily determined. Finite element numerical method can be roughly generalized in four steps as follow [37]

- First step, stiffness and force are introduced to the finite elements according to defined material and loading information.
- Second step, equilibrium condition is checked by considering global stiffness matrix constructed by summation of the local stiffness matrices.
- Third step, boundary condition is defined to the global matrix established in preceding step.
- Fourth step, different equation solving methods are employed to obtain desired results.

In this thesis, finite element program is selected as ABAQUS software, since ABAQUS offers the ability of user defined subroutine which enables advanced material models not included in finite element softwares.

5.2 Extended Finite Element Method

Cracks are the structural discontinuities and require the special treatment to correctly model in the finite element approach. Appropriate discretization

surrounding the discontinuity is needed to obtain desired output at the crack tip, and mesh refinement is necessity to rearrange appropriate discretization at the crack tip as crack grows in the traditional finite element approach. This numerical burden have been overcome with the introduction of the extended finite element method by Belytschko and Black [32].

Extended finite element method has been constructed by implementing additional enrichment term which contains functions defining for near tip asymptotic and discontinuous representing jump in displacement to the displacement vector [33].

A function can be divided into sub-functions whose summation equal to main function in according to partition of unity principle as given in below

$$\sum_{I=1}^{N} N_I(x) = 1 \tag{27}$$

$$\sum_{I=1}^{N} N_I(x) f(x) = f(x) \tag{28}$$

Displacement vector defined in classical finite element method can be written as

$$\boldsymbol{u} = \sum_{I=1}^{N} N_I(x) \boldsymbol{u}_I \tag{29}$$

where $N_I(x)$ is nodal shape function and $\boldsymbol{u}_I$ finite element degrees of freedom of the region without discontinuity.

Enriched displacement vector is defined by introducing enrichment terms into the Equation (28) as in below

$$\boldsymbol{u} = \sum_{I=1}^{N} N_I(x)[\boldsymbol{u}_I + H(x)\boldsymbol{a}_I + \sum_{\alpha=1}^{4} F_\alpha(x)\boldsymbol{b}_I^\alpha] \tag{30}$$

where *H(x)* is the heaviside function for the crack surfaces, $\boldsymbol{b}_I^\alpha$ is the crack tip extra degree of freedom defined and $F_\alpha(x)$ is the set of enrichment functions defined for crack tip.

The heaviside function, *H(x)*, is defined as follow [33]

$$H(x) = \begin{cases} 1 & y \geq 0 \\ -1 & y < 0 \end{cases} \tag{31}$$

y is the numeric indicator that defines two side of the crack surface.

Enrichment function to be used at the crack tip, $F_\alpha(x)$, is coming from Westergaard displacement solution [34] by reducing following basis

$$F_\alpha(x) = \left[\sqrt{r}\, sin\frac{\theta}{2}, \sqrt{r}\, cos\frac{\theta}{2}, \sqrt{r}\, sin\,\theta\, sin\frac{\theta}{2}, \sqrt{r}\, sin\,\theta\, cos\frac{\theta}{2}\right] \tag{32}$$

where (r, θ) is a polar coordinates components defined at the crack tip.

Enrichment function given in Equation (30) is employed only for immobile crack definitions in ABAQUS, since accuracy of the crack model depends on the tracking crack tip location. On the other hand, ABAQUS offers the method of XFEM based on linear elastic fracture mechanics (LEFM) to model crack initiation and evolution just by considering heaviside function. Thus, nonstationary cracks are modeled without considering enrichment function by propagating crack throughout an element to prevent the presence of stress singularity in the element. This method extinguish the necessity of crack path definition at the beginning of the model [33].

In XFEM based on LEFM method, the presence of the crack within an element is modeled by implementing phantom nodes coincident to the corresponding original element nodes and is established when the damage criterion is equal to the threshold value. Hereupon, the element reached to damage threshold starts to cleave into two parts, phantom nodes and corresponding original nodes are not tied any more as indicated in Figure 5.2.1.

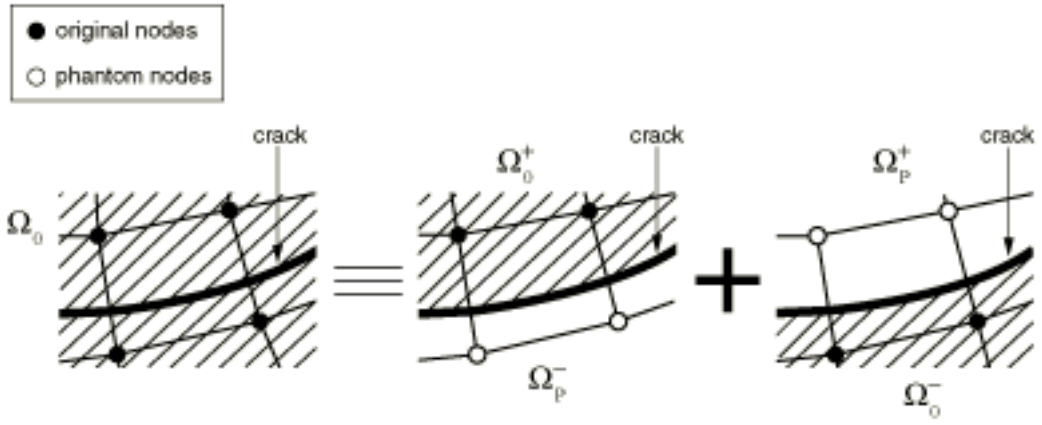

Figure 5.2.1 XFEM - Phantom Node Method

The degradation of an enriched element undertakes, when the stress or strain resulting in element reach to the specified threshold value. Namely, fracture criterion which is ratio of the stress/strain value to the threshold value is equal to 1, crack initiation takes place. After that, the separation of the phantom nodes from original nodes takes place, at the time of the strain energy release rate at the crack tip equal to critical strain energy release rate. Eventually, fully separation of the phantom and original nodes occurs and separated element can move apart from each other.

Crack initiation criteria can be utilized as the criteria embedded into ABAQUS such as the maximum principal stress and the maximum principal strain or user-defined damage initiation criteria which can be constructed by user subroutine of UDMGINI in the finite element model.

CHAPTER 6

DAMAGE INITIATION AND EVOLUTION

Damage initiation and evolution laws used throughout finite element models are given in this section.

6.1 Damage Initiation

6.1.1 Maximum Principal Stress (MAXPS) Criterion

The maximum principal stress criterion checks whether the magnitude of the maximum principal stress at the element centroid reached to the permissible stress magnitude. Crack direction is defined as the unit normal to the maximum principal stress plane, when the maximum principal stress criterion met.

$$f = \frac{< max(\sigma_1, \sigma_2, \sigma_3) >}{\sigma_{allowable}} \tag{33}$$

where σ_1, σ_2 and σ_3 are the principal stresses and $\sigma_{allowable}$ is the threshold stress to define damage initiation stress value. The Macaulay brackets are implemented to neglect that the compressive stress does not contribute crack initiation, since

$$< x > = \begin{cases} 0 \; if \; x < 0 \\ x \; if \; x > 0 \end{cases} \tag{34}$$

Damage is automatically introduced to the element, as soon as fracture criterion, *f*, is equal to one.

6.1.2 Maximum Principal Strain (MAXPE) Criterion

The maximum principal strain criterion checks whether the magnitude of the maximum principal strain at the element centroid reached to permissible strain magnitude. Crack direction is defined as the unit normal of the maximum principal strain plane, when the maximum principal strain criterion met.

$$f = \frac{< max(\varepsilon_1, \varepsilon_2, \varepsilon_3) >}{\varepsilon_{allowable}} \tag{35}$$

where ε_1, ε_2 and ε_3 are the principal strains and $\varepsilon_{allowable}$ is the threshold strain to define damage initiation strain value.

6.1.3 Maximum Resolved Shear Stress (MAXRSS) Criterion

Resolved shear stresses are calculated separately for all the slip systems according to Equation (1) given in Section 3. The maximum resolved shear stress criterion checks whether the resolved shear stress values calculated for each individual slip systems reached to critical resolved shear stress. Crack direction is defined as the unit normal to the slip plane in which maximum resolved shear stress occurs.

$$f = \frac{max\left(\left|\tau_r^{(\alpha)}\right|\right)}{\tau_{cr}} \tag{36}$$

where $\tau_r^{(\alpha)}$ is the resolved shear stress of the α^{th} slip system and τ_{cr} is the critical resolved shear stress.

6.1.4 Maximum Accumulated Shear Strain (MAXACSS) Criterion

Maximum accumulated shear strain are calculated for all the slip systems in according to Equation (25) given in Section 4.1.3. The maximum accumulated shear strain criterion checks whether the shear strain for each individual slip systems accumulated along with loading reached to allowable strain value. Crack

direction is defined as the unit normal to the slip plane in which maximum accumulated shear strain occurs.

$$f = \frac{max\left(\left|\sum_{\alpha} \gamma^{(\alpha)}\right|\right)}{\gamma_{cr}} \tag{37}$$

where $\gamma^{(\alpha)}$ is the accumulated shear strain of the αth slip system and γ_{cr} is the critical accumulated shear strain.

6.2 Damage Evolution

In ABAQUS, damage evolution takes place in according to Figure 6.2.1.

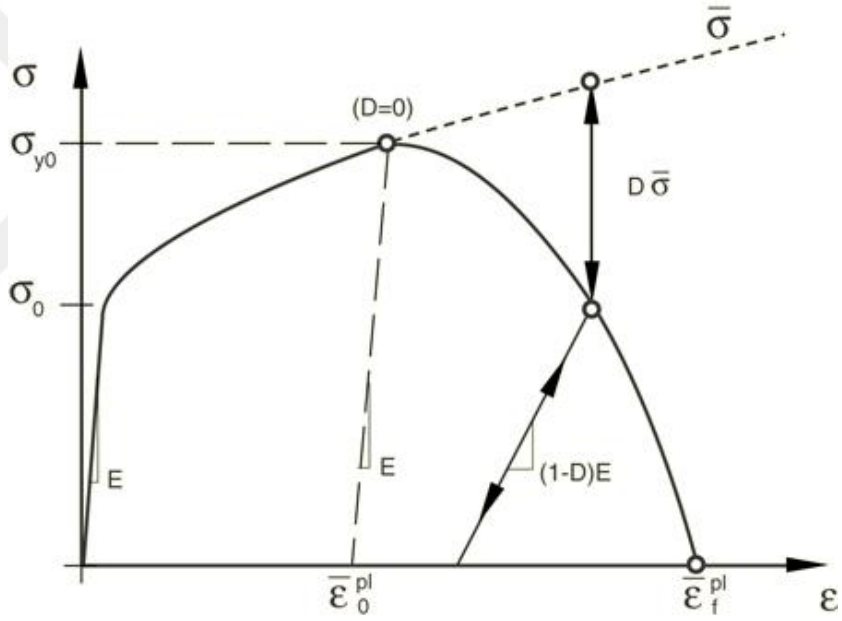

Figure 6.2.1 Representation of the stress-strain curve of a damaged material [33]

After having exceeded onset of the damage which is quantified in terms of σ_{Y0} or $\bar{\varepsilon}_0^{pl}$, softening of the yield stress and stiffness degradation take place.

ABAQUS offers two options to model damage evolution: defining by equivalent plastic strain at the failure, $\bar{\varepsilon}_f^{pl}$, or fracture energy, G_f. For example, when strain

energy release rate reached to the defined fracture energy, the finite element located at the crack tip is going to be fully damaged. In this thesis, damage evolution is carried out by defining fracture energy. Fracture energy is calculated as

$$G_f = \int_{\bar{\varepsilon}_0^{pl}}^{\bar{\varepsilon}_f^{pl}} L\sigma_Y d\bar{\varepsilon}^{pl} \tag{38}$$

where L is the characteristic length which depends on the element geometry and formulation [33].

CHAPTER 7

RESULTS AND DISCUSSION

7.1 Introduction

In this section, finite element models are created to investigate crack initiation and propagation through the use of Huang's UMAT subroutine [25] within ABAQUS XFEM. In addition to the Maximum Principal Stress (MAXPS) and Maximum Principal Strain (MAXPE) criteria which exist in the ABAQUS software, two more damage initiation criteria; the Maximum Resolved Shear Stress (MAXRSS) and Maximum Accumulated Shear Strain (MAXACSS) are defined by modifying Huang's code and employed. Finite element models are constructed by meshing square plates under the consideration of the plane stress condition to overcome excessive computational cost and time.

Firstly, single crystal square plates with V-notch is analyzed to investigate crack initiation behavior as a function of grain orientation according to mentioned damage criteria for nickel-based superalloy (MD2) material. Then, nickel-based superalloy (MD2), AA2024 aluminum alloy and 316L stainless steel polycrystal plates are modeled to examine crack propagation behavior by changing intrinsic material parameters, i.e. grain orientation and grain size. Additionally, finite element analyses of AA2024 aluminum polycrystal plates having different grain sizes are performed to capture the effect of grain size.

7.2 Crack Initiation and Propagation for MD2 Single Crystal

The geometry of the plate which is used in the analyses is shown in Figure 7.2.1. It is taken in plane stress condition with an edge length is 600 micrometers. Dimensions of the width and depth of the notch created in the middle of the upper

edge are 64 micrometers and 54 micrometers, respectively as illustrated in Figure 7.2.1. The plate has been discretized by the element type of CPS4, 4-node bilinear plane stress quadrilateral, with an average size of 3 micrometers. The total number of the elements in the mesh is forming 40477 as can be seen in Figure 7.2.2.

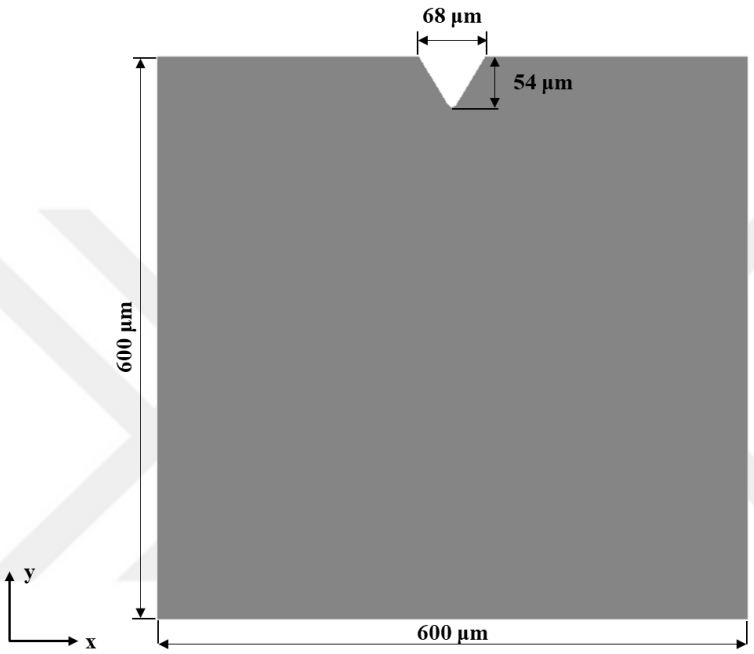

Figure 7.2.1 Two-dimensional V-Notched plate geometry

Boundary conditions of the plate are defined by assigning $u = 0$ for all the nodes at the left side edge of the plate along y-axis except the node at the upper left corner for which $u = v = 0$. A prescribed incremental displacement up to 15 micrometers is defined for the nodes at the right side of the plate in x-direction only. Boundary condition and load definition of the model is given in Figure 7.2.3.

Cubic elastic and viscoplastic material parameters of the nickel-based supper alloy (MD2) to be introduced in the crystal plasticity constitutive model are tabulated in Table 7.2.1.

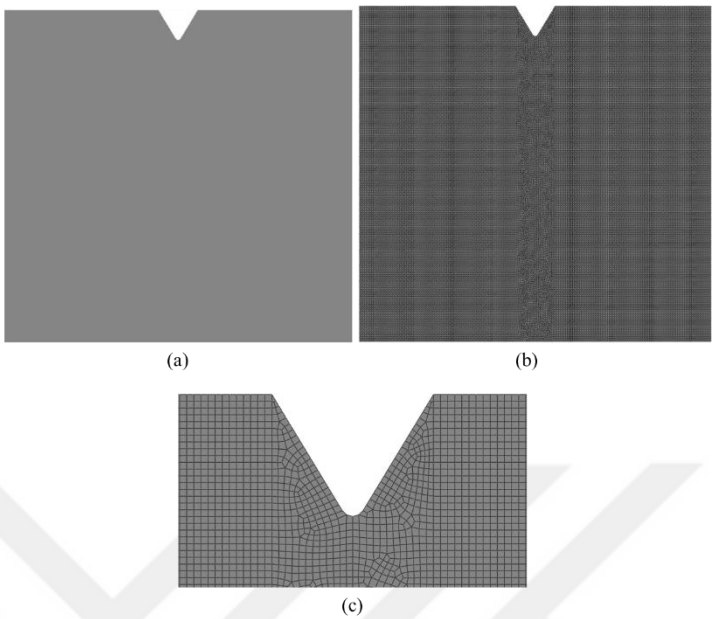

Figure 7.2.2 Mesh view of two-dimensional plate (a) unmeshed plate (b) general mesh view (c) mesh view at the notch vicinity

Figure 7.2.3 Boundary conditions and load definition of the plate

Table 7.2.1 MD2 material constants [17]

Parameters	Units	Description	Value
C11	MPa	Elastic Constant	174030
C12	MPa	Elastic Constant	77380
C44	MPa	Elastic Constant	118520
m	-	Strain Rate Sensitivity	10
$\dot{a}$	1/s	Reference Strain Rate	0.00001
h_0	MPa	Initial Hardening Modulus	173.5
τ_0	MPa	Critical Resolved Shear Stress	216.8
τ_s	MPa	Saturated Resolved Shear Stress	266.5

The grain orientations have been defined by the unit vectors in terms of Euler-Bunge convention which are described in Appendix-A and introduced into the Huang's Crystal Plasticity subroutine [25]. The new final axes are shown by x* and y* and the assigned grain orientations are tabulated in Table 7.2.2.

Table 7.2.2 Grain orientation of the single crystal MD2

Orientation Name	Euler-Bunge Orientation	x*			y*		
		x	y	z	x	y	z
O1	(15,0,0)	0.966	0.259	0	-0.256	0.966	0
O2	(30,0,0)	0.866	0.500	0	-0.500	0.866	0
O3	(45,0,0)	0.707	0.707	0	-0.707	0.707	0

The maximum principal stress, maximum principal strain, maximum resolved shear stress and maximum accumulated shear strain criteria are utilized to initiate and propagate crack within the element. The observations made from single crystal experiments demonstrate that slip band which takes place at the critical resolved shear stress is the indicator of the crack nucleation according to McDowell and

Dunne [38]. Therefore, for the maximum principal stress and resolved shear stress criteria allowable values given in Table 7.2.1 are used for predicting crack initiation. For maximum principal strain criterion 10^{-5} mm/mm is defined as the significant strain level to cause irreversible dislocation motion in Ref. [41] and used as the allowable strain value in the current study. Allowable values for each criterion are given in Table 7.2.3.

Table 7.2.3 Damage criteria allowable values for MD2 single crystal

Criterion	**Unit**	**Value**	**Fracture Energy (N/mm)**
MAXPS	MPa	216.8	0.005
MAXPE	mm/mm	10^{-5}	0.005
MAXRSS	MPa	216.8	0.005
MAXACSS	mm/mm	10^{-5}	0.005

After having constructed finite element model, the grain orientation of the MD2 has been assigned according to Table 7.2.2. Crack propagation directions obtained according to maximum resolved shear stress, maximum accumulated shear strain, maximum principal stress and maximum principal strain damage criteria are given throughout Figure 7.2.4 to Figure 7.2.7. Also note that, angle informations embedded in figures defines the crack initiation angle.

The results obtained by employing different criteria are compared in terms of crack initiation angle and activated slip system in Table 7.2.4.

Crack initiation due to stress concentration, i.e., V-notch, analyses have been performed for three grain orientations according to four different criteria. MAXRSS and MAXACSS criteria captured same crack initiation angles and

activated slip systems for the same orientations. On the other hand, MAXPS and MAXPE criteria as software built-in criteria showed similar performance regarding crack initiation angles.

Crack propagation direction according to MAXRSS criterion was led by either 1st or 2nd slip systems depending on the grain crystal orientation, while other slip systems were also activated causing the crack propagation in MAXACSS criterion at the crack initiation region.

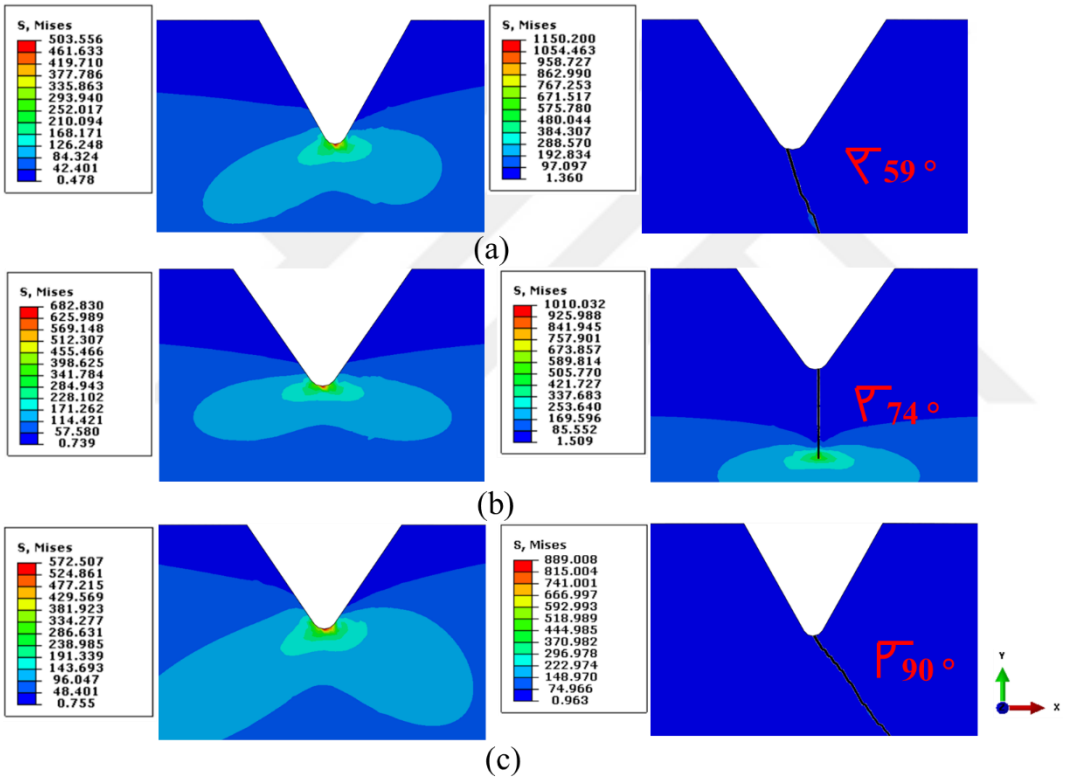

Figure 7.2.4 Grain orientation effect on crack initiation under MAXRSS damage criterion: (a) Orientation 1 (b) Orientation 2 (c) Orientation 3

The maximum principal stress and maximum strain criteria are based on stress and strain tensors calculated by the UMAT CPFEM subroutine for each element without referring the slip systems. Hence, the microscale parameters reflecting the slip system properties that define the preferable slip directions were not considered with these criteria. As a result, the crack propagation paths were observed almost as straight lines.

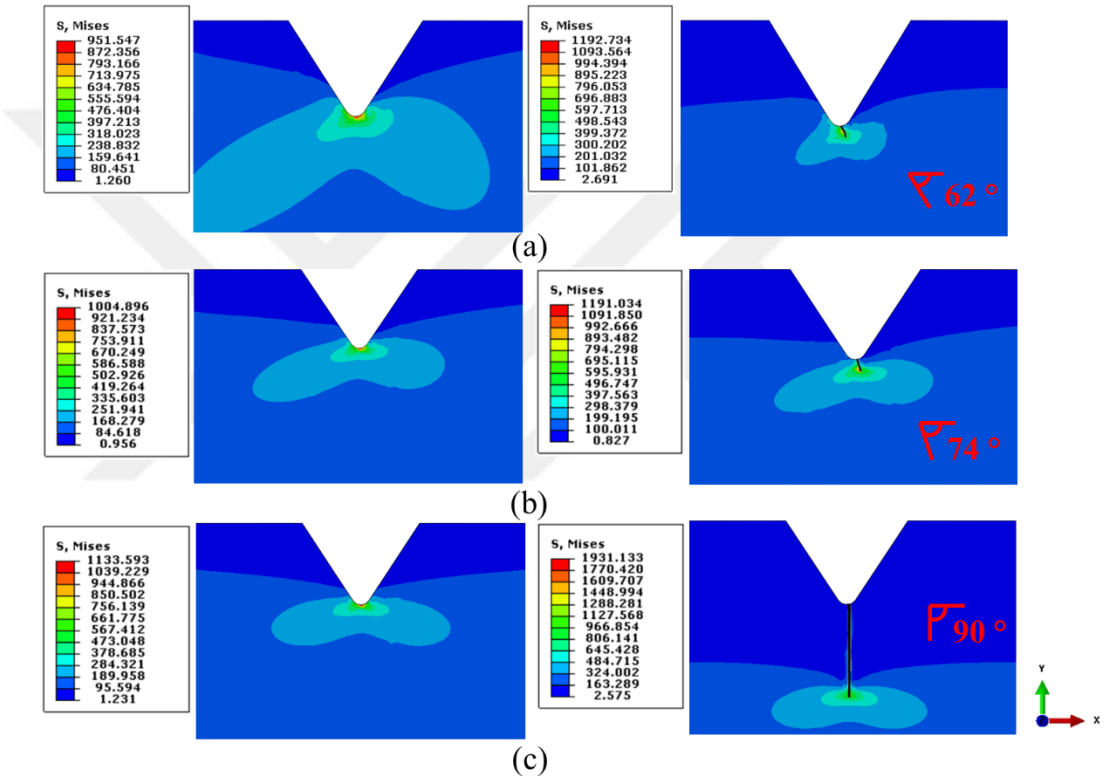

Figure 7.2.5 Grain orientation effect on crack initiation behavior under MAXACSS damage criterion: (a) Orientation 1 (b) Orientation 2 (c) Orientation 3

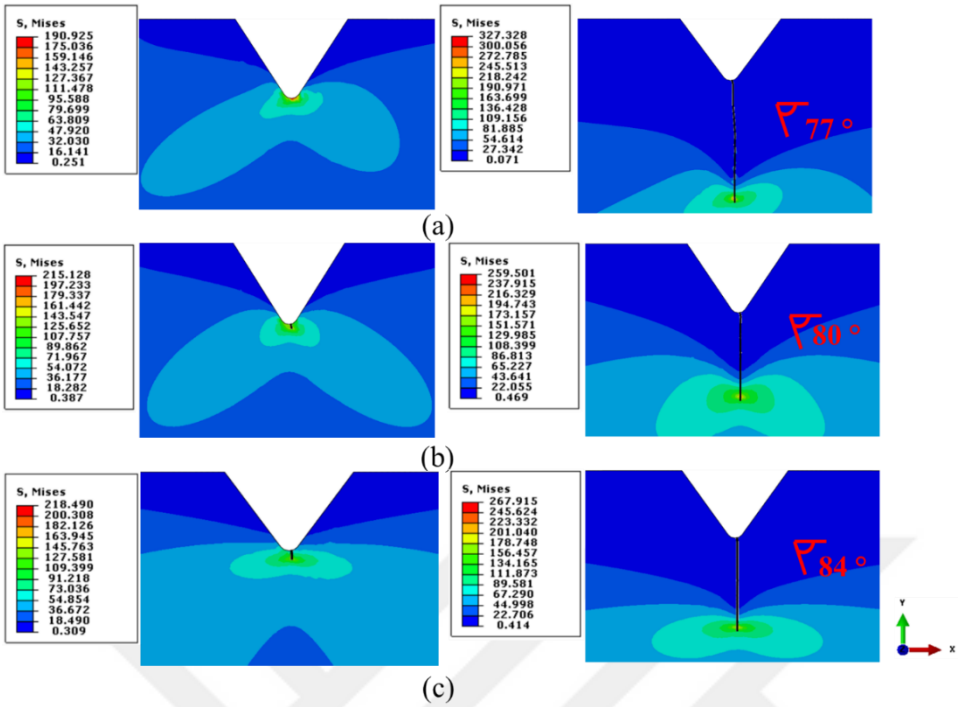

Figure 7.2.6 Grain orientation effect on crack propagation behavior under MAXPS damage criterion: (a) Orientation 1 (b) Orientation 2 (c) Orientation 3

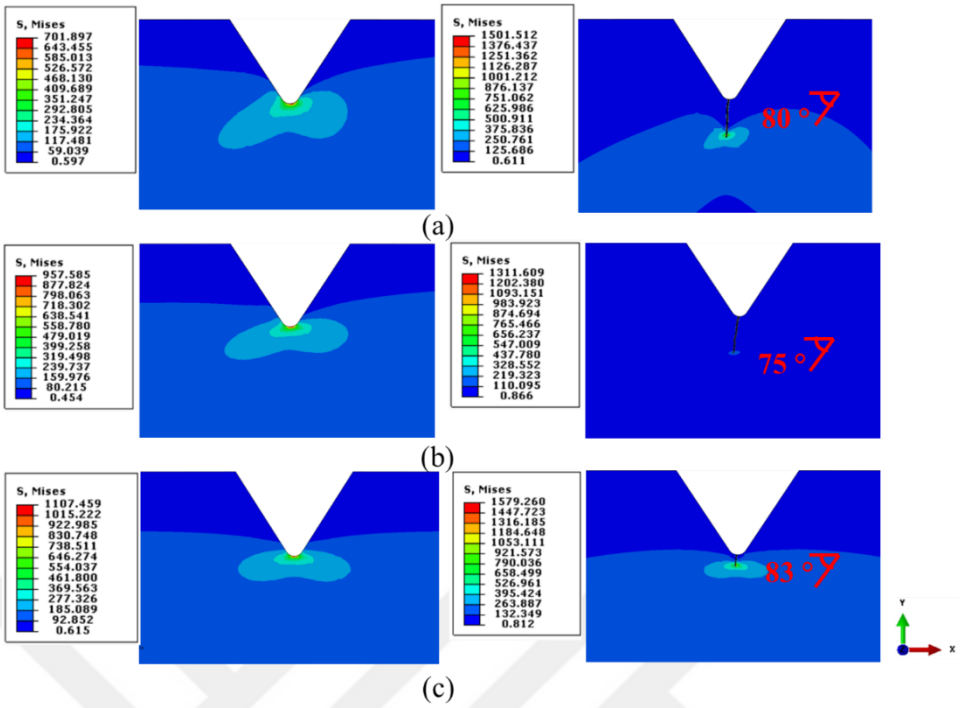

Figure 7.2.7 Grain orientation effect on crack propagation behavior under MAXPE damage criterion: (a) Orientation 1 (b) Orientation 2 (c) Orientation 3

Table 7.2.4 Crack initiation comparison about wrt orientation and criteria

Criterion	Orientation	Crack Initiation Angle [°]	Activated Slip Systems
MAXRSS	O1	59	2
MAXRSS	O2	74	2
MAXRSS	O3	90	1
MAXACSS	O1	62	2,11
MAXACSS	O2	74	2
MAXACSS	O3	90	1, 10
MAXPS	O1	77	NA
MAXPS	O2	80	NA
MAXPS	O3	84	NA
MAXPE	O1	80	NA
MAXPE	O2	75	NA
MAXPE	O3	83	NA

7.3 Effect of Grain Orientation on Crack Initiation and Propagation in Polycrystals

7.3.1 The Finite Element Model

The plate whose shape is rectangular and edge length is 600 micrometers was divided into subdomains which corresponds to grains by the open-source software Neper [36] through Voronoi tessellation. In this analysis, Neper software provided 48 grains whose grain orientations randomly assigned by considering statistical distribution of the solidification [36] as can be seen in Figure 7.3.1. Then, tessellated geometry has been imported to ABAQUS finite element software program. A pre-crack with the length of 18 micrometers was introduced to the tessellated model as can be seen in Figure 7.3.2. Discretization of the model was performed by the element type of CPS4, 4-node bilinear plane stress quadrilateral, with an average size of 3 micrometers. The mesh view of the model is given in Figure 7.3.3.

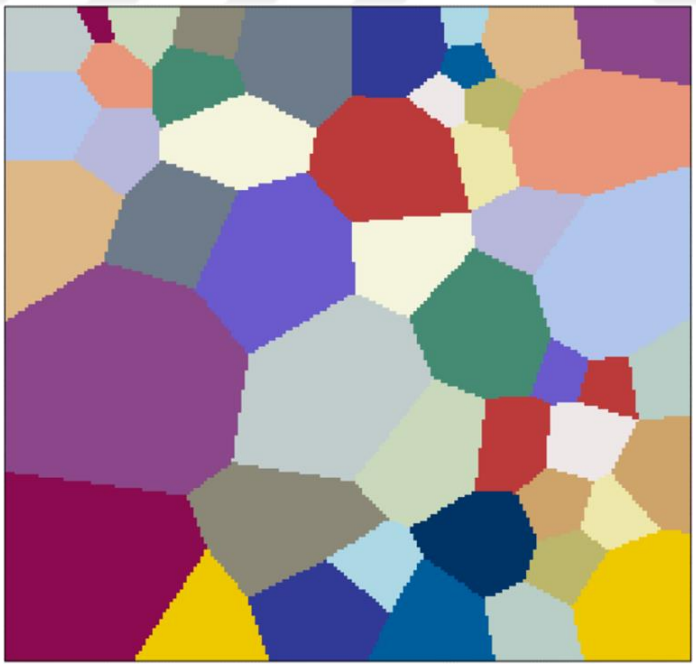

Figure 7.3.1 Two-dimensional plate model of MD2 polycrystal

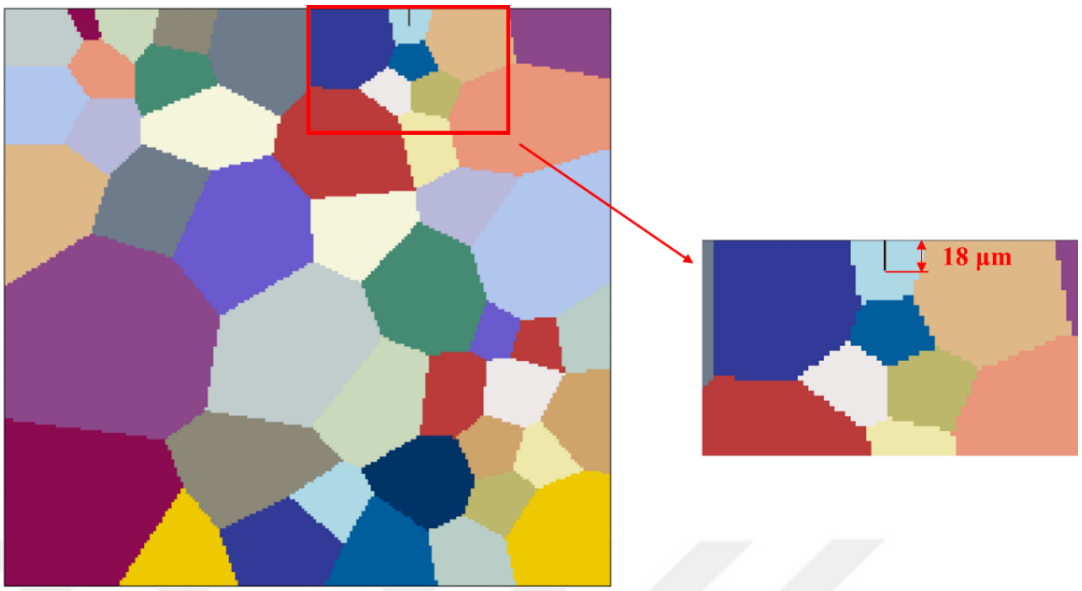

Figure 7.3.2 Two-dimensional plate model of MD2 polycrystal with pre-crack definition

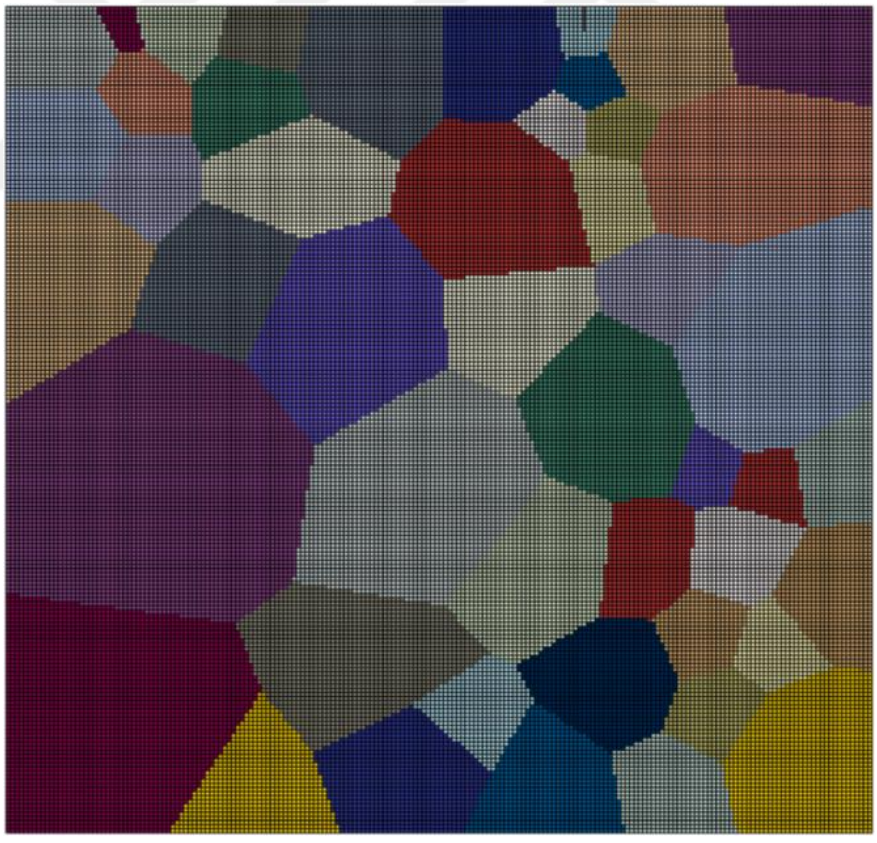

Figure 7.3.3 Mesh definition of the model

Boundary conditions of the plate are defined by assigning $u = 0$ for all the nodes at the left side edge of the plate along y-axis except the node at the upper left corner for which $u = v = 0$. A prescribed incremental displacement up to 15 micrometers is defined for the nodes at the right side of the plate in x-direction only. Boundary condition and load definition of the model is given in Figure 7.3.4.

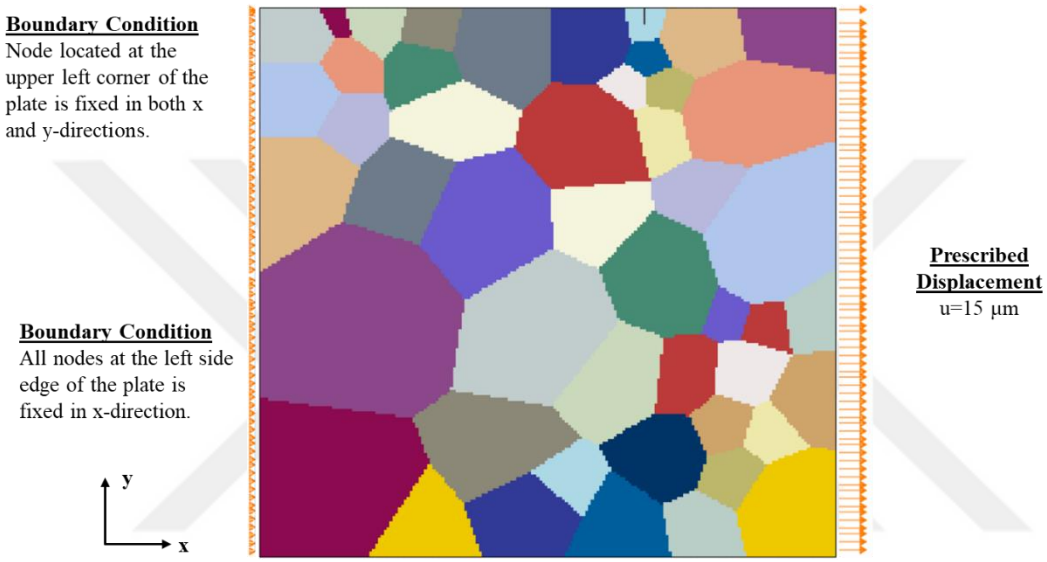

Figure 7.3.4 Boundary conditions and load definition of the model

The set of analyses were carried out by defining different grain orientations to understand the effect on the crack growth behavior since there are infinite number of combinations of grain orientation that can be generated. The grain orientation configurations and the related materials are tabulated in Table 7.3.1.

Table 7.3.1 Grain orientation configurations of MD2 polycrystal model

Orientation Name	**Euler-Bunge Orientation**	**x***			**y***			**Material**
		x	y	z	x	y	z	
O1	(15,0,0)	0.966	0.259	0	-0.256	0.966	0	MD2 Aluminum Steel
O2	(30,0,0)	0.866	0.500	0	-0.500	0.866	0	MD2 Aluminum Steel
O3	(45,0,0)	0.707	0.707	0	-0.707	0.707	0	MD2 Aluminum Steel
O4	(60,0,0)	0.500	0.866	0	-0.866	0.500	0	MD2 Aluminum Steel
O5	(75,0,0)	0.259	0.966	0	-0.966	0.259	0	MD2 Aluminum Steel
O6	(0,15,0)	1	0	0	0	0.966	0.259	MD2
O7	(0,30,0)	1	0	0	0	0.866	0.500	MD2
O8	(0,45,0)	1	0	0	0	0.707	0.707	MD2
O9	(0,60,0)	1	0	0	0	0.500	0.866	MD2

7.3.2 Pre-cracked MD2 Polycrystal

Crystal plasticity constitutive material parameters of the nickel-based supper alloy (MD2) that were tabulated in Table 7.2.2 have been defined into the polycrystalline model also, the damage criteria allowable values are given in Table 7.3.2.

Table 7.3.2 Damage criteria allowable values for MD2 polycrystal

Criterion	Unit	Value	Fracture Energy (N/mm)
MAXPS	MPa	216.8	0.015
MAXRSS	MPa	216.8	0.015

The orientation of the grain including pre-crack has been changed in according to Table 7.3.1. MD2 polycrystal model was evaluated by employing MAXPS and MAXRSS damage criteria. Results of the crack propagation of the MD2 polycrystal are given in Figure 7.3.5, Figure 7.3.6 for MAXRSS criterion and Figure 7.3.7 for MAXPS criterion.

For the MAXPS criterion, the finite element models were constructed for first five orientations, since MAXPS criterion was not found sensitive to grain orientation change.

Detailed results of the analyses are presented throughout Figure 7.3.8 to Figure 7.3.17.

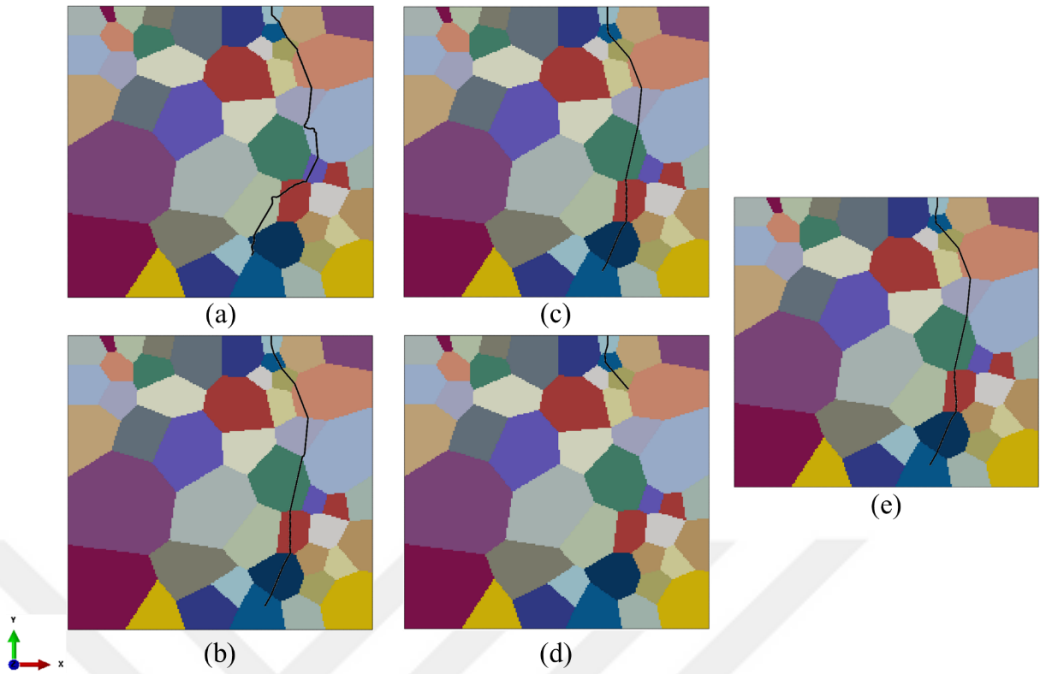

Figure 7.3.5 MAXRSS criterion – MD2 polycrystal crack propagation directions of (a) Orientation 1 (b) Orientation 2 (c) Orientation 3 (d) Orientation 4 (e) Orientation 5

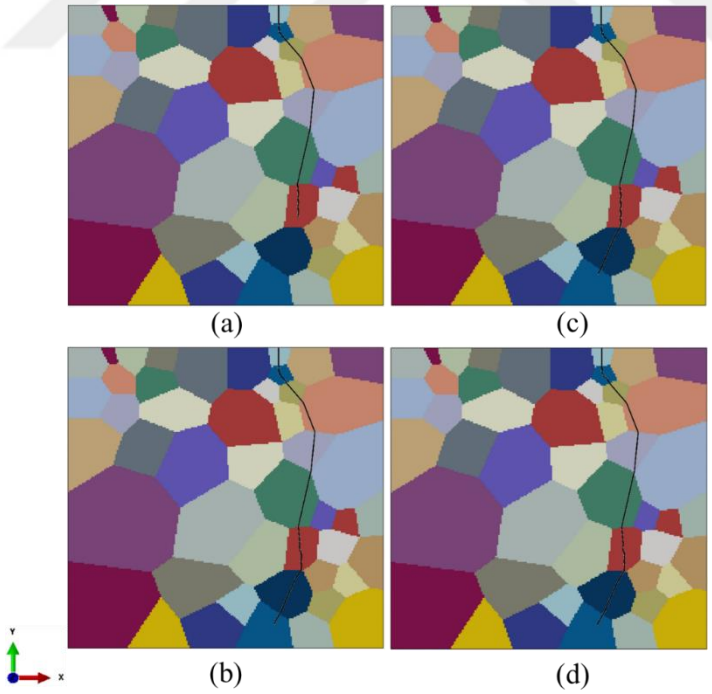

Figure 7.3.6 MAXRSS criterion – MD2 polycrystal crack propagation directions of a-) Orientation 6 b-) Orientation 7 c-) Orientation 8 d-) Orientation 9

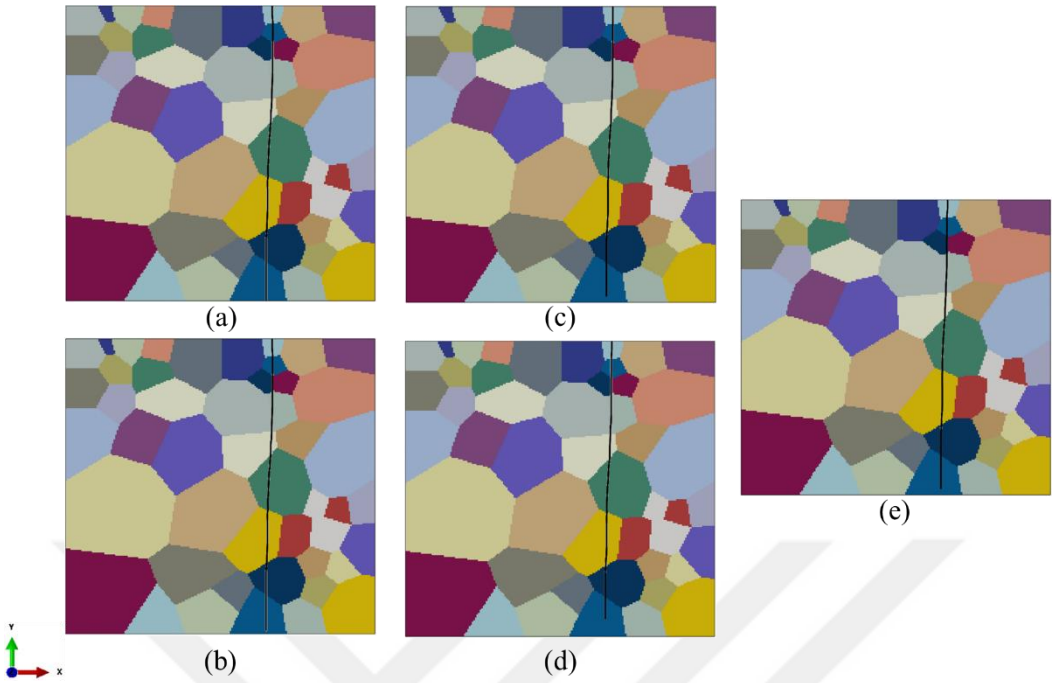

Figure 7.3.7 MAXPS criterion – MD2 polycrystal crack propagation directions of (a) Orientation 1 (b) Orientation 2 (c) Orientation 3 (d) Orientation 4 (e) Orientation 5

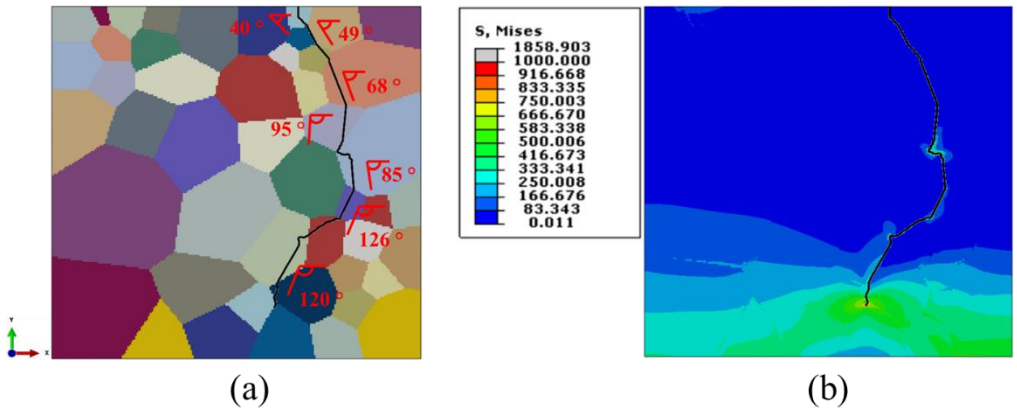

Figure 7.3.8 MAXRSS criterion - MD2 polycrystal crack propagation directions of Orientation 1 (a) Crack Propagation Path (b) Final Stress State

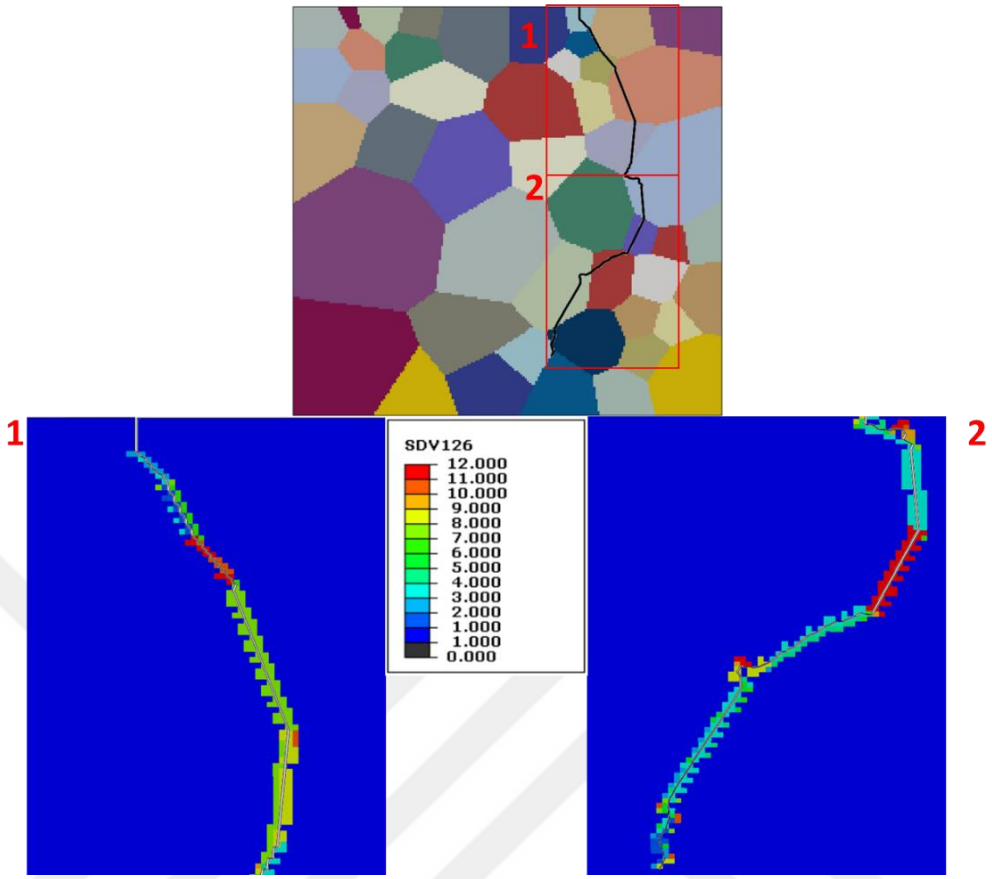

Figure 7.3.9 MAXRSS criterion - MD2 polycrystal crack propagation of Orientation 1 - activated slip systems throughout crack

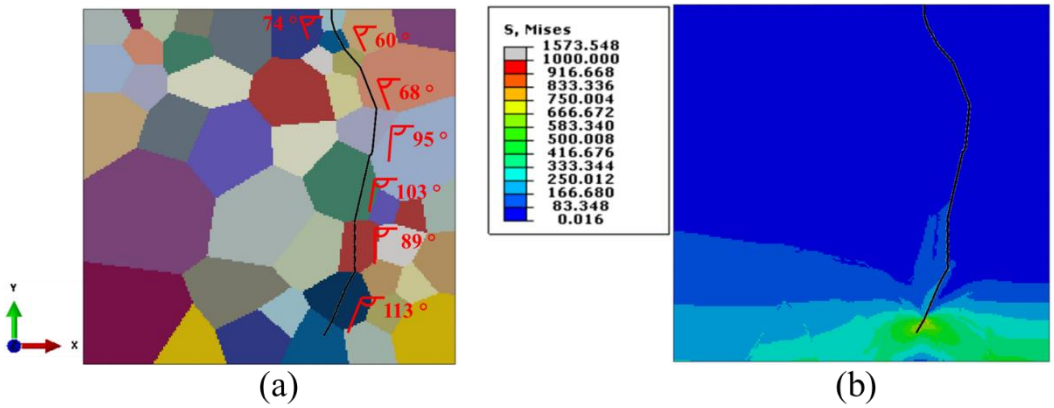

Figure 7.3.10 MAXRSS criterion - MD2 polycrystal crack propagation of Orientation 2 (a) Crack Propagation Path (b) Final Stress State

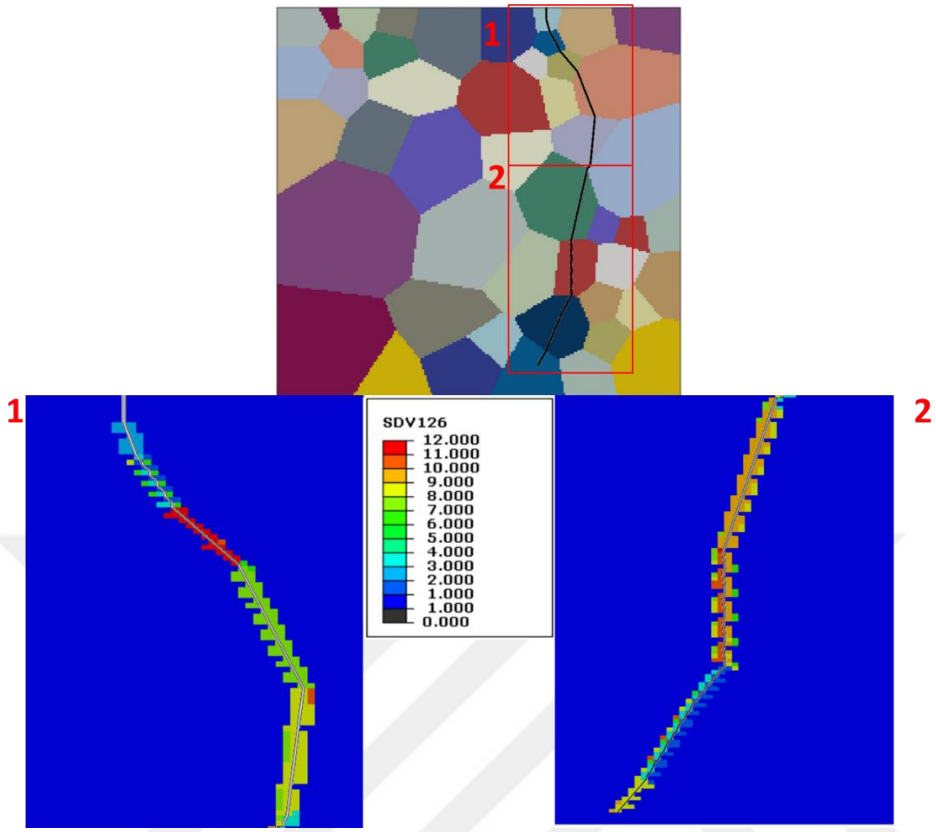

Figure 7.3.11 MAXRSS criterion - MD2 polycrystal crack propagation of Orientation 2 - activated slip systems throughout crack

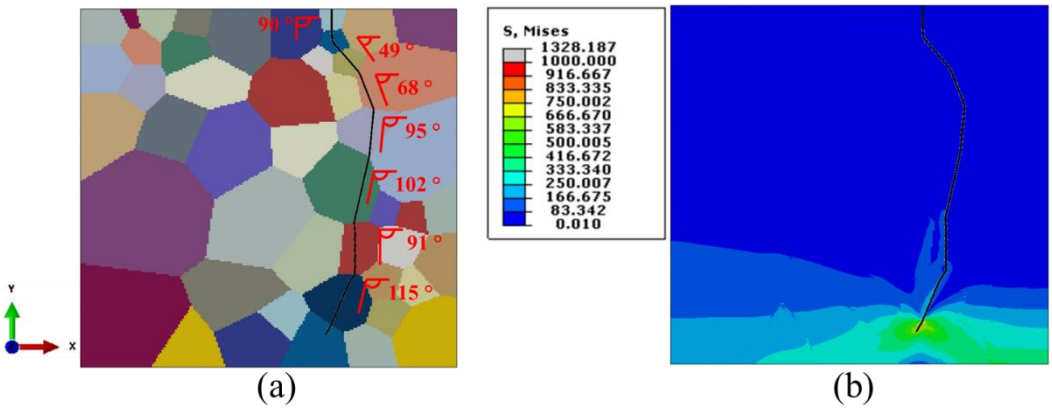

Figure 7.3.12 MAXRSS criterion - MD2 polycrystal crack propagation of Orientation 3 (a) Crack Propagation Path (b) Final Stress State

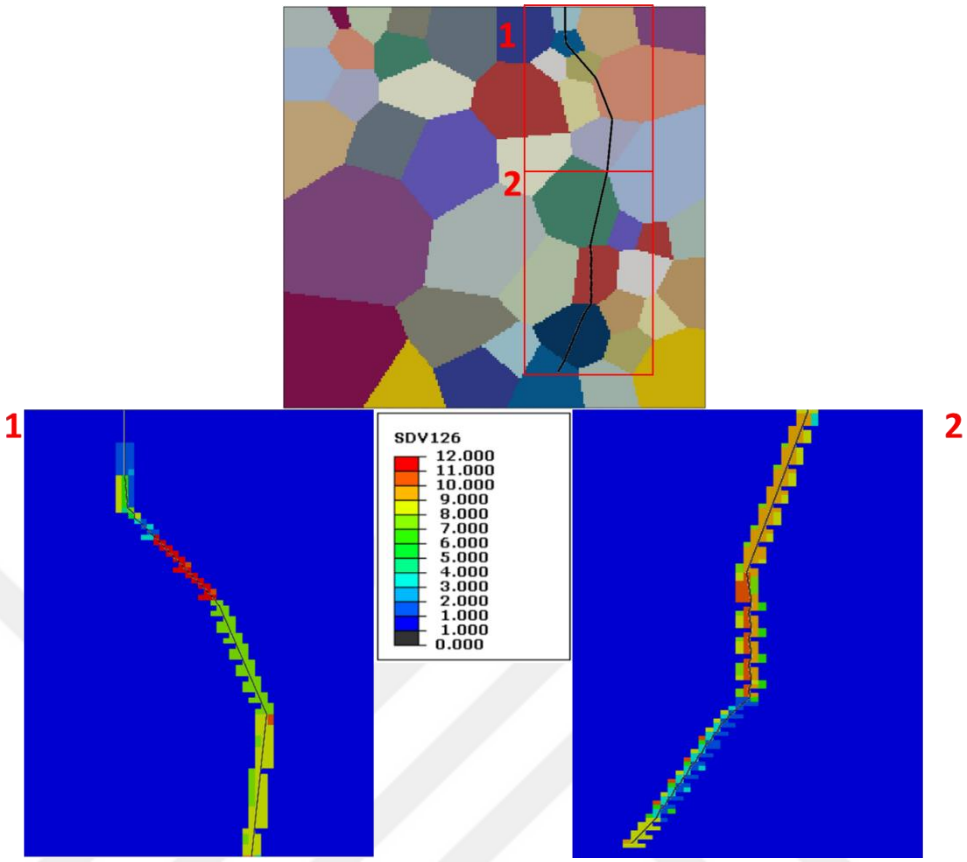

Figure 7.3.13 MAXRSS criterion - MD2 polycrystal crack propagation of Orientation 3 - activated slip systems throughout crack

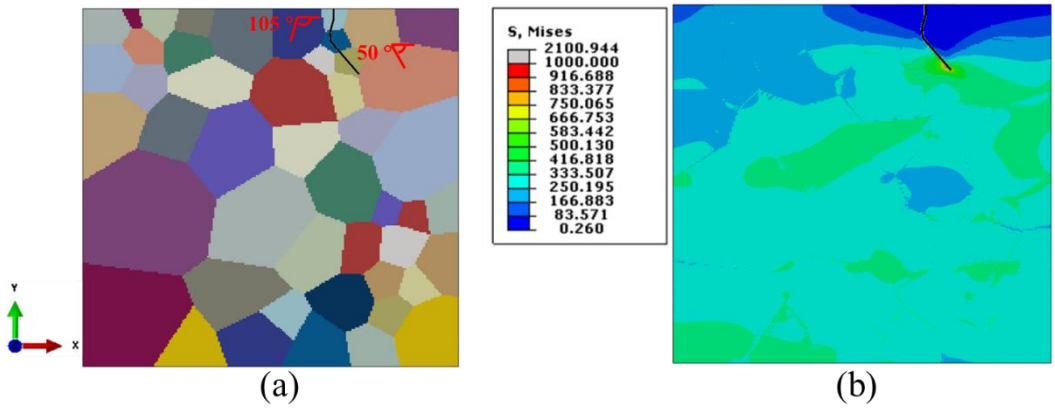

Figure 7.3.14 MAXRSS criterion - MD2 polycrystal crack propagation of Orientation 4 (a) Crack Propagation Path (b) Final Stress State

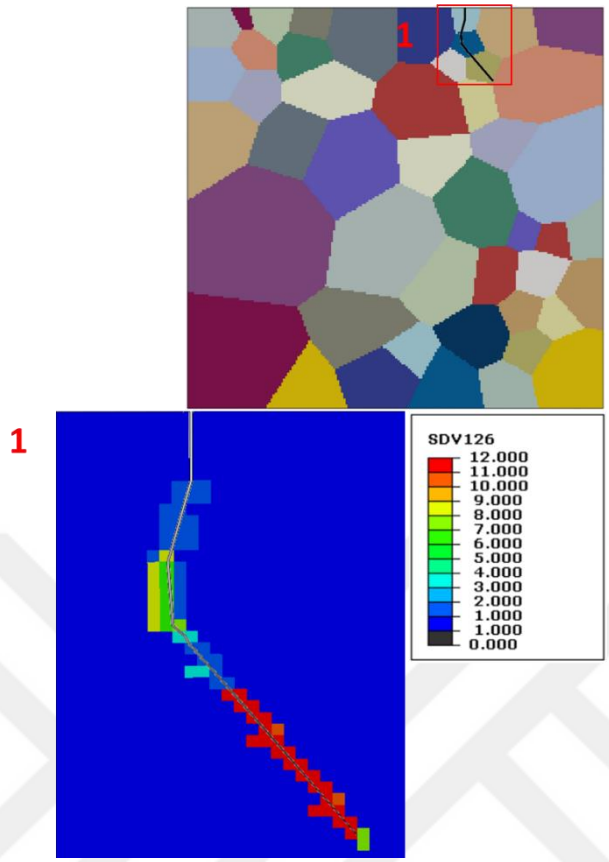

Figure 7.3.15 MAXRSS criterion - MD2 polycrystal crack propagation of Orientation 4 - activated slip systems throughout crack

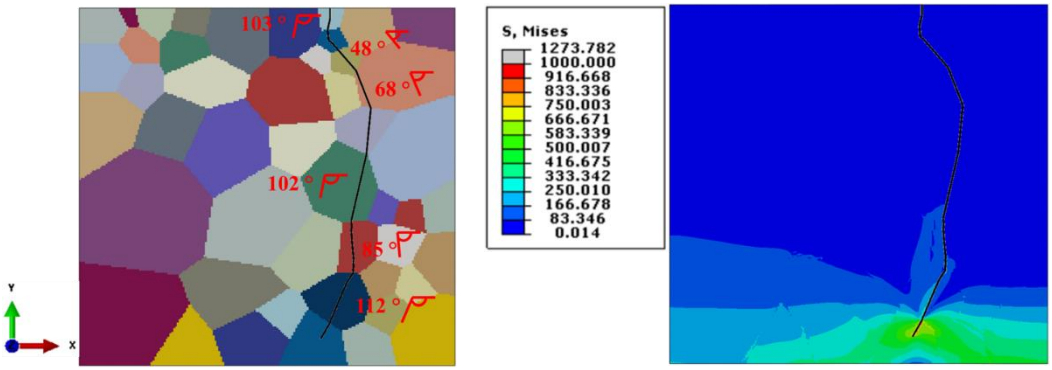

Figure 7.3.16 MAXRSS criterion - MD2 polycrystal crack propagation of Orientation 5 (a) Crack Propagation Path (b) Final Stress State

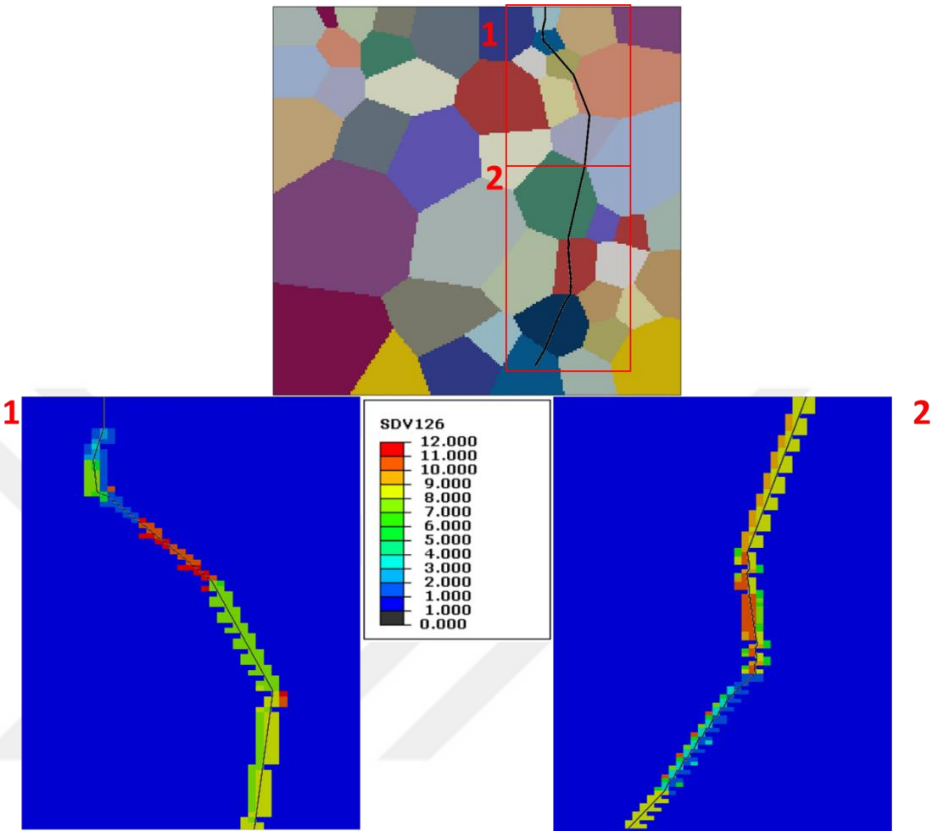

Figure 7.3.17 MAXRSS criterion - MD2 polycrystal crack propagation of Orientation 5 - activated slip systems throughout crack

Also, the graphical representations of the force needed to propagate crack versus crack length for each orientation are given for MAXRSS and MAXPS criteria in Figure 7.3.18 and Figure 7.3.19, respectively.

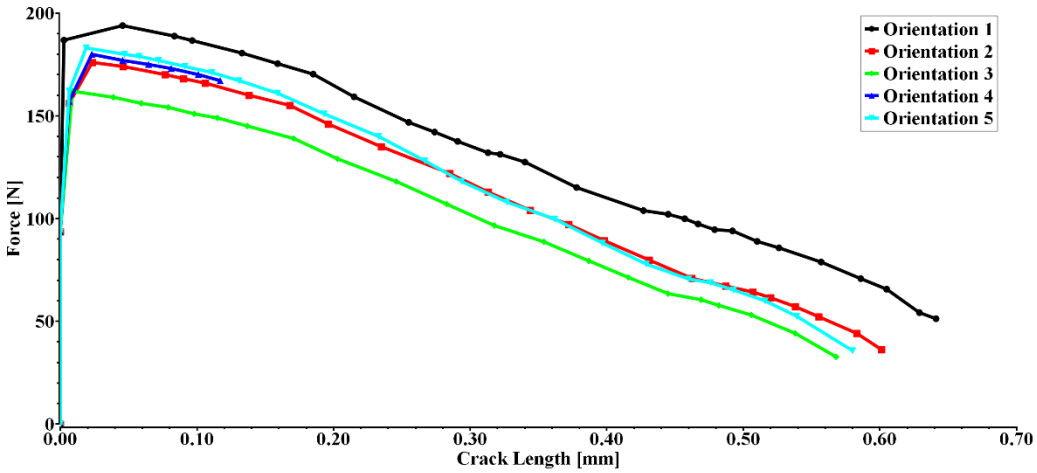

Figure 7.3.18 MAXRSS criterion - MD2 Ni-based superalloy - force vs. crack length

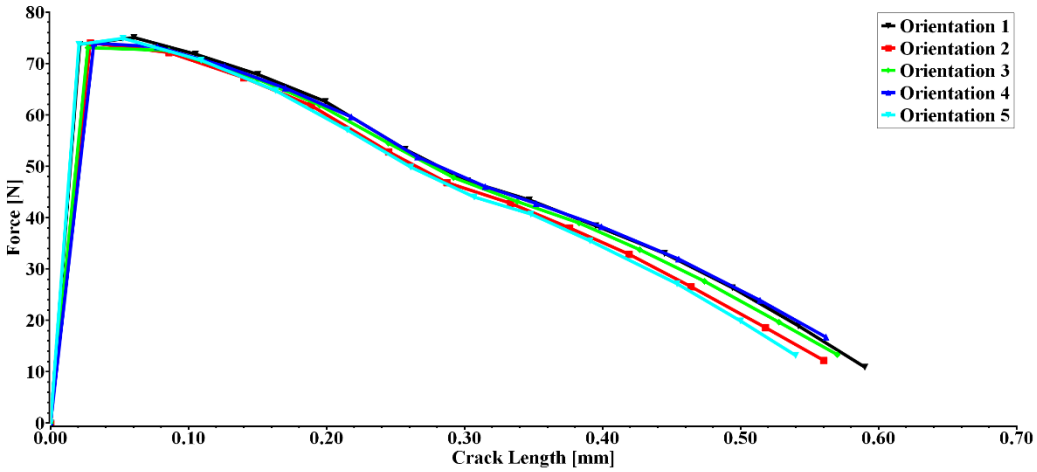

Figure 7.3.19 MAXPS criterion - MD2 Ni-based superalloy - force vs. crack length

Crack propagation in the crystalline scale behaves highly dependent on grain orientation; the grain orientation of the grain including pre-crack dramatically effects the crack path in different grains in MAXRSS criterion as can be seen in Figure 7.3.5 and Figure 7.3.6. Crack propagation direction in MAXRSS criterion is defined as unit normal to the slip plane in which the highest resolved shear stress

takes place. Therefore, crack growth differs in each grain whose slip plane in which maximum resolved shear stress occurs due to the grain orientation.

On the contrary, crack path obtained under consideration of MAXPS criterion is not sensitive to grain orientation since crack propagation direction is simply defined according to normal direction of the principal plane on which the maximum principal stress is obtained rather than the unit normal of the slip plane.

Also, activated slip system alters in the grains due to mainly the angle between loading direction and grain orientation as can be seen in Figure 7.3.9, Figure 7.3.11, Figure 7.3.13, Figure 7.3.15 and Figure 7.3.17. Different activated slip systems lead to variety of crack propagation behavior depending on individual grain properties.

Applied force to propagate in MAXRSS criterion crack notably deviates depending on the orientation of grain including pre-crack. First five orientations have been obtained by rotating crystalline about the z-axis which is out of plane direction of the plate, the others are obtained by rotating about the x-axis which in the plane of the plate. Rotations performed about z-axis causing variations in the force values to propagate crack, since Schmid's factor changes by considerable amounts. But, the effect of rotation about x-axis is less than the rotation about z-axis as can be seen in Figure 7.3.18, as Schmid's factor changes with the orientation. Yet, the MAXPS criterion could not capture the dependency of crack propagation to the grain orientation. Still, it can be said that grain orientation plays important role for the material crack resistance.

7.3.3 Pre-cracked AA2024 Aluminum Alloy Polycrystal

Geometry, discretization, boundary conditions and loading given in Section 7.3.1 have been maintained to capture effect of material change to the crack propagation behavior of AA2040 aluminum.

Crystal plasticity constitutive material parameters of the AA2040 aluminum alloy are tabulated in Table 7.3.3 have been defined into the polycrystalline model. The damage criteria allowable values are given in and Table 7.3.4, respectively.

Table 7.3.3 AA2040 aluminum alloy material constants [39]

Parameters	Units	Description	Value
C11	MPa	Elastic Constant	112000
C12	MPa	Elastic Constant	59500
C44	MPa	Elastic Constant	24700
m	-	Strain Rate Sensitivity	10
$\dot{a}$	1/s	Reference Strain Rate	0.001
h_0	MPa	Initial Hardening Modulus	37
τ_0	MPa	Critical Resolved Shear Stress	82.5
τ_s	MPa	Saturated Resolved Shear Stress	100

Table 7.3.4 Damage criteria allowable values for AA2040 aluminum alloy

Criterion	Unit	Value	Fracture Energy (N/mm)
MAXPS	MPa	82.5	0.05
MAXPE	mm/mm	10^{-5}	0.05
MAXRSS	MPa	82.5	0.05
MAXACSS	mm/mm	10^{-5}	0.05

AA2024 aluminum alloy polycrystal model has been evaluated by employing MAXPS, MAXPE, MAXRSS and MAXACSS damage criteria, and results of the crack propagation of the AA2024 aluminum alloy polycrystal are given in Figure 7.3.20, Figure 7.3.21, Figure 7.3.22 and Figure 7.3.23, respectively. Also, detailed results of the analyses are presented throughout Figure 7.3.24 to Figure 7.3.33 for MAXRSS and MAXACSS criteria.

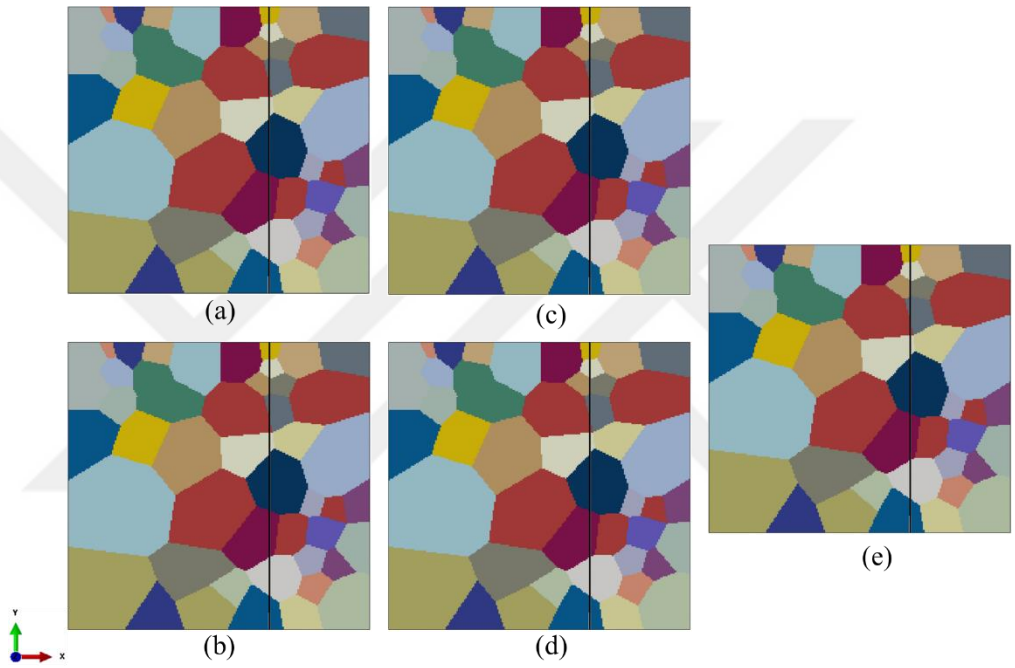

Figure 7.3.20 MAXPS criterion - AA2024 aluminum alloy polycrystal crack propagation directions of (a) Orientation 1 (b) Orientation 2 (c) Orientation 3 (d) Orientation 4 (e) Orientation 5

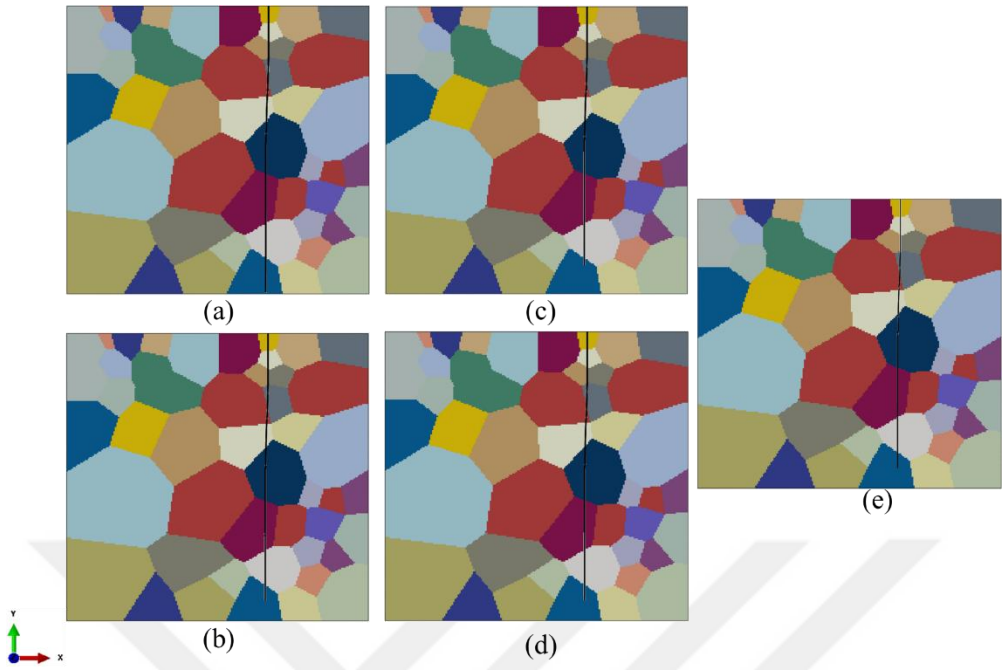

Figure 7.3.21 MAXPE criterion - AA2024 aluminum alloy polycrystal crack propagation directions of (a) Orientation 1 (b) Orientation 2 (c) Orientation 3 (d) Orientation 4 (e) Orientation 5

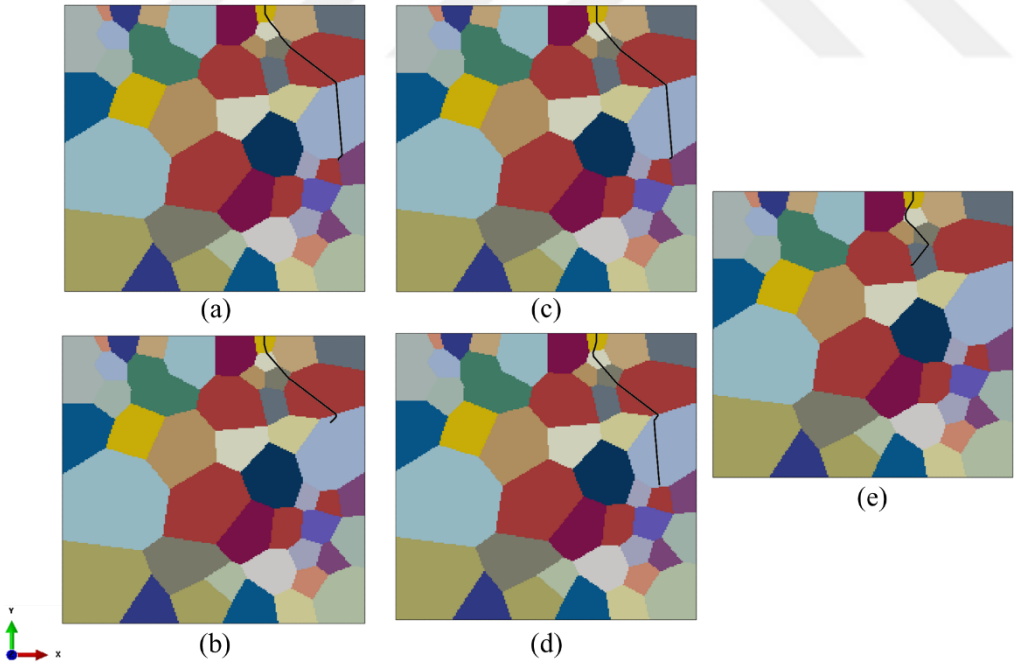

Figure 7.3.22 MAXRSS criterion - AA2024 aluminum alloy polycrystal crack propagation directions of (a) Orientation 1 (b) Orientation 2 (c) Orientation 3 (d) Orientation 4 (e) Orientation 5

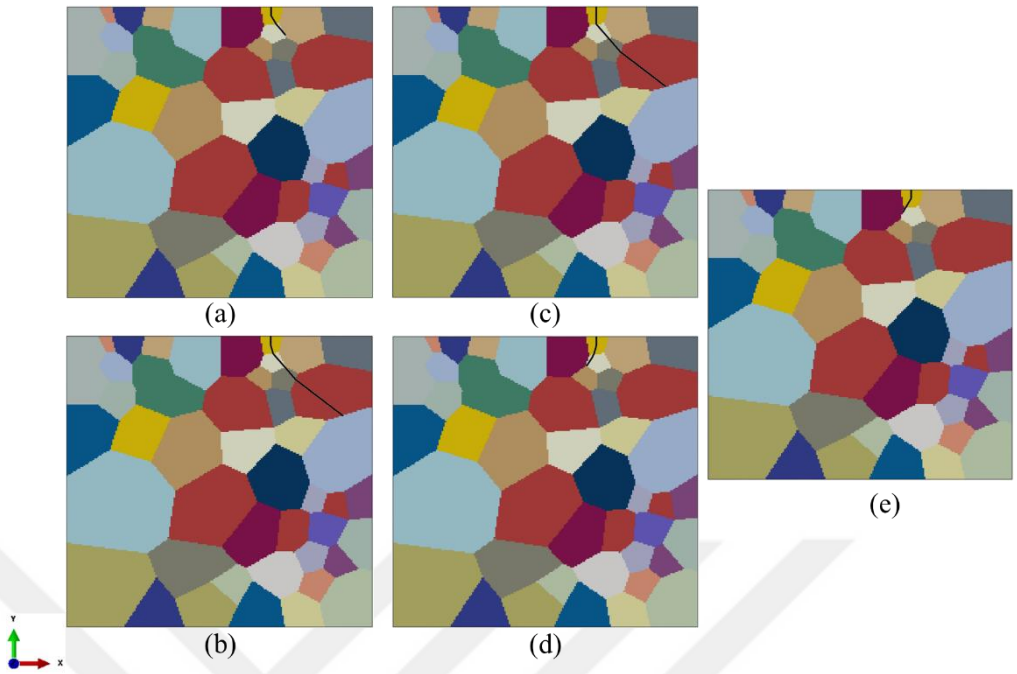

Figure 7.3.23 MAXACSS criterion - AA2024 aluminum alloy polycrystal crack propagation directions of (a) Orientation 1 (b) Orientation 2 (c) Orientation 3 (d) Orientation 4 (e) Orientation 5

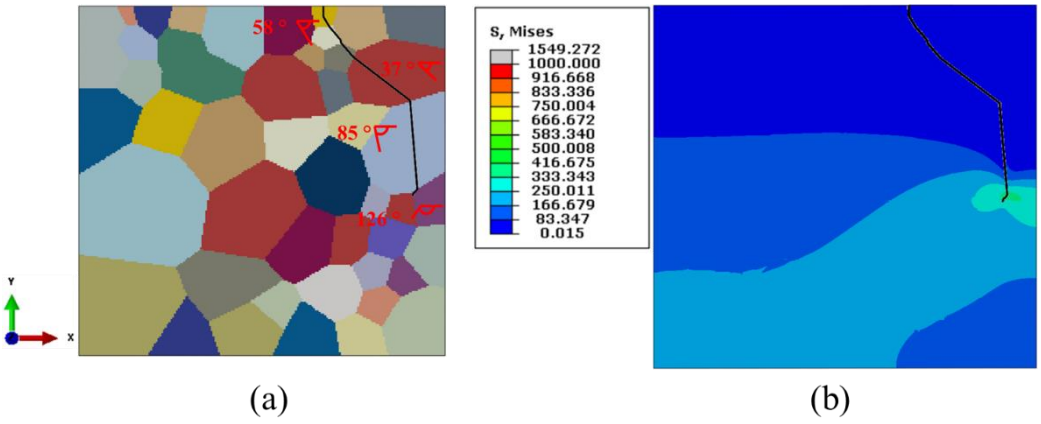

Figure 7.3.24 MAXRSS criterion – AA2024 aluminum alloy polycrystal crack propagation of Orientation 1 (a) Crack Propagation Path (b) Final Stress State

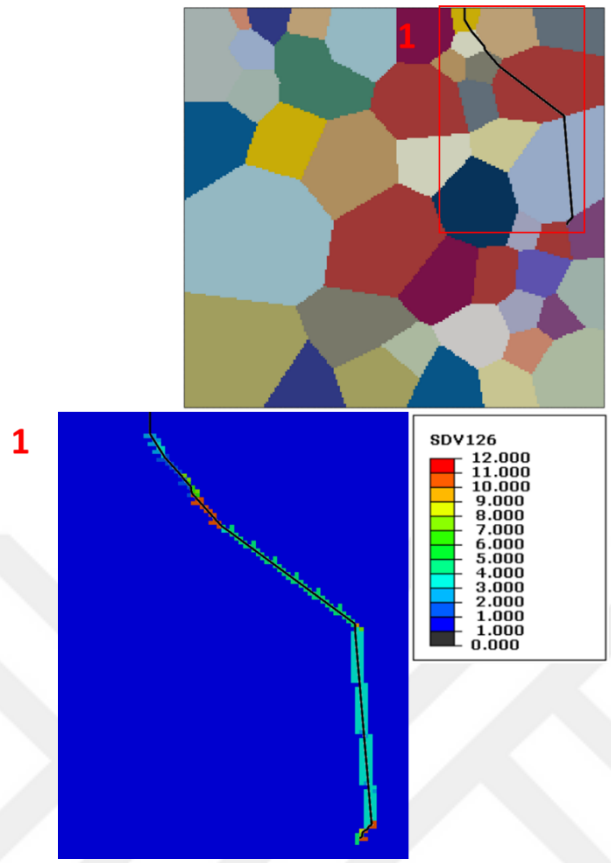

Figure 7.3.25 MAXRSS criterion - AA2024 aluminum alloy crack propagation of Orientation 1 - activated slip systems throughout crack

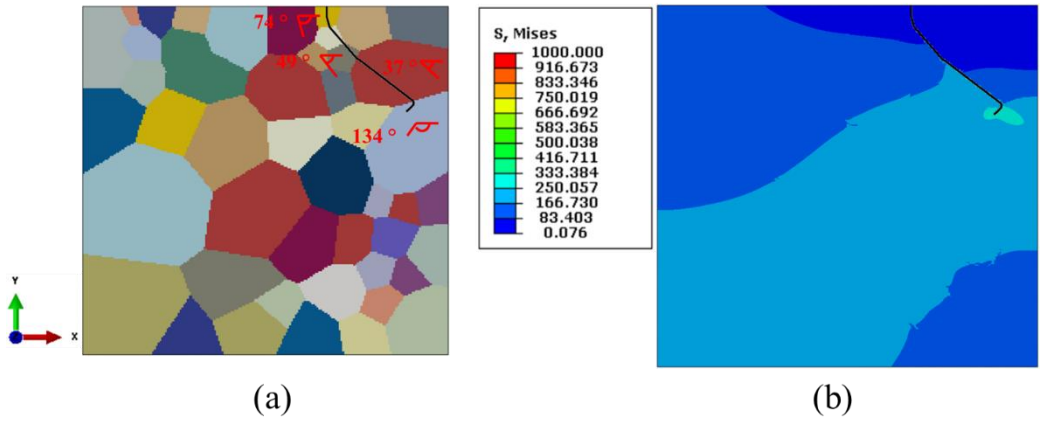

Figure 7.3.26 MAXRSS criterion – AA2024 aluminum alloy polycrystal crack propagation of Orientation 2 (a) Crack Propagation Path (b) Final Stress State

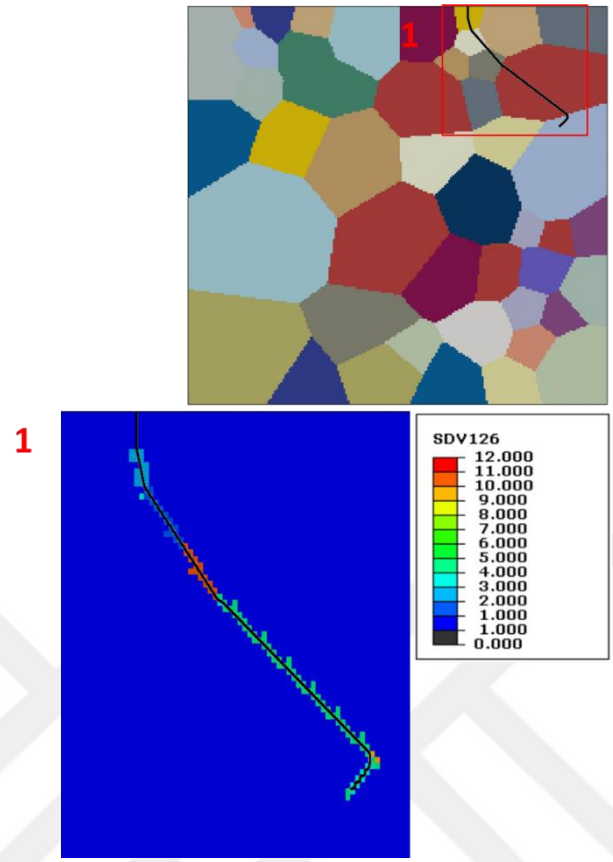

Figure 7.3.27 MAXRSS criterion - AA2024 aluminum alloy crack propagation of Orientation 2 - activated slip systems throughout crack

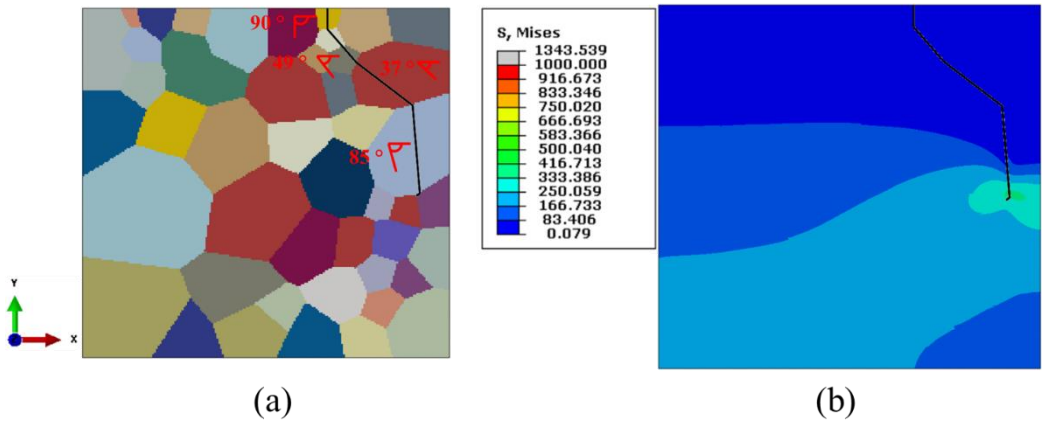

Figure 7.3.28 MAXRSS criterion – AA2024 aluminum alloy polycrystal crack propagation of Orientation 3 (a) Crack Propagation Path (b) Final Stress State

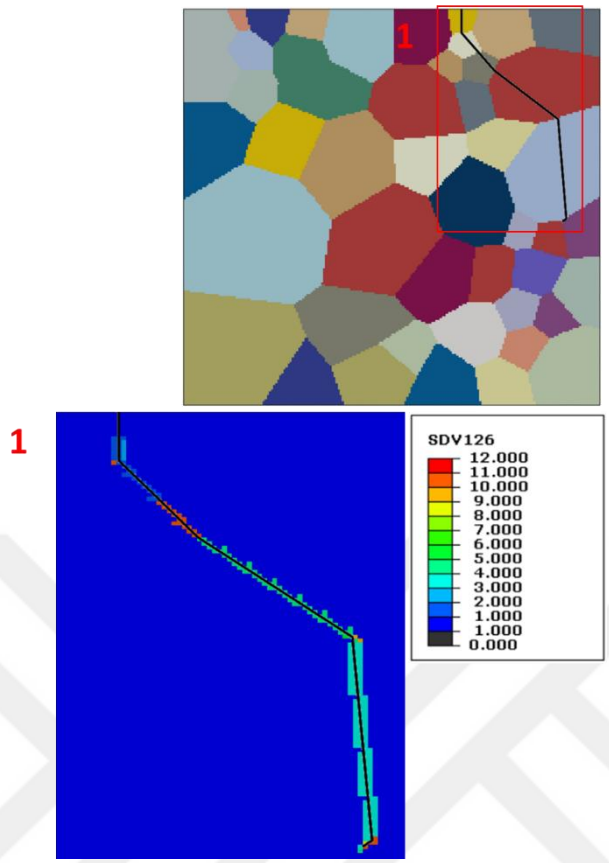

Figure 7.3.29 MAXRSS criterion - AA2024 aluminum alloy crack propagation of Orientation 3 - activated slip systems throughout crack

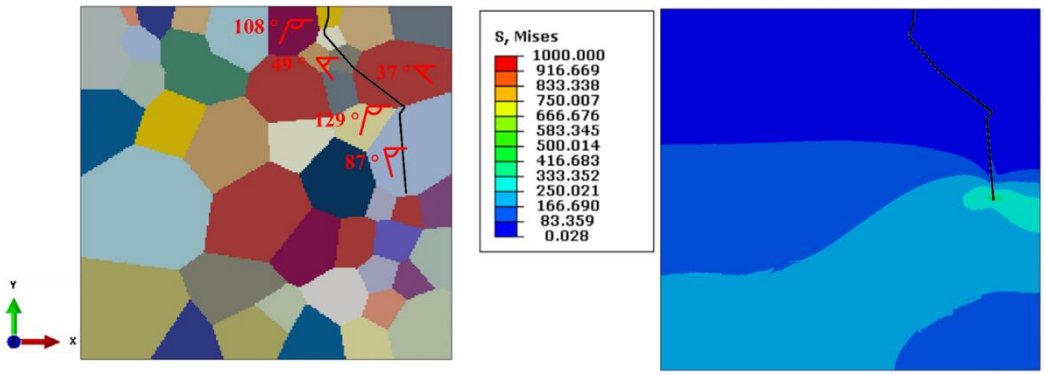

Figure 7.3.30 MAXRSS criterion – AA2024 aluminum alloy polycrystal crack propagation of Orientation 4 (a) Crack Propagation Path (b) Final Stress State

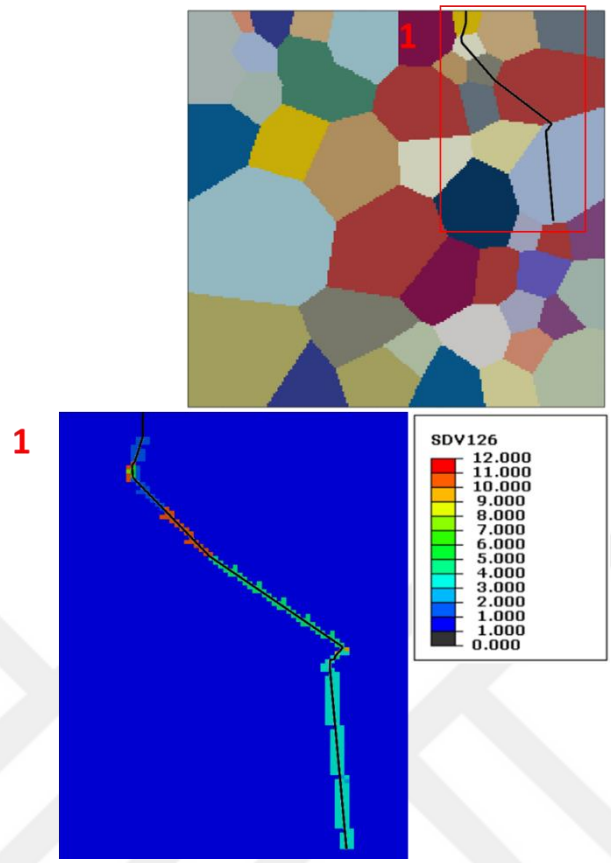

Figure 7.3.31 MAXRSS criterion - AA2024 aluminum alloy crack propagation of Orientation 4 - activated slip systems throughout crack

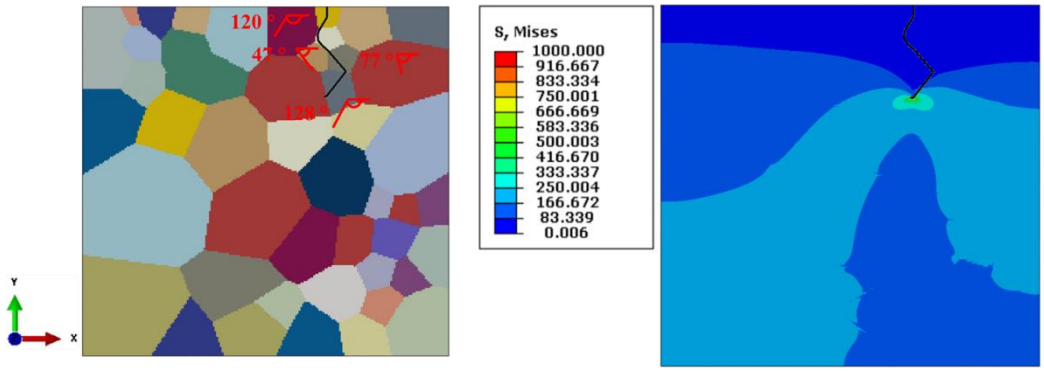

(a) (b)

Figure 7.3.32 MAXRSS criterion – AA2024 aluminum alloy polycrystal crack propagation of Orientation 5 (a) Crack Propagation Path (b) Final Stress State

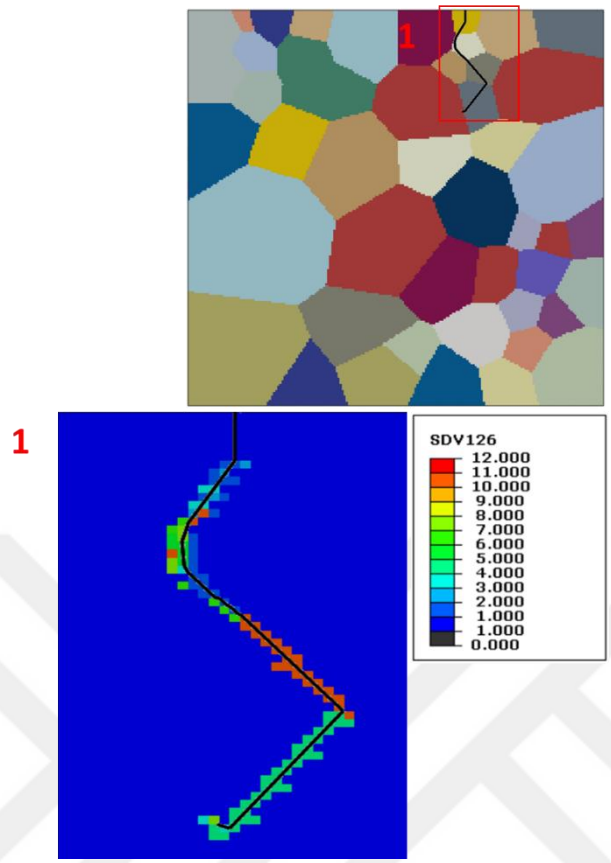

Figure 7.3.33 MAXRSS criterion - AA2024 aluminum alloy crack propagation of Orientation 5 - activated slip systems throughout crack

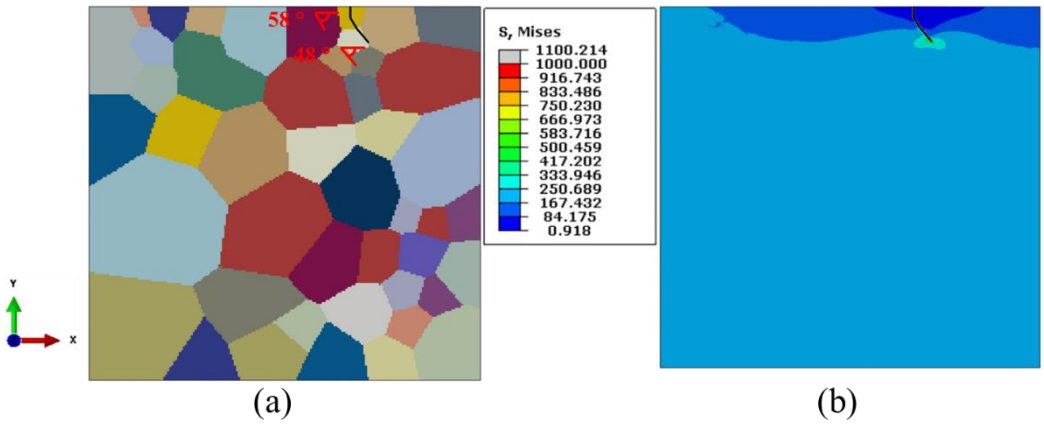

Figure 7.3.34 MAXACSS criterion – AA2024 aluminum alloy polycrystal crack propagation of Orientation 1 (a) Crack Propagation Path (b) Final Stress State

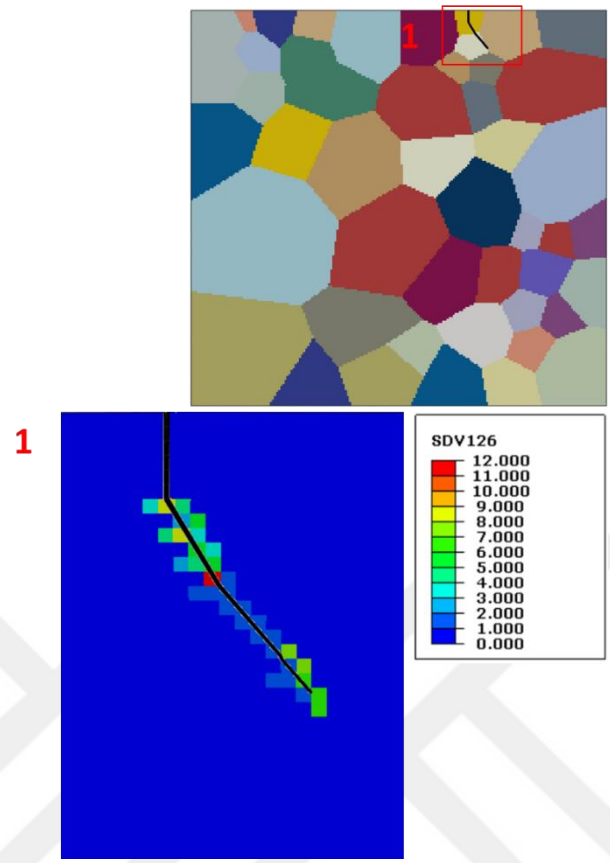

Figure 7.3.35 MAXACSS criterion - AA2024 aluminum alloy crack propagation of Orientation 1 - activated slip systems throughout crack

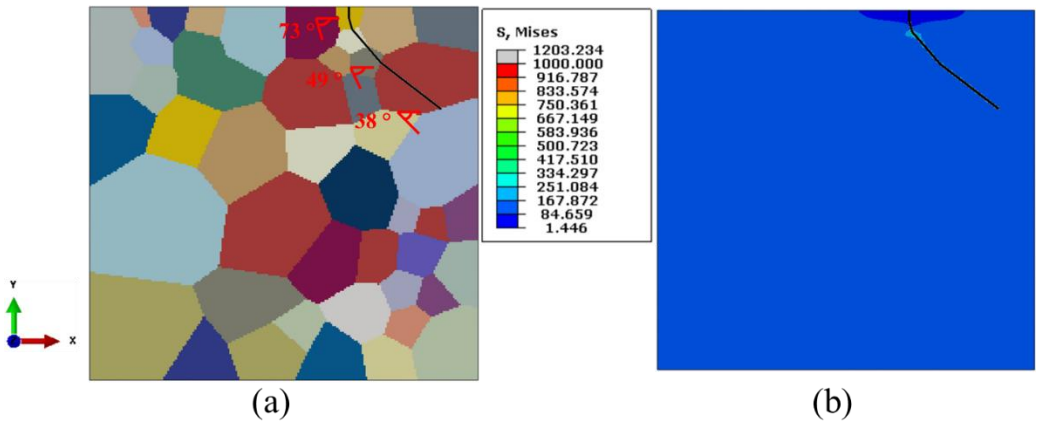

Figure 7.3.36 MAXACSS criterion – AA2024 aluminum alloy polycrystal crack propagation of Orientation 2 (a) Crack Propagation Path (b) Final Stress State

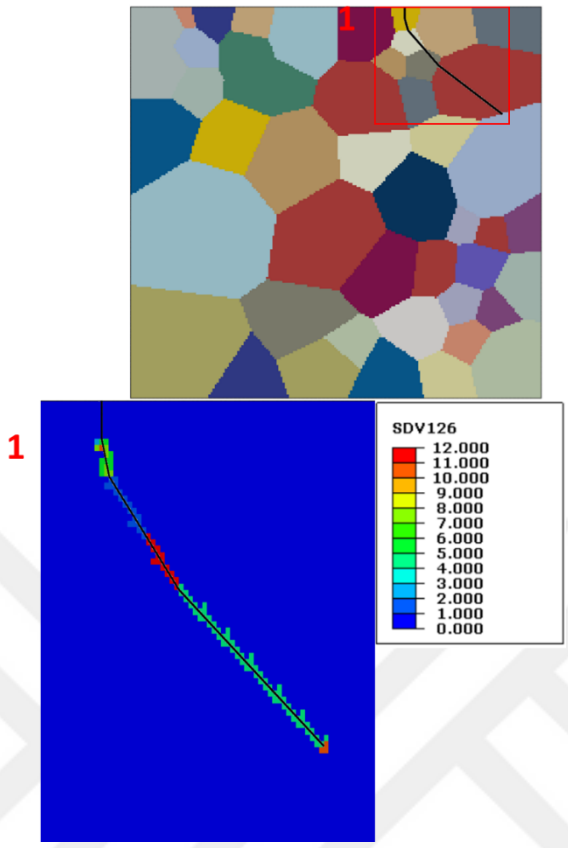

Figure 7.3.37 MAXACSS criterion - AA2024 aluminum alloy crack propagation of Orientation 2 - activated slip systems throughout crack

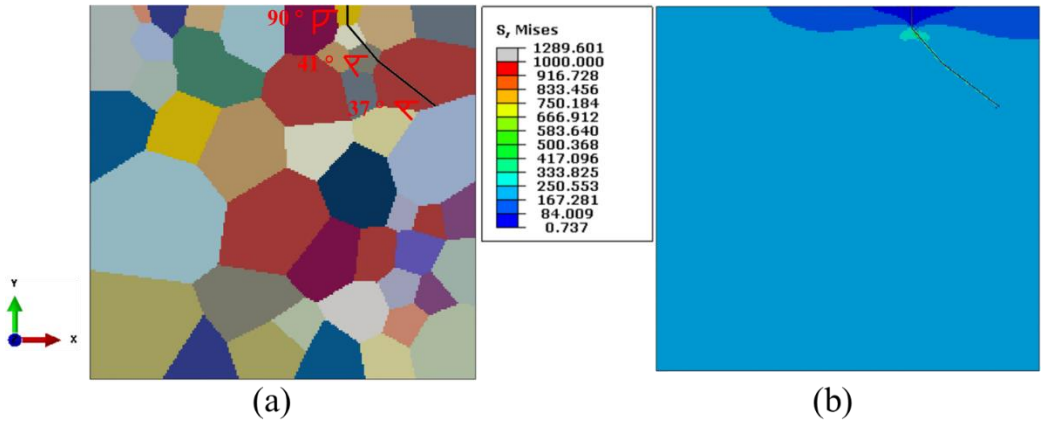

Figure 7.3.38 MAXACSS criterion – AA2024 aluminum alloy polycrystal crack propagation of Orientation 3 (a) Crack Propagation Path (b) Final Stress State

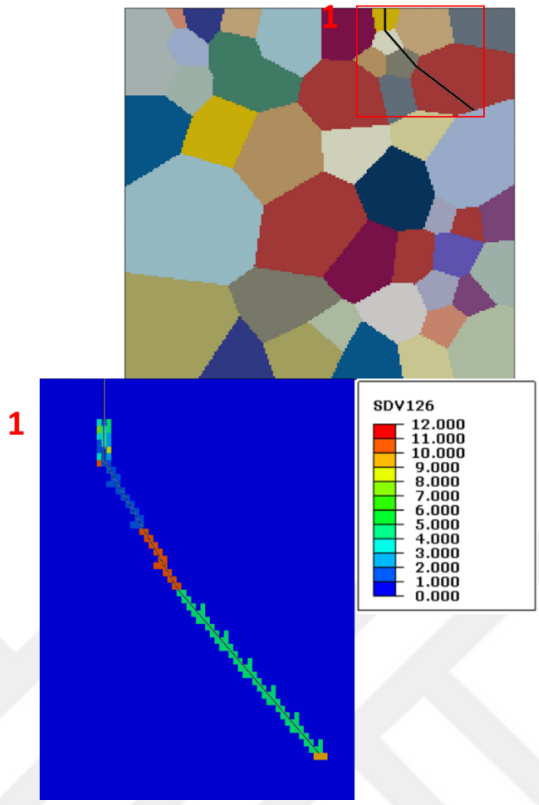

Figure 7.3.39 MAXACSS criterion - AA2024 aluminum alloy crack propagation of Orientation 3 - activated slip systems throughout crack

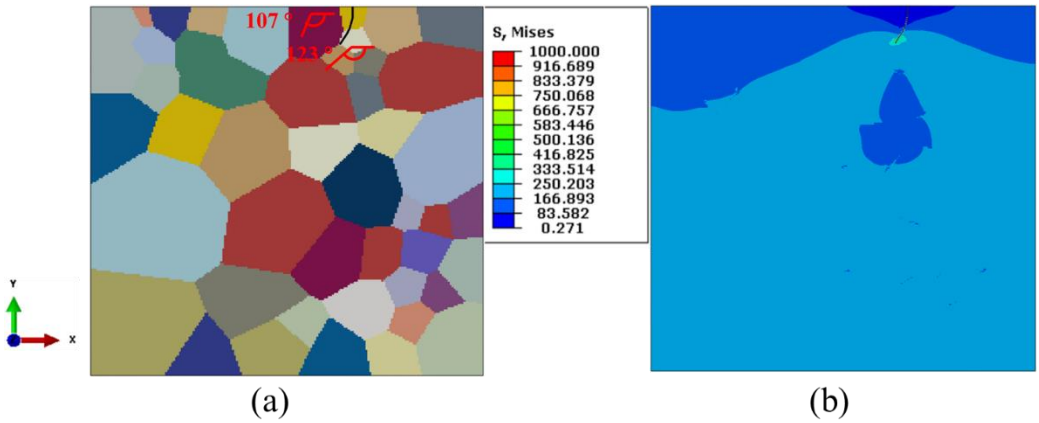

Figure 7.3.40 MAXACSS criterion – AA2024 aluminum alloy polycrystal crack propagation of Orientation 4 (a) Crack Propagation Path (b) Final Stress State

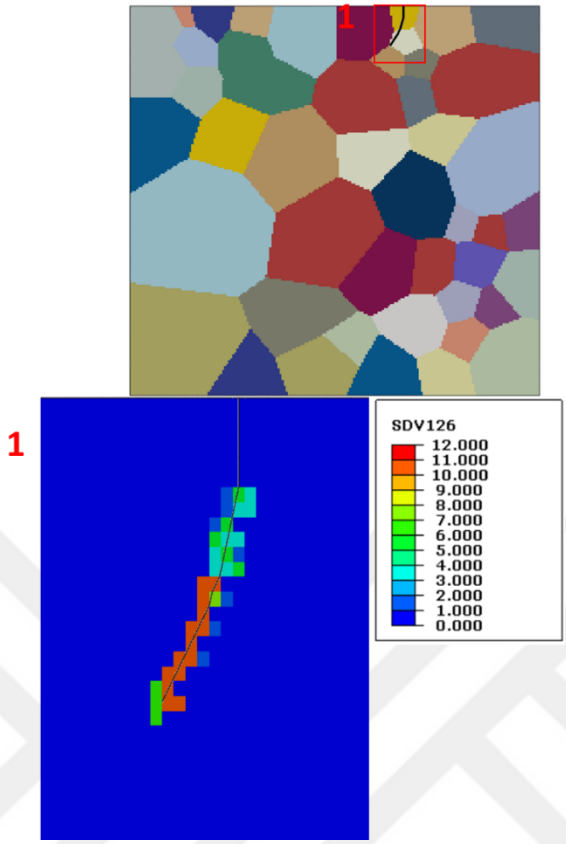

Figure 7.3.41 MAXACSS criterion - AA2024 aluminum alloy crack propagation of Orientation 4 - activated slip systems throughout crack

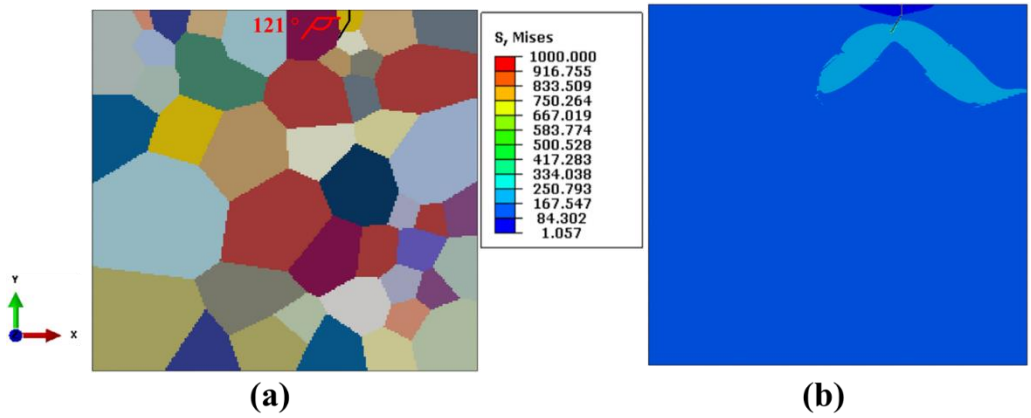

Figure 7.3.42 MAXACSS criterion – AA2024 aluminum alloy polycrystal crack propagation of Orientation 5 (a) Crack Propagation Path (b) Final Stress State

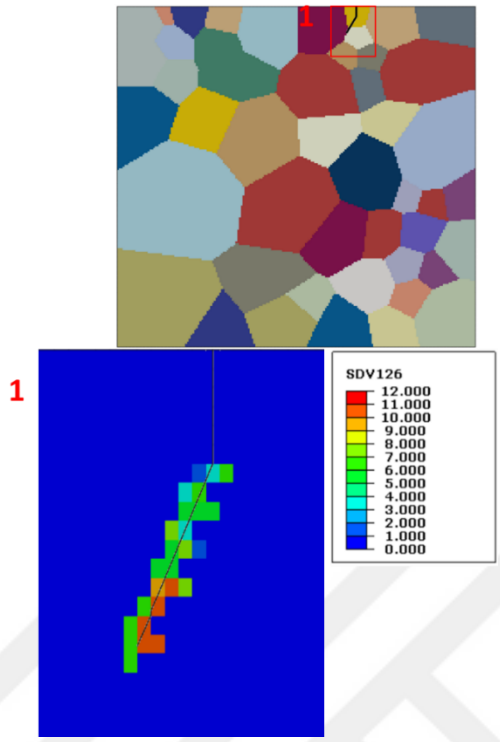

Figure 7.3.43 MAXACSS criterion - AA2024 aluminum alloy crack propagation of Orientation 5 - activated slip systems throughout crack

The graphical representations of the force needed to propagate crack versus crack length for each orientation are given for MAXPS, MAXPE, MAXRSS and MAXACSS criteria throughout Figure 7.3.44 to Figure 7.3.47, respectively.

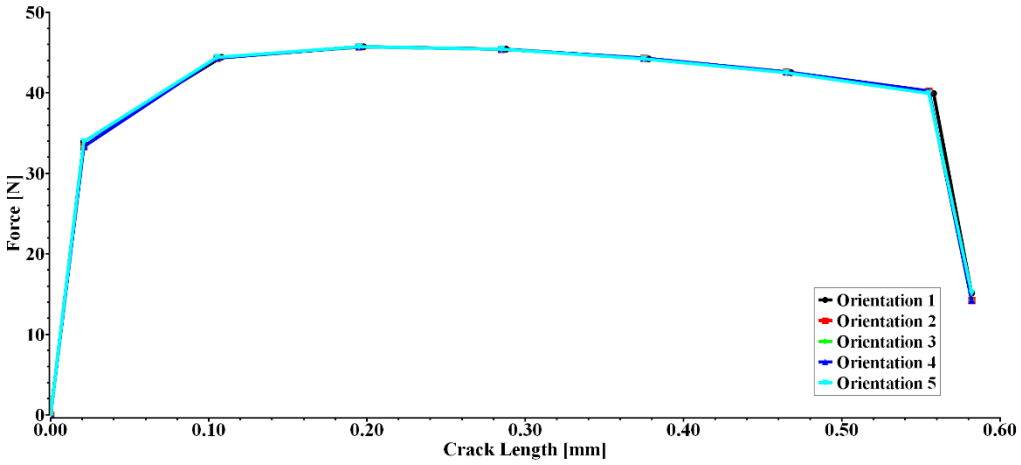

Figure 7.3.44 MAXPS criterion - AA2024 aluminum alloy - force vs. crack length

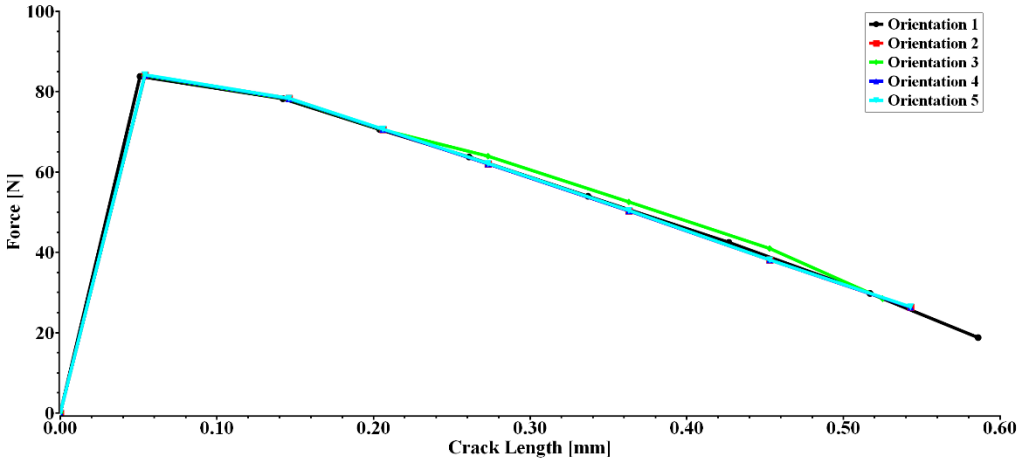

Figure 7.3.45 MAXPE criterion - AA2024 aluminum alloy - force vs. crack length

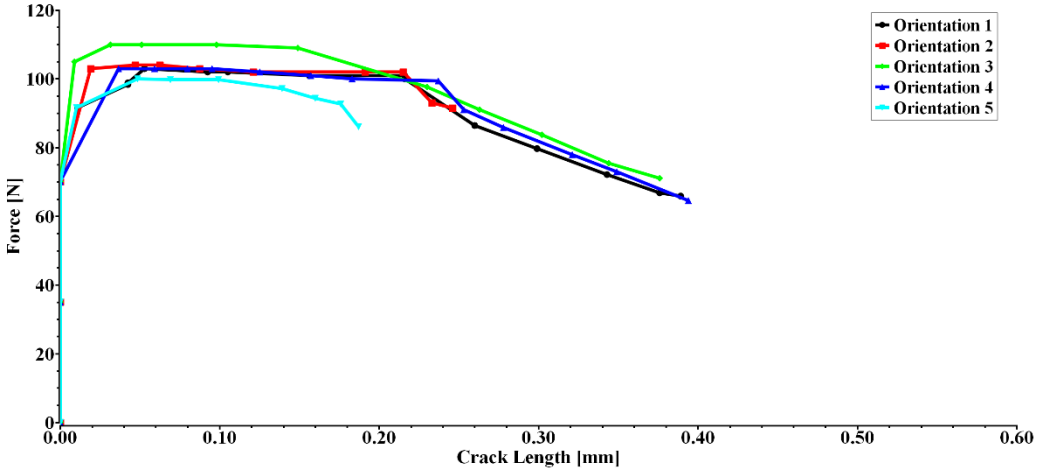

Figure 7.3.46 MAXRSS criterion - AA2024 aluminum alloy - force vs. crack length

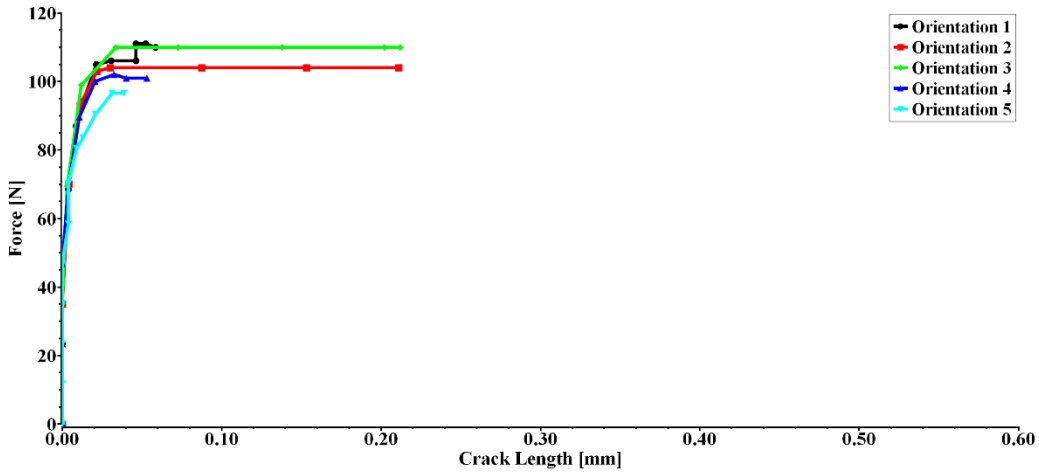

Figure 7.3.47 MAXACSS criterion - AA2024 aluminum alloy - force vs. crack length

MAXPS and MAXPE criteria give results that were not affected from grain orientation as can be seen in Figure 7.3.44 and Figure 7.3.45. These criteria found crack propagation direction as a straight line which is in the case of Farukh et al. [15] as can be seen in Figure 7.3.20 and Figure 7.3.21. In AA2024 aluminum analysis, MAXPS criterion shows same sensitivity to the grain orientation with that of MD2.

On the other hand, crack propagation behavior has been found highly dependent on grain orientation under the use of MAXRSS and MACSS criteria. AA2024 aluminum alloy separates from MD2 material in terms of required force to propagate crack and the variation of the force with respect to crack length due to the different hardening attribute and anisotropy. Another interpretation can be made that crack resistance depends on the material properties by considering total crack lengths obtained for MD2 and AA2024 aluminum which differ from each other. Also, crack propagation path obtained by employing MAXRSS differs from that of MAXACSS due to change of crack driving parameter.

7.3.4 Pre-cracked 316L Stainless Steel Polycrystal

Geometry, discretization, boundary conditions and loading given in Section 7.3.1 is applied to capture effect of material change to the crack propagation behavior of 316L stainless steel.

Crystal plasticity constitutive material parameters of the 316L stainless steel are tabulated in Table 7.3.5 have been defined in the polycrystalline model. Also, damage criteria allowable values are given in

Table 7.3.6.

Table 7.3.5 316L stainless steel material constants [40]

Parameters	**Units**	**Description**	**Value**
C11	MPa	Elastic Constant	204600
C12	MPa	Elastic Constant	137700
C44	MPa	Elastic Constant	126200
m	-	Strain Rate Sensitivity	10
$\dot{a}$	1/s	Reference Strain Rate	0.001
h_0	MPa	Initial Hardening Modulus	675
τ_0	MPa	Critical Resolved Shear Stress	90
τ_s	MPa	Saturated Resolved Shear Stress	175

Table 7.3.6 Damage criteria allowable values for 316L stainless steel

Criterion	**Unit**	**Value**	**Fracture Energy (N/mm)**
MAXPS	MPa	90	0.015
MAXPE	mm/mm	5.10^{-6}	0.015
MAXRSS	MPa	90	0.015
MAXACSS	mm/mm	5.10^{-6}	0.015

Crack initiation and propagatin in 316L stainless steel polycrystal model has been evaluated by employing MAXPS, MAXPE, MAXRSS and MAXACSS damage criteria. Results of the crack propagation of the 316L stainless steel polycrystal are given in Figure 7.3.48, Figure 7.3.49, Figure 7.3.50 and Figure 7.3.51, respectively.

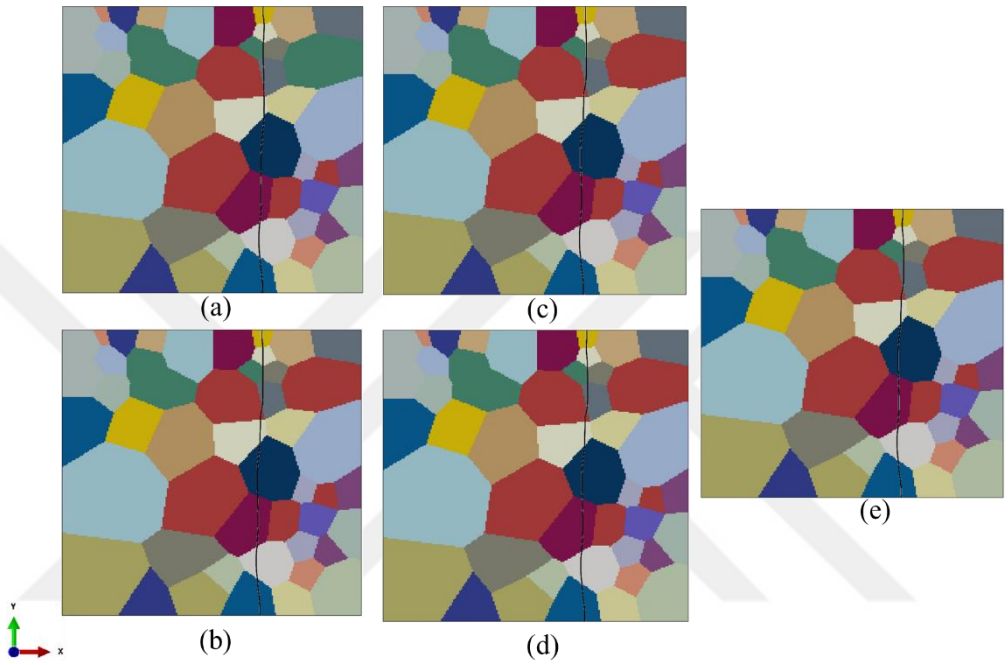

Figure 7.3.48 MAXPS criterion – 316L stainless steel polycrystal crack propagation directions of (a) Orientation 1 (b) Orientation 2 (c) Orientation 3 (d) Orientation 4 (e) Orientation 5

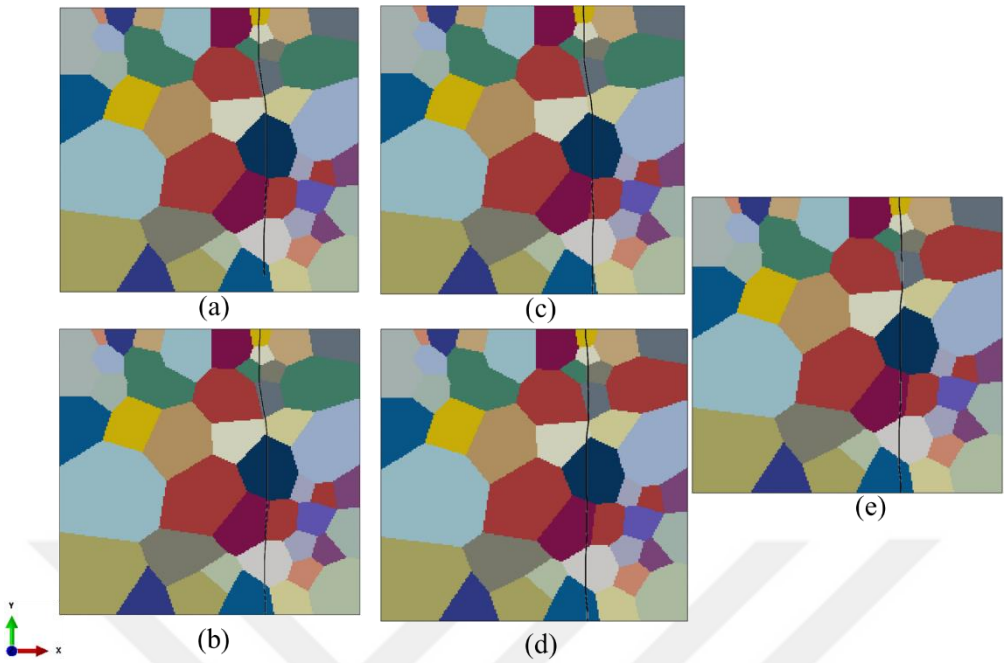

Figure 7.3.49 MAXPE criterion – 316L stainless steel polycrystal crack propagation directions of (a) Orientation 1 (b) Orientation 2 (c) Orientation 3 (d) Orientation 4 (e) Orientation 5

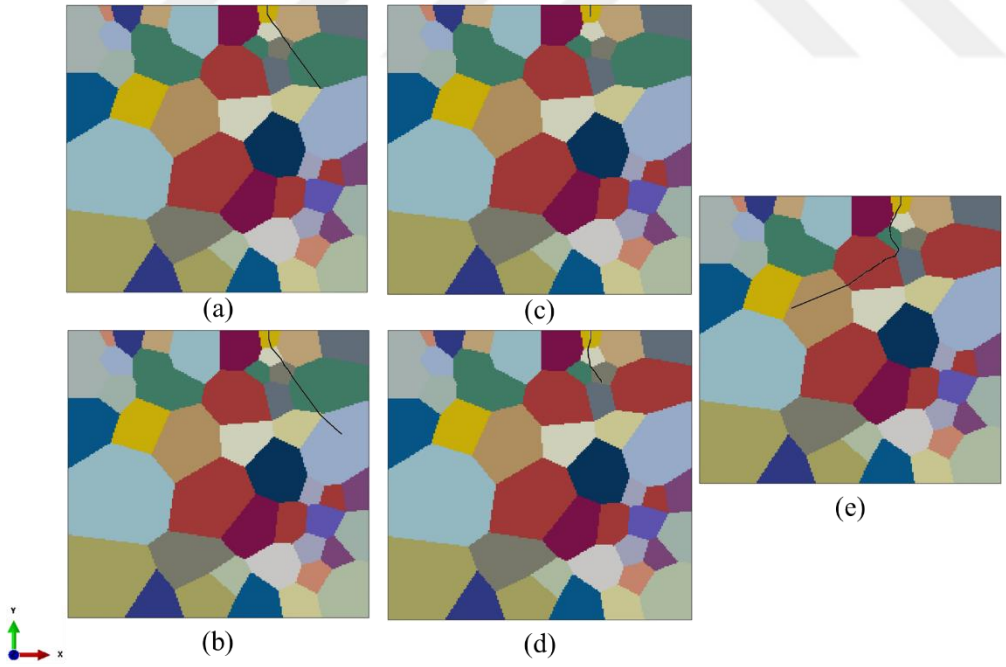

Figure 7.3.50 MAXRSS criterion – 316L stainless steel polycrystal crack propagation directions of (a) Orientation 1 (b) Orientation 2 (c) Orientation 3 (d) Orientation 4 (e) Orientation 5

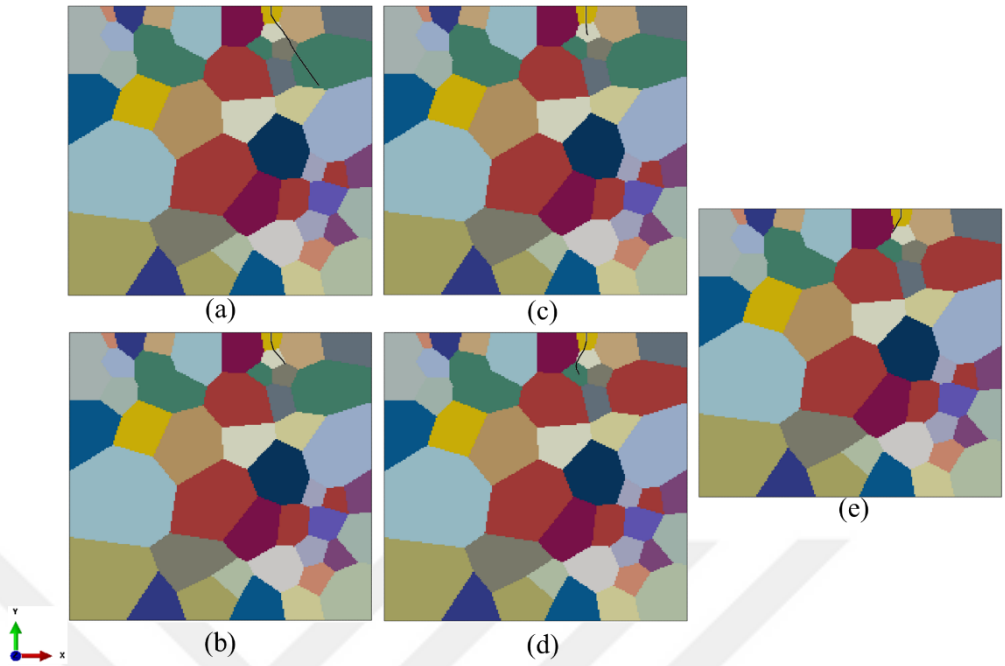

Figure 7.3.51 MAXACSS criterion – 316L stainless steel polycrystal crack propagation directions of (a) Orientation 1 (b) Orientation 2 (c) Orientation 3 (d) Orientation 4 (e) Orientation 5

Also, detailed results of the analyses are presented throughout Figure 7.3.52 to Figure 7.3.71 for MAXRSS and MAXACSS criteria.

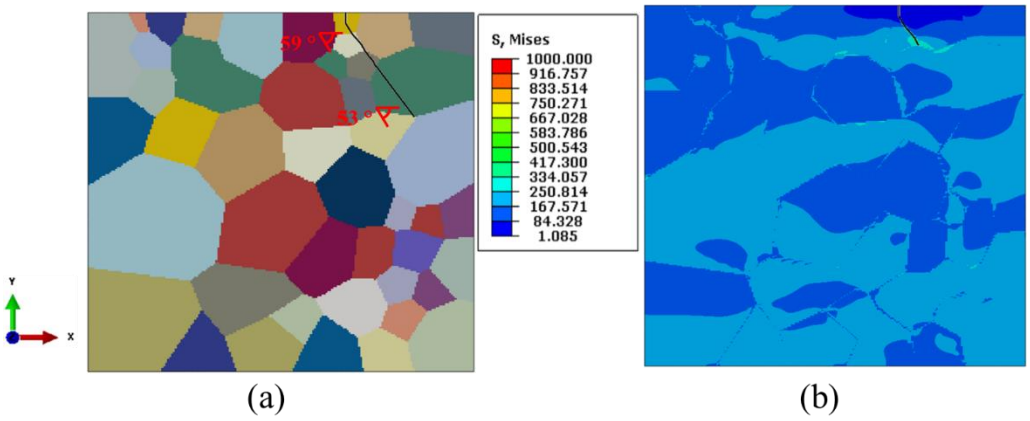

Figure 7.3.52 MAXRSS criterion – 316L stainless steel polycrystal crack propagation of Orientation 1 (a) Crack Propagation Path (b) Final Stress State

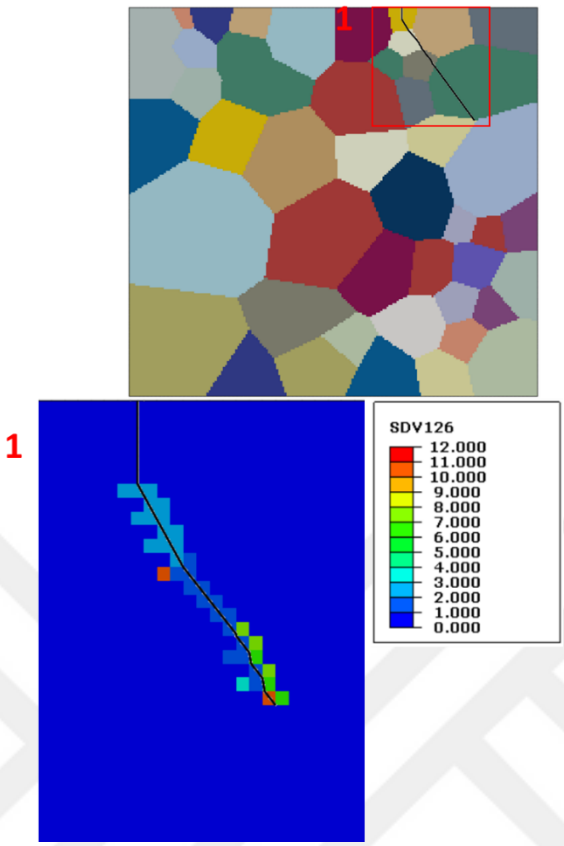

Figure 7.3.53 MAXRSS criterion - 316L stainless steel crack propagation of Orientation 1 - activated slip systems throughout crack

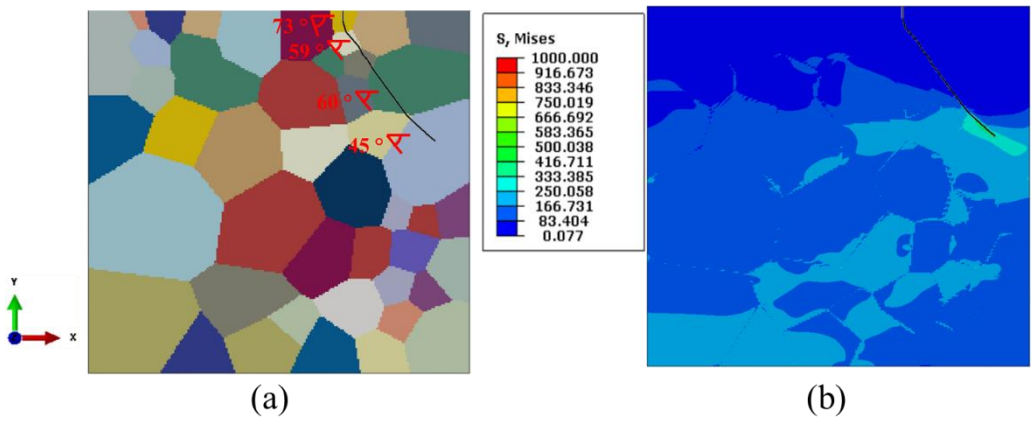

Figure 7.3.54 MAXRSS criterion – 316L stainless steel polycrystal crack propagation of Orientation 2 (a) Crack Propagation Path (b) Final Stress State

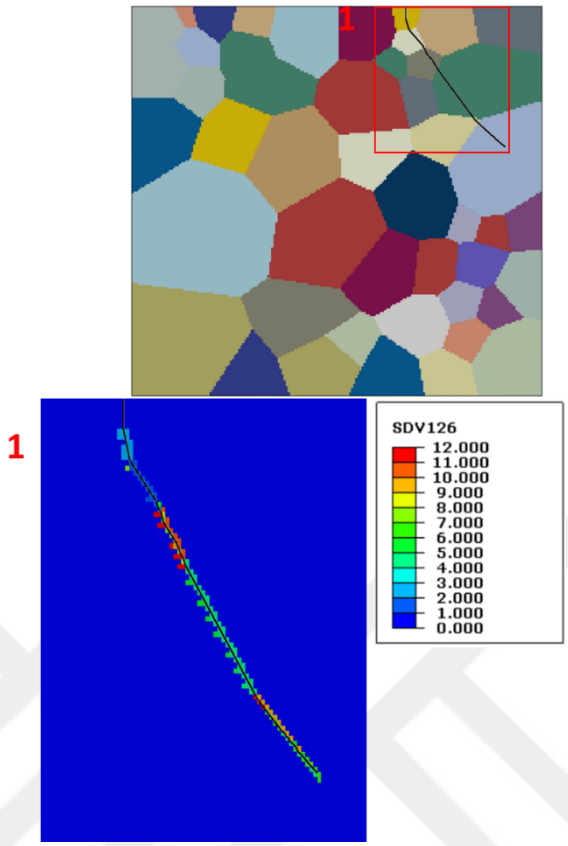

Figure 7.3.55 MAXRSS criterion - 316L stainless steel crack propagation of Orientation 2 - activated slip systems throughout crack

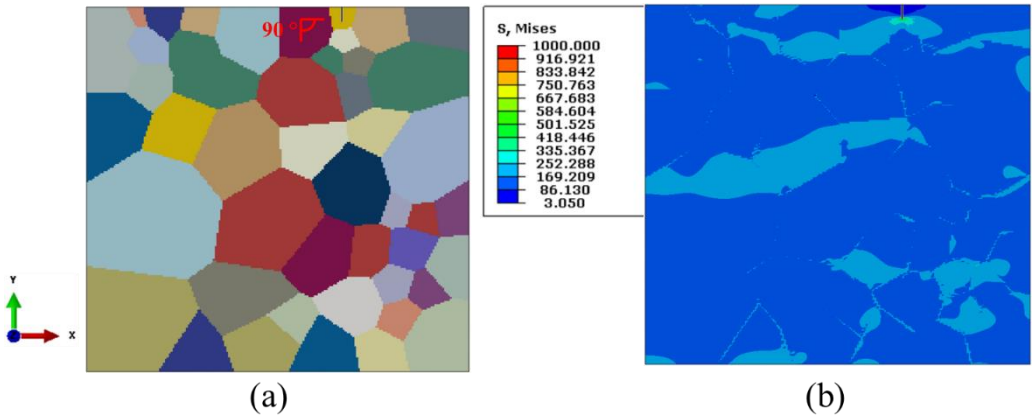

Figure 7.3.56 MAXRSS criterion – 316L stainless steel polycrystal crack propagation of Orientation 3 (a) Crack Propagation Path (b) Final Stress State

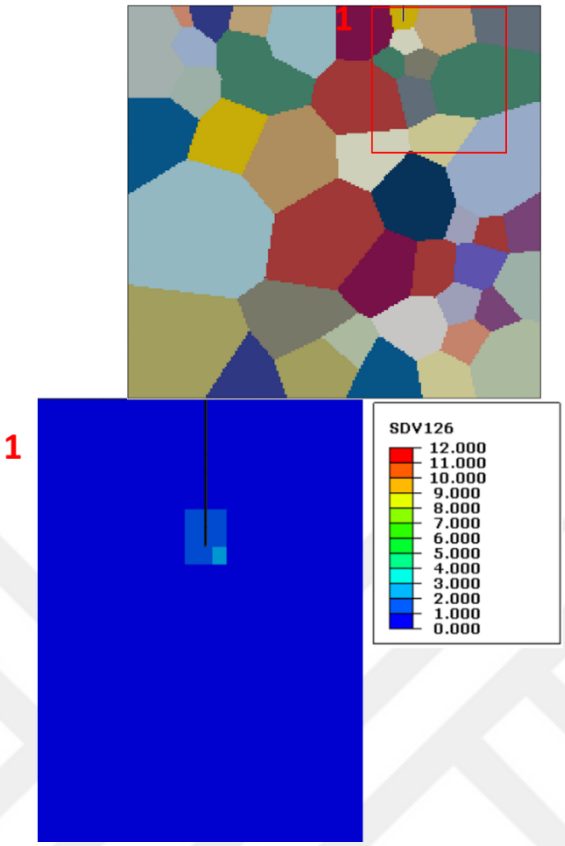

Figure 7.3.57 MAXRSS criterion - 316L stainless steel crack propagation of Orientation 3 - activated slip systems throughout crack

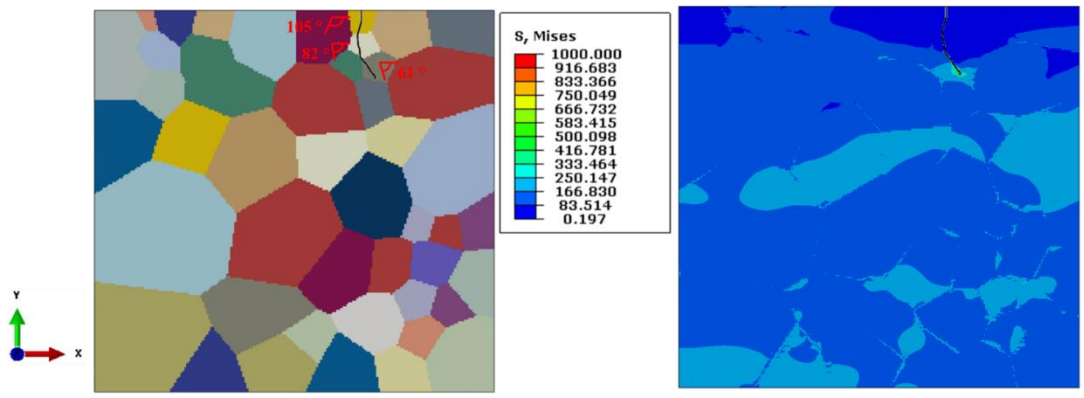

Figure 7.3.58 MAXRSS criterion – 316L stainless steel polycrystal crack propagation of Orientation 4 (a) Crack Propagation Path (b) Final Stress State

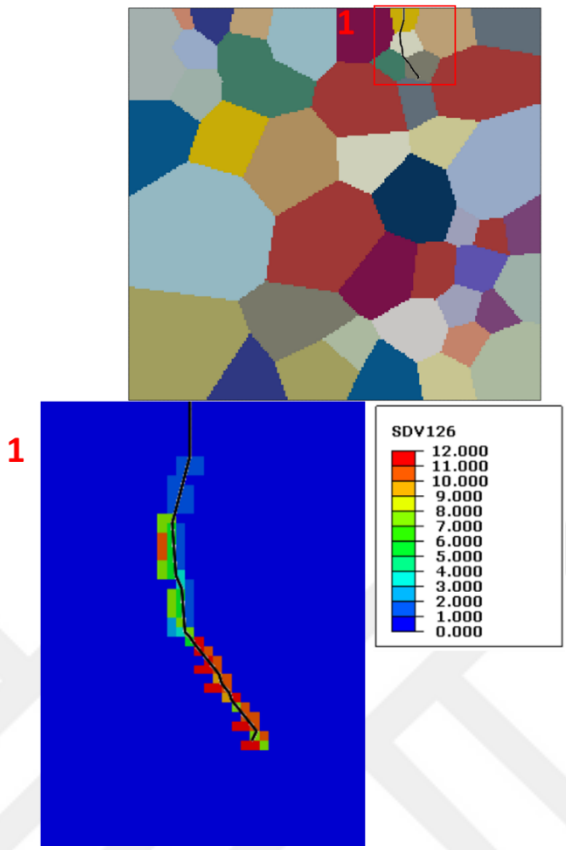

Figure 7.3.59 MAXRSS criterion - 316L stainless steel crack propagation of Orientation 4 - activated slip systems throughout crack

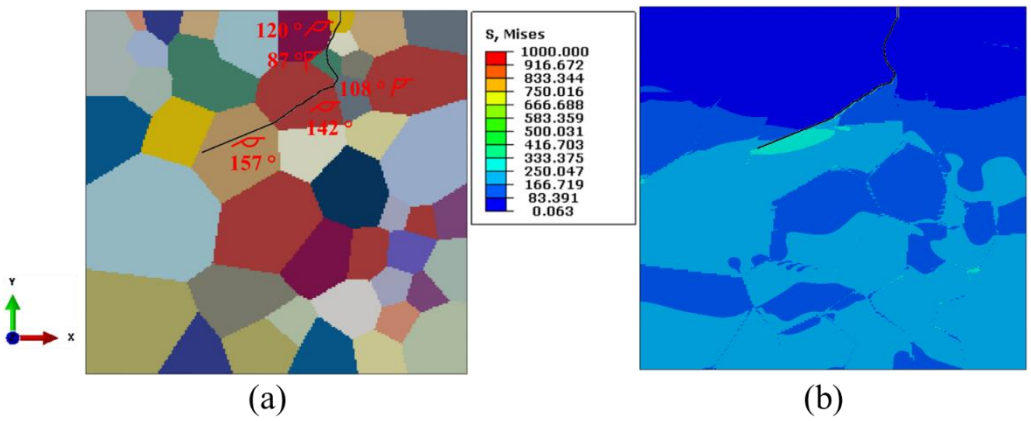

Figure 7.3.60 MAXRSS criterion – 316L stainless steel polycrystal crack propagation of Orientation 5 (a) Crack Propagation Path (b) Final Stress State

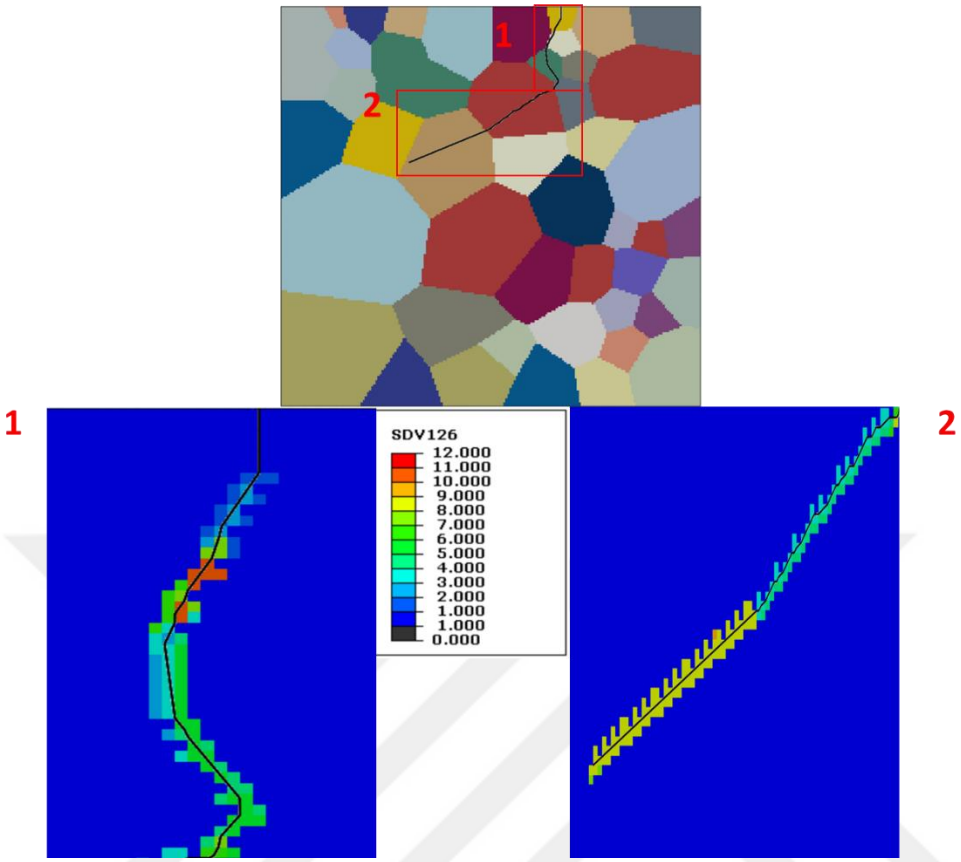

Figure 7.3.61 MAXRSS criterion - 316L stainless steel crack propagation of Orientation 5 - activated slip systems throughout crack

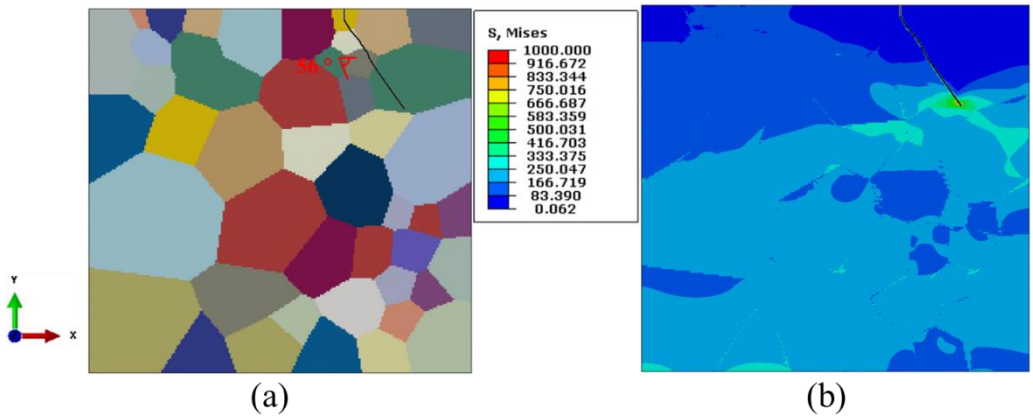

Figure 7.3.62 MAXACSS criterion – 316L stainless steel polycrystal crack propagation of Orientation 1 (a) Crack Propagation Path (b) Final Stress State

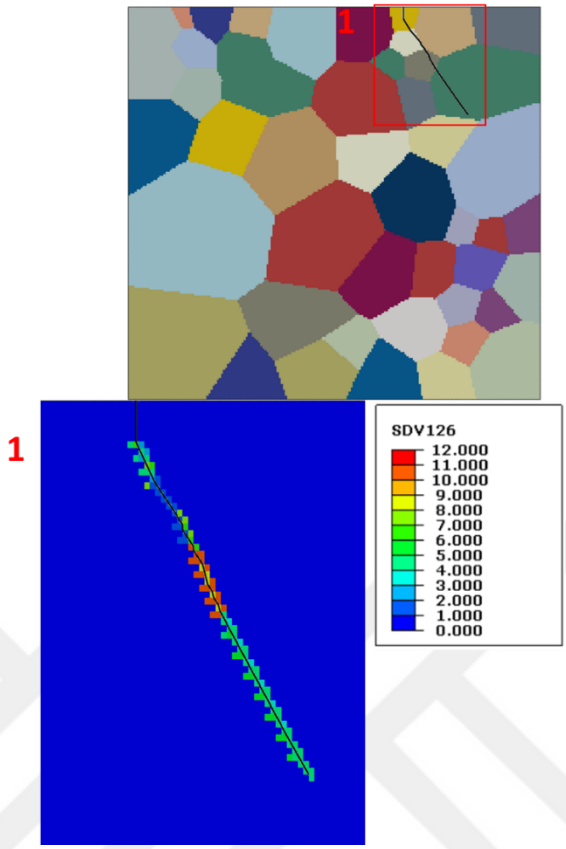

Figure 7.3.63 MAXACSS criterion - 316L stainless steel crack propagation of Orientation 1 - activated slip systems throughout crack

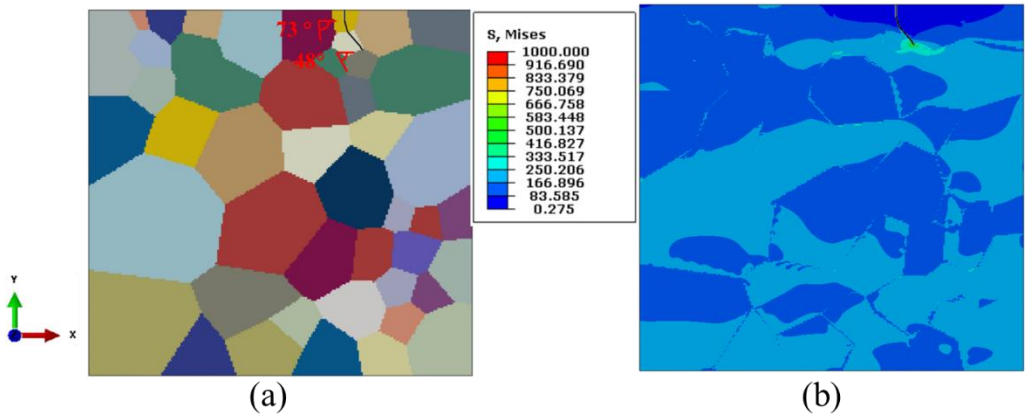

Figure 7.3.64 MAXACSS criterion – 316L stainless steel polycrystal crack propagation of Orientation 2 (a) Crack Propagation Path (b) Final Stress State

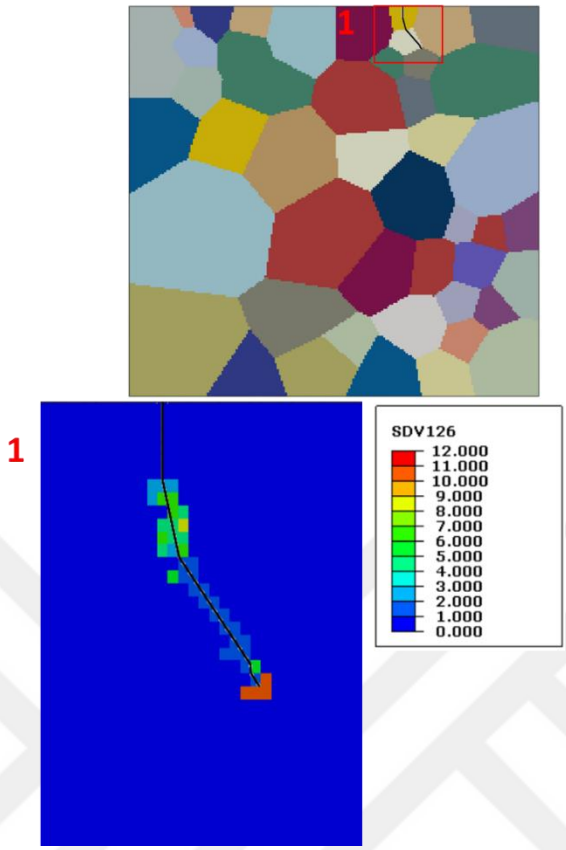

Figure 7.3.65 MAXACSS criterion - 316L stainless steel crack propagation of Orientation 2 - activated slip systems throughout crack

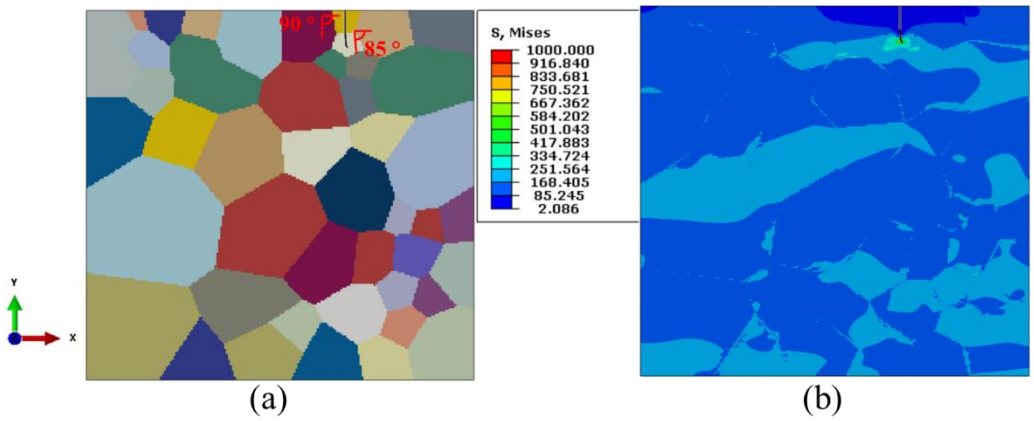

Figure 7.3.66 MAXACSS criterion – 316L stainless steel polycrystal crack propagation of Orientation 3 (a) Crack Propagation Path (b) Final Stress State

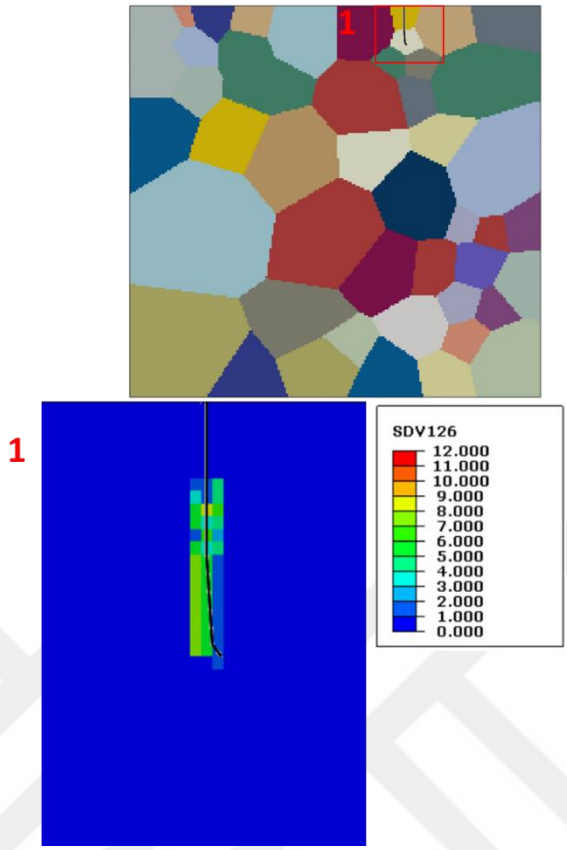

Figure 7.3.67 MAXACSS criterion - 316L stainless steel crack propagation of Orientation 3 - activated slip systems throughout crack

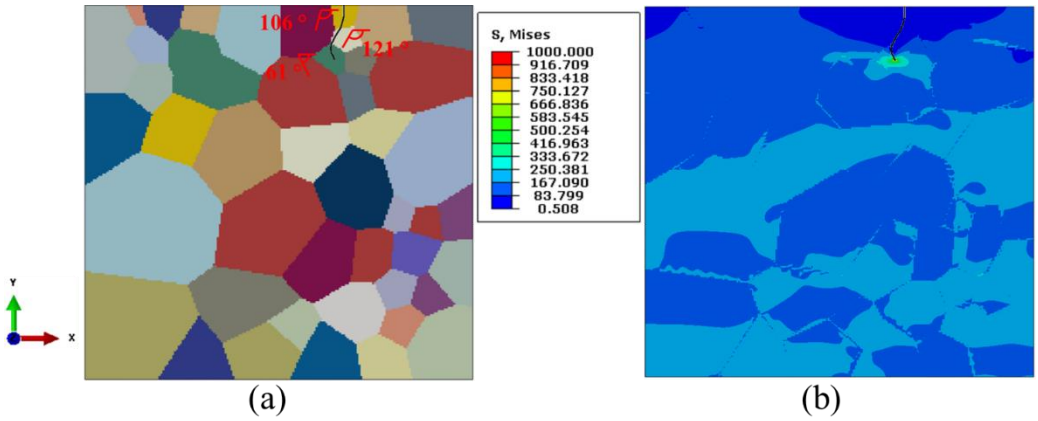

Figure 7.3.68 MAXACSS criterion – 316L stainless steel polycrystal crack propagation of Orientation 4 (a) Crack Propagation Path (b) Final Stress State

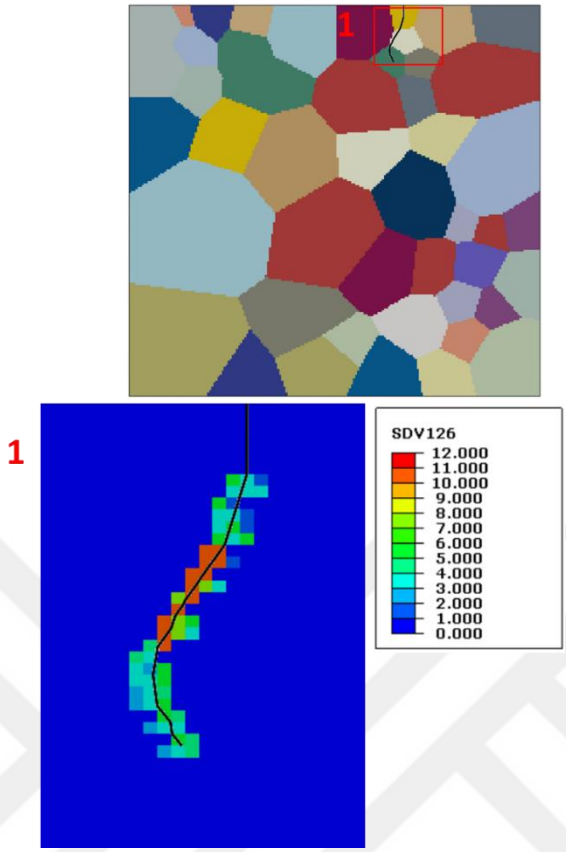

Figure 7.3.69 MAXACSS criterion - 316L stainless steel crack propagation of Orientation 4 - activated slip systems throughout crack

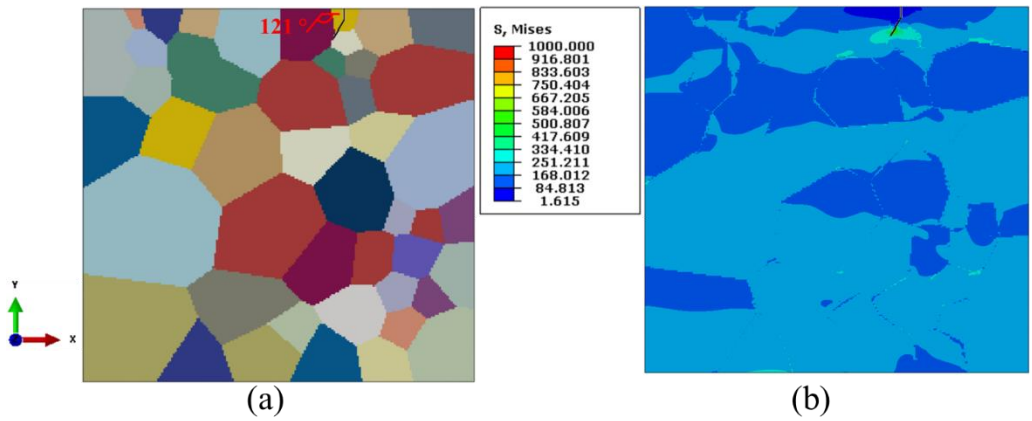

Figure 7.3.70 MAXACSS criterion – 316L stainless steel polycrystal crack propagation of Orientation 5 (a) Crack Propagation Path (b) Final Stress State

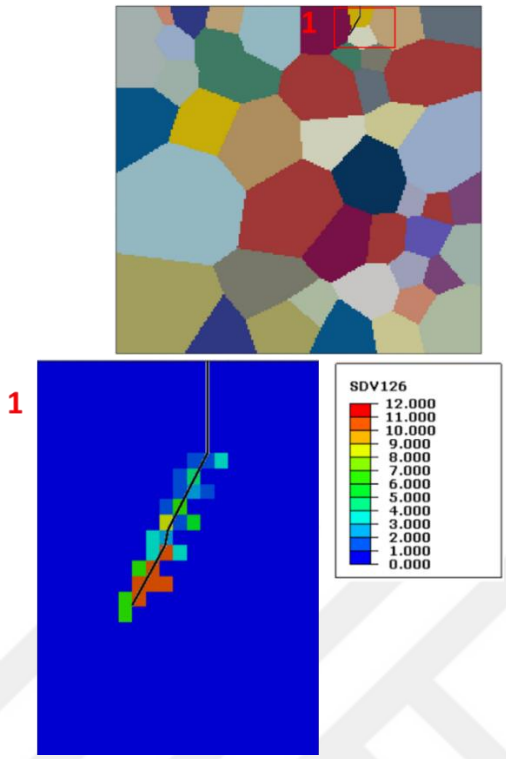

Figure 7.3.71 MAXACSS criterion - 316L stainless steel crack propagation of Orientation 5 - activated slip systems throughout crack

Also, the variation of the force needed to propagate crack versus crack length for each orientation are given for MAXPS, MAXRSS and MAXPS criteria throughout Figure 7.3.72 to Figure 7.3.75.

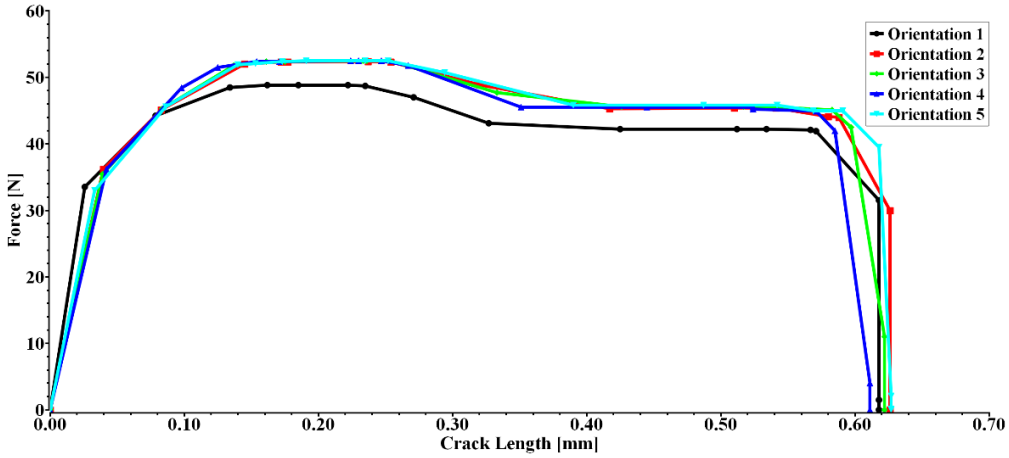

Figure 7.3.72 MAXPS criterion - 316L stainless steel - force vs. crack length

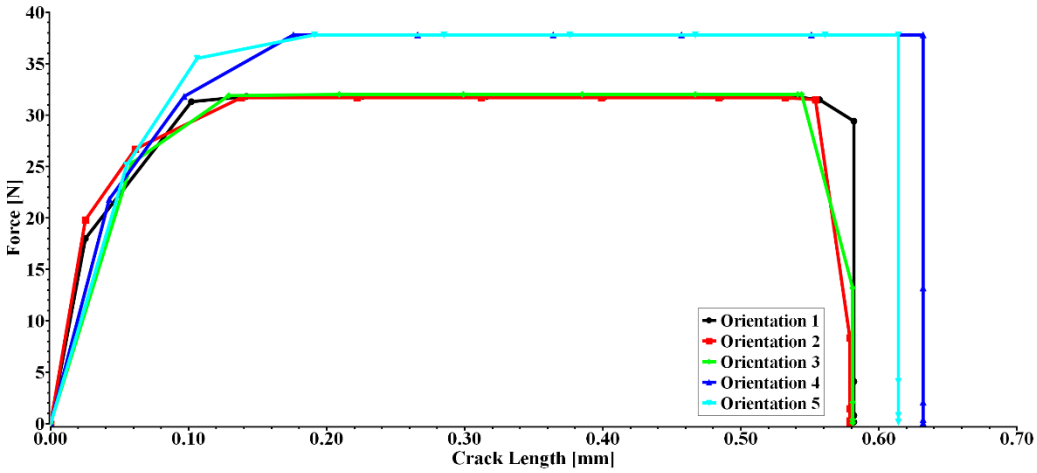

Figure 7.3.73 MAXPE criterion - 316L stainless steel - force vs. crack length

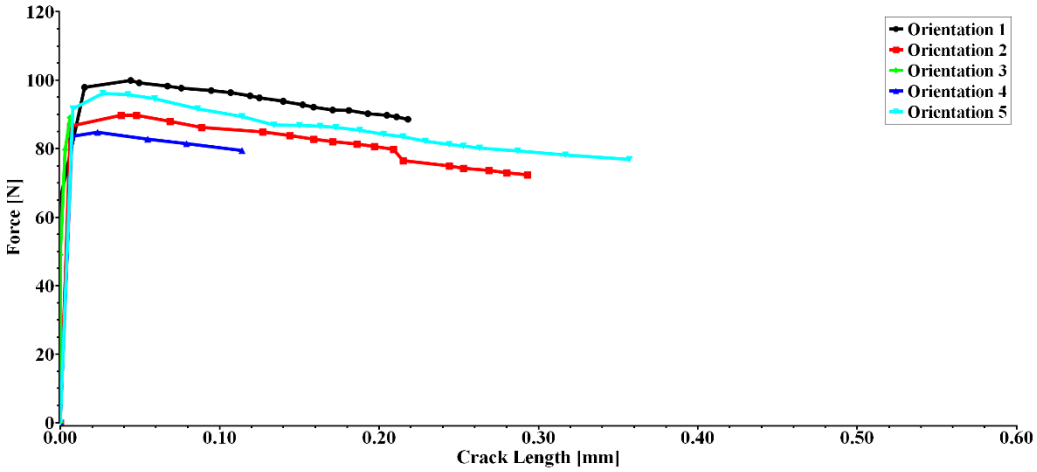

Figure 7.3.74 MAXRSS criterion - 316L stainless steel - force vs. crack length

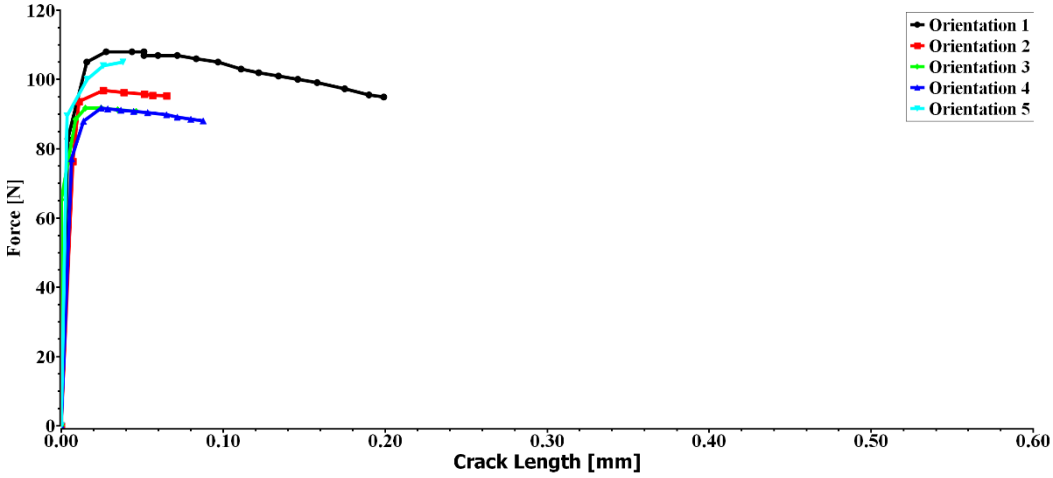

Figure 7.3.75 MAXACSS criterion - 316L stainless steel - force vs. crack length

Similar results are observed for the effect of grain orientation on crack propagation for streel polycrystal with the ones for aluminum polycrystals when MAXRSS and MAXACSS criteria are used. On the other hand, the variation of the force needed to propagate with respect to crack length differs from other materials due to its hardening behavior and anisotropy.

7.4 Material Effect on Crack Propagation Behavior

In this section, crack propagation results of the different materials corresponding to orientation 1 of MD2, Al 2024 and 316L under MAXRSS criteria are compared to investigate crack propagation behavior for different materials under same configuration, i.e., same grain orientations, loadings etc. Crack propagation directions of the corresponding materials are summarized in Figure 7.4.1. Also, force needed to propagate crack is given in Figure 7.4.2.

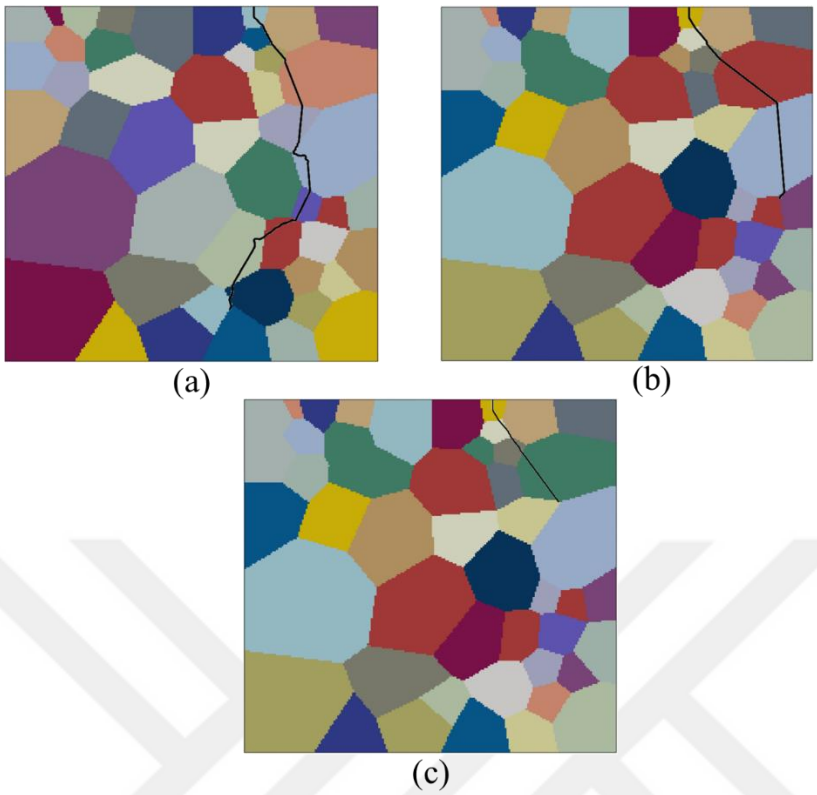

Figure 7.4.1 Crack propagation directions (a) MD2 (b) AA2024 Aluminum (c) MD2 Stainless Steel

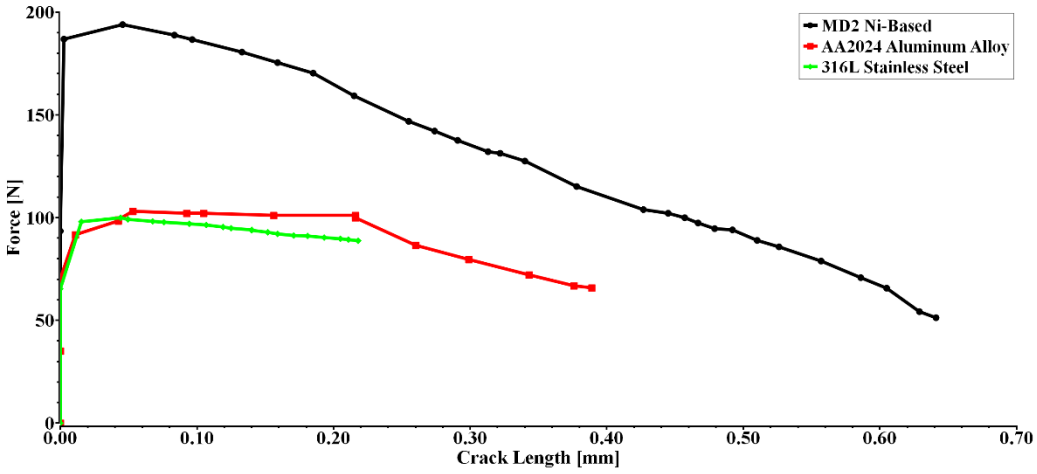

Figure 7.4.2 MAXRSS criterion different materials force vs. crack length comparison

Different material properties could affect the crack propagation direction and total crack length as can be seen in Figure 7.4.1 due to the different hardening and

anisotropy characteristic. Also, the force to cause crack propagation is captured at different levels for MD2, AA2024 Aluminum, and 316L stainless steel. As to give idea, yield strength of MD2, AA2024 and 316L are 900 MPa [42], 324 MPa, and 205 MPa in macroscale. Hence, force versus crack length curves reflect the tendency with macroscale mechanical values.

7.5 Grain Size Effect on Crack Propagation Behavior of AA2024 Aluminum Alloy Polycrystal

In this section, AA2024 aluminum alloy polycrystal finite element models whose grain sizes differ from each other are analyzed by considering the MAXRSS criterion. Grain sizes defined in finite element models are given in Table 7.5.1. The same boundary conditions and loading described in Section 7.3.1 are applied. The material properties given in Table 7.3.3 and damage allowable values given in Table 7.3.4 are introduced into finite element models.

Table 7.5.1 Grain size configurations of AA2024 aluminum alloy polycrystal

Averaged Grain Size [μm]	**Number of Grain**
60	108
70	80
90	48

Grain texture of the finite element models are given throughout Figure 7.5.1 to Figure 7.5.3.

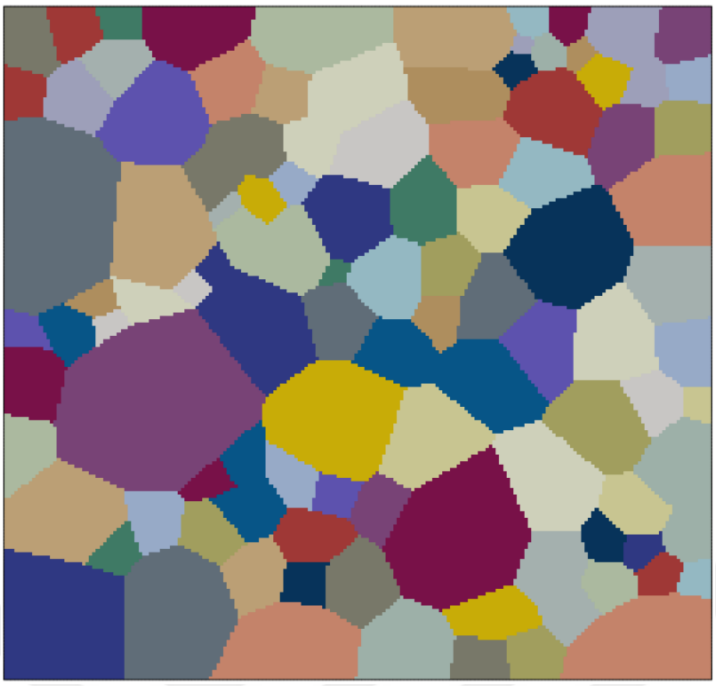

Figure 7.5.1 Grain texture of averaged grain size of 60 micrometers

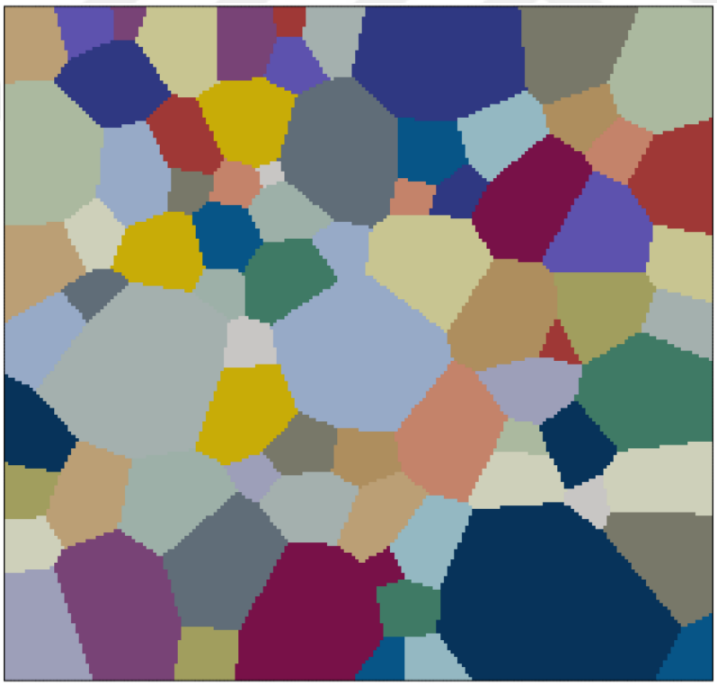

Figure 7.5.2 Grain texture of averaged grain size of 70 micrometers

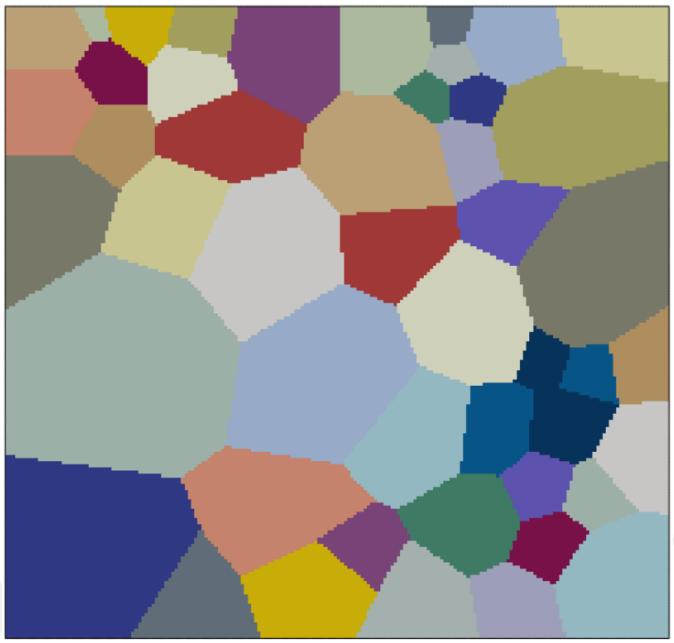

Figure 7.5.3 Grain texture of averaged grain size of 90 micrometers

Crack propagation directions of each grain size are given throughout Figure 7.5.4 to Figure 7.5.6 for MAXRSS criterion.

Figure 7.5.4 MAXRSS criterion - crack propagation direction of averaged grain size of 60 micrometers

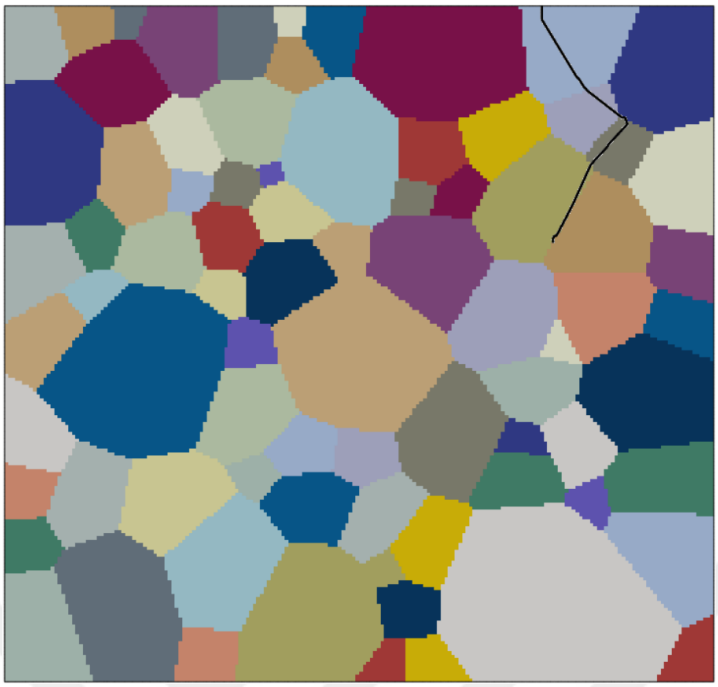

Figure 7.5.5 MAXRSS criterion - crack propagation direction of averaged grain size of 70 micrometers

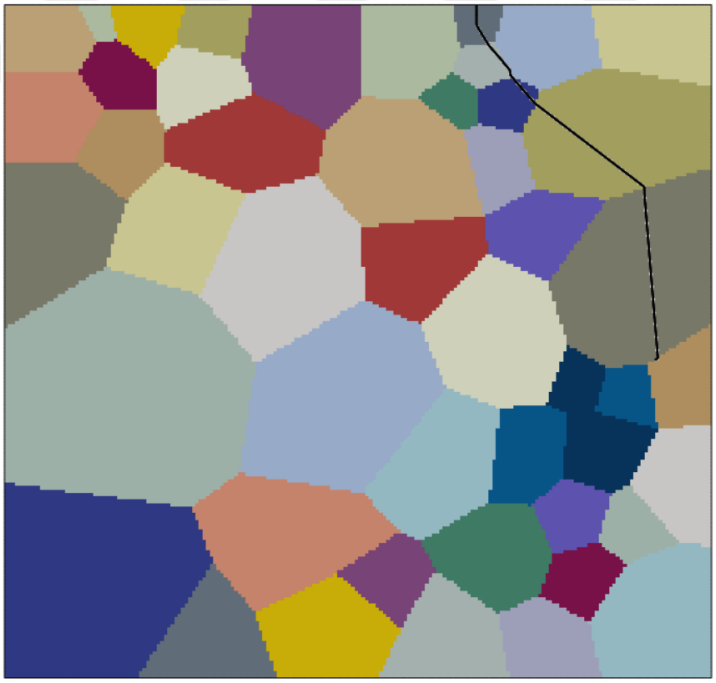

Figure 7.5.6 MAXRSS criterion - crack propagation direction of averaged grain size of 90 micrometers

The force needed to propagate crack is given in Figure 7.5.7. This graphic is obtained by considering MAXRSS criterion, since MAXRSS criterion is found more sensitive to the microscale.

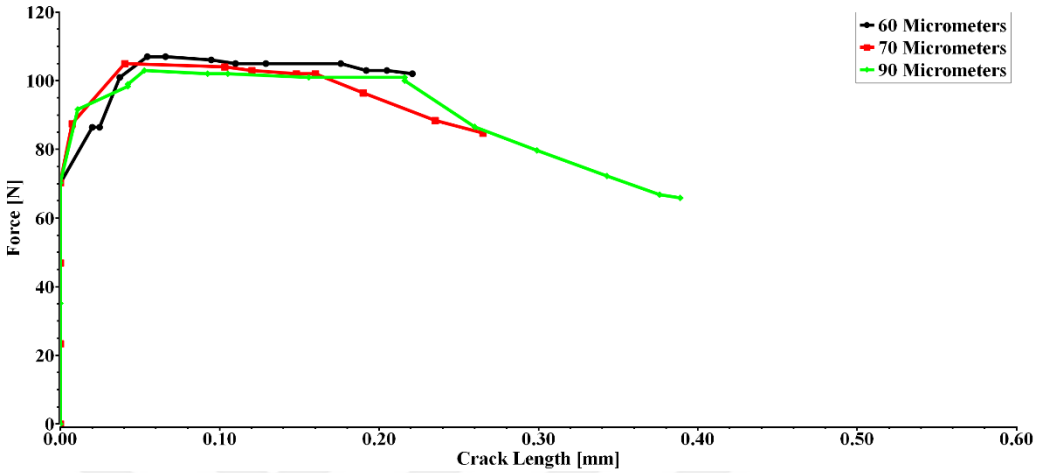

Figure 7.5.7 MAXRSS criterion - force vs. crack Length comparison

Different grain size assignment to the volume to be analyzed provokes different number of grains with arbitrary orientations. Therefore, the observation regarding grain size effect on the crack propagation behavior can be implicitly made by considering force-crack length curve constructed for different models including different grain sizes. Peak force values for different averaged grain sizes have different magnitudes from each other as it is anticipated, since resistance to crack growth increases as grain size is going to decrease. The maximum force needed to propagate crack has been obtained for grain size of 60 micrometers. Further, the longest final crack length has been detected for grain size of 90 micrometers as can be seen in Figure 7.5.7.

CHAPTER 8

CONCLUSION AND FUTURE WORKS

8.1 Conclusion

In this thesis, microscale crack propagation is investigated by employing four different damage criteria and by considering of several grain orientations and sizes for different materials which are nickel-based super alloy (MD2), AA2024 aluminum alloy and 316L stainless steel. Grain textures have been obtained through numerical tessellation by the open-source software Neper. After importing grain texture to the extended finite element software ABAQUS, crystal plasticity finite element model (CPFEM) is introduced to by means of the user subroutine UMAT. Then, the damage criteria are defined in the crystal plasticity model by user subroutine. The results achieved from numerical analyses are the following:

1. Crack propagation behavior is found highly dependent on grain orientation where activated slip systems are considered, since activated slip systems differ according to angle between loading direction and slip planes.
2. The MAXPS and MAXPE criteria determines the crack initiation due to the maximum principal stress and strain values defining the normal of the crack plane as parallel to the normal to the maximum principal plane for the stress and strain tensors, respectively. On the other hand, MAXRSS and MAXACSS criteria, that are introduced by user defined subroutines, use the maximum shear stress that occur among the slip systems for crack initiation by defining the normal of the crack plane parallel to the normal of the related slip plane. Hence it is expected that the criterion based on the slip systems reflects the actual behavior more realistically.
3. It is seen that the material selection plays important role on the crack propagation since intrinsic material properties such as hardening

characteristics, critical resolved shear stress values and anisotropic stiffnesses differ significantly from each other.

4. The general trend of the force required to propagate a crack is observed to decrease as the crack advances in the microstructure, as expected. However, the shape of the force-crack length curve varies depending on the material selection and grain orientation, which are indicators of the hardening characteristics and stiffness of the microstructure that crack propagates.
5. It is observed that grain size difference affects the crack propagation behavior by changing the number of grains in the material. This can be attributed to the increasing number of the grains that have arbitrary orientations.
6. The grain orientation and size, and material properties all are found as factors in the scatter of crack resistance of crystalline materials as well as the direction of crack propagation.

8.2 Future Works

Future works which would be provide more accuracy to model microscale crack propagation can be listed as follows:

1. Experiments are essential to evaluate the accuracy of models used in microscale. Therefore, single crystal experiments could be conducted to obtain the actual behavior of the materials. Digital image correlation from specimen could be employed to be able to simulate realistic grain texture.
2. Analyses results could be enhanced by introduction of the grain boundary and its interactions.
3. Finite element models can be constructed for fatigue loading to get better understanding crack formation in microscale depending on microscale fatigue experiments.

REFERENCES

[1] Reed, R.P., Smith, J.H., and Christ, B.W., *"Economic effects of fracture in the United States. Part 1. A synopsis of the September 30, 1982 report to NBS by Battelle Columbus Laboratories"*, United States, 1983.

[2] Campbell, G.S., Lahey, R., *"A survey of serious aircraft accidents involving fatigue fracture",* International Journal of Fatigue, vol. 6, p. 25-30, 1984.

[3] Griffith, A.A., *"The Phenomena of Rupture and Flow in Solids"*, Philosophical Transactions, Series A, vol. 221, p. 163-198, 1920.

[4] Westergaard, H.M., *"Bearing Pressures and Cracks"*, Journal of Applied Mechanics, vol. 6, p. A49-53, 1939.

[5] Irwin, G.R., *"Analysis of Stresses and Strains Near the End of a Crack Traversing a Plate"*, Journal of Applied Mechanics, vol. 24, p. 361-364, 1957.

[6] Schivje, J., *"Fatigue of Structures and Materials"*, 2nd Edition, p. 15, Springer, 2009.

[7] Taylor, G.I., *"The mechanism of plastic deformation of crystals. Part I.- Theoretical"*, Proc. Roy. Soc. A, vol. 145, 1934.

[8] Peirce, D., Asaro, R.J., Needleman, A., *"An analysis of nonuniform and localized deformation in ductile single crystals"*, Acta Metallurgica, vol. 30, p. 1087-1119, 1982.

[9] Hill, R., *"Generalized constitutive relations for incremental deformation of metal crystals by multislip"*, Journal of the Mechanics and Physics of Solids, vol. 14, p. 95-102, 1966.

[10] Rice, J.R., *"Inelastic constitutive relations for solids: An internal-variable theory and its application to metal plasticity"*, vol. 19., p. 433-455, 1971.

[11] Hill, R., Rice, J.R., *"Constitutive analysis of elastic-plastic crystals at arbitrary strain"*, Journal of the Mechanics and Physics of Solids, vol.20, p. 401-413, 1972.

[12] Peirce, D., Asaro, R.J., Needleman, A., *"Material rate dependence and localized deformation in crystalline solids"*, Acta Metallurgica, vol. 31, p. 1951-1976, 1983.

[13] Asaro, R.J., *"Micromechanics of Crystals and Polycrystals"*, Advances in Applied Mechanics, vol. 23, p. 1-115, 1983.

[14] Wu, T., Bassani, J.L, Lairde, C., *"Latent hardening in single crystals – I. Theory and experiments"*, Proc. Roy. Soc. A, vol. 435, 1991.

[15] Farukh, F., Zhao, L.G., Jiang, R., Reed, P., Proprentner, D., Shollock, B.A., *"Realistic microstructure-based modelling of cyclic deformation and crack growth using crystal plasticity"*, Computational Materials Science, vol. 111, p. 395-405, 2016.

[16] Wilson, D., Wan, W., Dunne, F.P.E., *"Microstructurally-sensitive fatigue crack growth in HCP, BCC and FCC polycrystals"*, Journal of the Mechanics and Physics of Solids, vol. 126, p. 204-225, 2019.

[17] Zhang., P., Zhang, L., Baxevanakis, K.P., Zhao, L.G., Bullough, C., *"Modelling short crack propagation in a single crystal nickel-based superalloy using crystal plasticity and XFEM"*, International Journal of Fatigue, vol. 136, 2020.

[18] Abdolvand, H., *"Development of microstructure-sensitive damage models for zirconium polycrystals",* International Journal of Plasticity, vol. 149, 2022.

[19] Zhang, X., Dunne, F.P.E., *"3D CP-XFEM modelling of short crack propagation interacting with twist/tilt nickel grain boundaries"*, Journal of the Mechanics and Physics of Solids, vol. 168, 2022.

[20] Mao, J., Yufei, X., Dianyin. H., Liu, X., Pan, J., Sun, H., Wang, R., *"Microstructurally short crack growth simulation combining crystal plasticity with extended finite element method"*, Engineering Fracture Mechanics, vol. 275, 2022.

[21] Wilson, D., Dunne, F.P.E., *"A mechanistic modelling methodology for microstructure-sensitive crack growth"*, Journal of the Mechanics and Physics of Solids, vol. 124, 2019.

[22] Karamitros, V., MacLahlan, D.W., Dunne, F.P.E., *"Mechanistic fatigue in Ni-Based superalloy single crystals: A study of crack paths and growth rates"*, Journal of the Mechanics and Physics of Solids, vol. 158, 2022.

[23] Zhang, J., Johnston, H., Chattopadhyay, A., *"Physics-based multiscale damage criterion for fatigue crack prediction in aluminum alloy",* Fatigue & Fracture of Engineering Materials & Structures, 37(2), p. 119-131, 2014.

[24] Efthymiadis, P., Pinna, C., Yaters, J.R., *"Fatigue crack initiation in AA2024: a coupled micromechanical testing and crystal plasticity study"*, Fatigue & Fracture of Engineering Materials & Structures, 24, 321-338, 2019.

[25] Huang, Y., *"A user-material subroutine incorporating single crystal plasticity in the ABAQUS finite element program."*, Cambridge, MA: Harvard Univ., 1991.

[26] Rice, J.R., *"Inelastic constitutive relations for solids: An internal-variable theory and its application to metal plasticity"*, Journal of the Mechanics and Physics Solids, vol. 19, p. 433-455, 1971.

[27] Callister, W.D, Rethwisch, Jr. D. G., *"Materials Science and Engineering An Introduction"*, 9th Edition, The Structure of Crysalline Solids, p. 57, Copyright © 2014, 2010, 2007, 2003, 2000 John Wiley & Sons, New York.

[28] Rosenhain, W., *"An Introduction to the Study of Physical Metallurgy"*, 2nd Edition, Constable & Company Ltd., London,1915.

[29] Hayden, H.W, Moffatt, H.G, Wulff J., *"The Structure and Properties of Materials"*, Vol. III, Mechanical Behavior, p.70, John Wiley & Sons, New York, 1965.

[30] Guy, A.g, *"Essentials of Materials Science"*, p.153, McGraw-Hill Book Company, New York, 1976.

[31] Yongjuan, G., Chen, B., Zou, J., Britton, T.B., Jiang, J., Dunne, F.P.E, *"Crystal plasticity modelling and HR-DIC measurement of slip activation*

and strain localization in single and oligo-crystal Ni alloys under fatigue", International Journal of Plasticity, vol. 88, p. 70-88, 2017.

[32] Belytschko, T., Black, T., *"Elastic Crack Growth in Finite Elements with Minimal Remeshing"*, International Journal for Numerical Methods for Engineering, vol. 45, p. 601-620, 1999.

[33] D. Systémes, "Abaqus 6.14: Analysis User's Manual, 10.7.1 Modeling discontinuities as an enriched feature using the extended finite element method"

[34] Westergaard, H.M., *"Bearing Pressures and Cracks"*, Journal of Applied Mechanics, vol. 6, p. A49-53, 1939.

[35] Aghabalaeivahid, A., Shalvandi, M., "*Microstructure-based crystal plasticity modeling of AA2024-T3 aluminum alloy defined as the α-Al, θ-Al_2Cu, S-Al_2CuMg phases based on real metallographic image"*, Material Research Express, vol. 8, 2021.

[36] Quey, R., Dawson, P.R., Barbe, F., *"Large-scale 3D random polycrystals for the finite element method: Generation, meshing and remeshing."*, Computational Methods Applied Mechanics Engineering, vol. 200, p. 1729-1745, 2011.

[37] Zienkiewicz, O.C., Taylor, R.L., Zhu, J.Z., *"The Finite Element Method: Its Basis & Fundamentals"*, 7th Edition, Copyright © 2013 Elseviers Ltd., Butterworth-Heinemann.

[38] McDowell, D.L., Dunne, F.P.E., *"Microstructure-sensitive computational modeling of fatigue crack formation"*, International Journal of Fatigue, vol. 32, p. 1521-1542, 2010.

[39] Ye, W., Efthymiadis, P., Pinna, C., Ma, A., Shollock, B., Dashwood, R., *"Experimental and modelling study of fatigue crack initiation in an aluminum beam with a hole under 4-point bending"*, International Journal of Solids and Structures, vol. 138, p. 87-96, 2018.

[40] Gonzalez, D., Simonovski, I., Withers, P.J., Quinta da Fonseca, J., *"Modelling the effect of elastic and plastic anisotropies on stresses at grain boundaries"*, International Journal of Plasticity, vol. 61, p. 49-63, 2014.

[41] Dieter, G.E., *"Mechanical Metallurgy"*, SI Metric Edition, Microstrain Behavior, p. 138, Copyright © 1988 McGraw-Hill Book Company (UK) Limited

[42] Pollock, T.M., Tin, S., *"Nickel-based superalloys for advanced turbine engines: Chemistry, microstructure, and properties"*, Journal of Propulsion and Power, vol. 54, p. 1679-1684, 2006.

[43] Dieter, G.E., *"Mechanical Metallurgy"*, SI Metric Edition, Slip by Dislocation Motion, p. 124, Copyright © 1988 McGraw-Hill Book Company (UK) Limited

[44] Hutchinson, J.W., *"Bounds and self-consistent estimates for creep of polycrystalline materials"*, Proc. Roy. Soc. Series, vol. 348, p. 101, 1976.

APPENDICES

A. Euler-Bunge Convention

According to Euler rotation theory, an object can be rotated to final configuration in total three subsequently rotations as can be seen in Figure 8.2.1. Euler-Bunge convention defined as the rotation in the order of Z, X and Z axes is generally chosen to define crystal orientation in material science. Namely, coordinate system is firstly rotated in Z-axis, after first rotation x and y axes are called as x* and y*; second rotation occurs in x*-axis and final rotation is around z* axis. Euler-Bunge rotation angles are subsequently called $\emptyset_1$, Φ and $\emptyset_2$ and its rotation matrix is given in Equation (39).

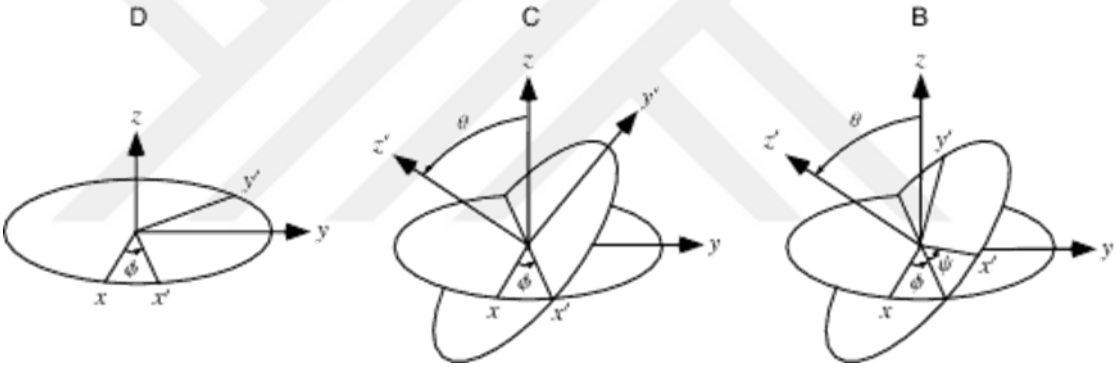

Figure 8.2.1 Euler rotation sequence

$$(\phi_1, \Phi, \phi_2) = \begin{bmatrix} \cos\phi_1 \cos\phi_2 - \cos\Phi \sin\phi_1 \sin\phi_2 & -\cos\phi_1 \sin\phi_2 - \cos\Phi \cos\phi_2 \sin\phi_1 & \sin\phi_1 \sin\phi_2 \\ \cos\phi_2 \sin\phi_1 + \cos\phi_1 \cos\Phi \sin\phi_2 & \cos\phi_1 \cos\Phi \cos\phi_2 - \sin\phi_1 \sin\phi_2 & -\cos\phi_1 \sin\Phi \\ \sin\Phi \sin\phi_2 & \cos\phi_2 \sin\Phi & \cos\Phi \end{bmatrix} \quad (39)$$